The Effects of Cell Culture Oxygen Levels on the Replicative Senescence Processes of Primary Human Fibroblasts

by

Bernd R. Stab II

Dissertation submitted to the Faculty of the Virginia Polytechnic Institute and State University in partial fulfillment of the requirements for the degree of

DOCTOR OF PHILOSOPHY
in
Biochemistry

APPROVED:

Richard F. Helm, Chairman

Jill C. Sible David R. Bevan

John M. McDowell

July 17, 2009
Blacksburg, Virginia

Key Words: replicative senescence, aging, oxygen, TCA, glycolysis, metabolites, oxidative stress

The Effects of Cell Culture Oxygen Levels on the Replicative Senescence Processes of Primary Human Fibroblasts

by

Bernd R. Stab II

(Abstract)

Serial passaging of primary human fibroblasts leads to the formation of non-dividing senescent cells by a process termed replicative senescence. This tissue culture-based methodology is currently used as a model system to determine the underlying mechanisms of *in vivo* cellular aging and tumor suppression. Senescence is regarded as an alternative pathway to apoptosis, where cells undergo multiple changes in metabolic and cellular signaling pathways in order to prevent proliferation but still maintain a metabolically-active cell. Whether or not this model accurately reflects *in vivo* processes is presently controversial; however, replicative senescence is currently the most applicable model through which one can investigate the underlying causes of human cellular aging in the context of controlled environmental stress over time. This work was directed at understanding the molecular processes involved in replicative senescence with specific emphasis on the role of the mitochondria.

A series of experiments were performed to assess changes during the induction of replicative senescence under conditions of low (3%) and high (20%) oxygen levels. Measurements were made at the transcriptional, protein, and metabolite levels. Microscopy was also utilized to monitor changes in mitochondrial morphology and volume. While previous studies have evaluated specific pathways and/or products; this work combines a more complete

metabolomic, genomic, proteomic, and morphological picture of cells undergoing senescence and oxidative stress.

Considering the low cell population densities of primary adherent fibroblasts and the subsequent low concentrations of small polar metabolites involved in glycolysis and the TCA cycle, methodologies needed to be developed in order to optimize metabolite extraction and liquid chromatography-mass spectrometric analysis. Protein kinase and transcriptional microarrays were also performed in order to quantify the changes in activated/deactivated signaling cascades as well as gene expression and relate these findings to metabolomic data. Mitochondrial dynamics of cells at different age time points and under different oxygen conditions were also assessed including mitochondrial size, shape, membrane potential, and percent volume per cell volume using confocal microscopy.

The results obtained not only confirm the major pathways involved in senescence (p53/p21, PTEN/p27, and RTK/Raf/MAPK) but also provide evidence at both the transcriptional and protein levels for additional senescence-associated pathways. The majority of the changes observed were related to pathways involved in cellular stress, cell cycle control, and the survival response. Metabolic data suggested a "pooling effect" of glycolysis and TCA precursor molecules due to attenuation in enzyme function; this theory was also supported by an observed up regulation of gene expression as a compensatory mechanism. Mitochondria exhibited changes in membrane potential as well as volume and percent volume per cell which suggested compensatory hypertrophy and/or attenuation of mitochondrial fission processes. When the aforementioned analyses are tied together, a "theoretical model of senescence" can be formulated and is characterized by increased metabolic protein and associated metabolite levels due to

attenuation in their respective enzyme function, resulting in increases in expression of their associated genes as a compensatory mechanism.

Acknowledgements

I first want to express my sincere appreciation and respect for my advisor, Dr. Richard R. Helm. I want to thank him for his guidance, inspiration, and patience over the past six years. I also want to thank my committee, Dr. David R. Bevan, Dr. Jill C. Sible, and Dr. John M. McDowell for their support. I also want to thank Dr. Keith W. Ray for his support and knowledge in regards to my work with mass spectrometry. Thanks to other members of the lab, past and present, especially Jody and soon to be Dr. Yvette Edmonds. Yvette provided me with the needed emotional support and encouragement during the difficult times of method development.

List of Abbreviations

2/3PG	2-phosphoglycerate and 3-phosphoglycerate
3PG	3-phosphoglycerate
α-KG	α-ketoglutarate
β-Gal	β-galactosidase
ATP	Adenosine triphosphate
ATPase	Adenosine triphosphate synthase
ADP	Adenosine diphosphate
AMP	Adenosine monophosphate
BJ	Human foreskin fibroblasts
CDK	Cyclin dependent kinase
CE	Capillary electrophoresis
CIT	Citrate
CLDN1	Claudin-1
CTHRC1	Collagen triple helix repeat containing 1
CTNNB	Beta-catenin
DAIME	Digital image analysis in microbial ecology
DAPI	4', 6-diamidino-2-phenyl indole
DEPDC1	DEP containing domain 1
DHAP	Dihydroxyacetone phosphate
DIC	Differential interference contrast
DMEM	Dulbelco's modified medium
DMSO	Dimethyl sulfoxide

DNA	Deoxyribonucleic acid
ERK	Extracellular regulated kinase
ESI	Electrospray ionization
FACS	Fluorescence acquired cell sorting
FBP	Fructose-1,6-bisphosphate
FBS	Fetal bovine serum
FUM	Fumarate
G0	Quiescence, reversible out of cell cycle state
G1	First growth phase of the cell cycle
G2	Second growth phase of the cell cycle
G3P	Glyceraldehyde-3-phosphate
GC	Gas chromatography
G/F6P	Glucose-6-phosphate and fructose-6-phosphate
GYS1	Glycogen synthetase
HDACs	Histone deacetylases
HDM2	Human double minute oncogene
HILIC	Hydrophilic interaction chromatography
IDH4	Human diploid foreskin fibroblasts
IL	Interleukin
IMR90	Human fetal lung fibroblasts
IPRP	Ion pairing reverse phase
ISO	Isocitrate
ISO/CIT	Isocitrate and citrate

JAK1	Janus kinase 1
JNK	Jun-N-terminal kinase
LAC	Lactate
LC	Liquid Chromatography
LDH	Lactate dehydrogenase levels
M	Mitosis phase of the cell cycle
MAL	Malate
MALDI	Matrix assisted laser desorption ionization
MAPK	Mitogen activated protein kinase
MCF7	Human breast cell carcinoma
MMP	Mitochondrial membrane potential
MRM	Multiple reaction monitoring
MS	Mass spectral
NAD	Nicotinamide adenine dinucleotide
NADP	Nicotinamide adenine dincleotide phosphate
NAG	N-acetyl glutamine
NMR	Nuclear magnetic resonance
NR4A2	Nuclear receptor subfamily 4
NSI	Nanospray ionization
OAA	Oxaloacetate
OD	Oxidative damage
PBS	Phosphate-buffered saline
PDs	Population doublings

PDK	Pyruvate kinase
PEP	Phosphoenolpyruvate
PEPCK	Phosphoenolpyruvate kinase
PFK2	Phosphofructose kinase 2
PGK	Phosphogylcerate kinase
PI3K	Phosphoinositol-3-phosphate kinase
PTEN	Phosphatase and tensin homolog
PTGIS	Prostaglandin I2 synthase
PTHLH	Parathyroid hormone like hormone
PYR	Pyruvate
Rb	Retinoblastoma tumor suppressor protein
ROS	Reactive oxygen species
RTK	Receptor tyrosine kinase
RYK	Receptor like tyrosine kinase
S	DNA synthesis phase of the cell cycle
SAHF	Senescence associated heterchromatin formation
SA β-Gal	Senescence associated β-galactosidase
SAPK	Signal activated protein kinase
SEPP1	Selonoprotein P
SOCS4	Suppressor of cytokine signaling 4
SUC	Succinate
TCA	Tricarboxylic acid cycle
TOF	Time of flight

WI-38	Human fetal lung fibroblasts
X-Gal	5-bromo-4-chloro-3-indolyl-β-galactopyranoside

Table of Contents

List of Figures

List of Tables

Chapter 1

Background and Research Objectives

Prolonged serial passaging of primary human fibroblasts in culture leads to the formation of non-proliferating senescent cells. Such cells exhibit features similar to cellular aging, including an increase in oxidative damage (OD), activation of pro-apoptotic and senescent signaling pathways, a decrease in proliferation, and an increase in the number of senescent cells (Fig. 1.1) [1-7]. Due to these similarities, serial passaging of primary fibroblasts is considered by some to be one of the better approaches to determining the underlying mechanisms of human cellular aging. However, whether or not tissue culture-induced senescence accurately reflects *in vivo* processes is presently controversial [3, 8-10].

'Replicative senescence' is a term used to describe senescence associated with cells grown in culture, while 'cellular senescence' is used to describe senescence associated with cells *in vivo* [3, 11-13]. Fibroblasts grown in culture have varying replicative life spans that show no correlation to the age of the donor [14-16], suggesting the senescence process in culture is different than *in vivo*. Also, the lifespan of cells grown in culture are dependent upon oxygen levels [5, 17]. Human cells *in vivo* are exposed to physiological oxygen levels between 2 and 8 percent, whereas standard culturing conditions are 20% O_2. The replicative lifespan of primary fibroblasts cultured at 3% O_2 is double that of the same cells grown at 20 % O_2 [5, 10, 17-22], suggesting that pathways to senescence are very much dependent on oxygen levels and hence oxidative damage (OD). As the fundamental biological processes involved in the OD response are likely to be very similar *in vivo* and *in vitro*, one can assume that there are at least some common senescent pathways between cells *in vivo* and *in vitro*. Therefore, replicative senescence can be considered the cellular response to environmental stresses over time. Inasmuch, prolonged serial passaging provides a methodology by which one can investigate the underlying causes of human cellular aging with respect to constant environmental stress [23, 24].

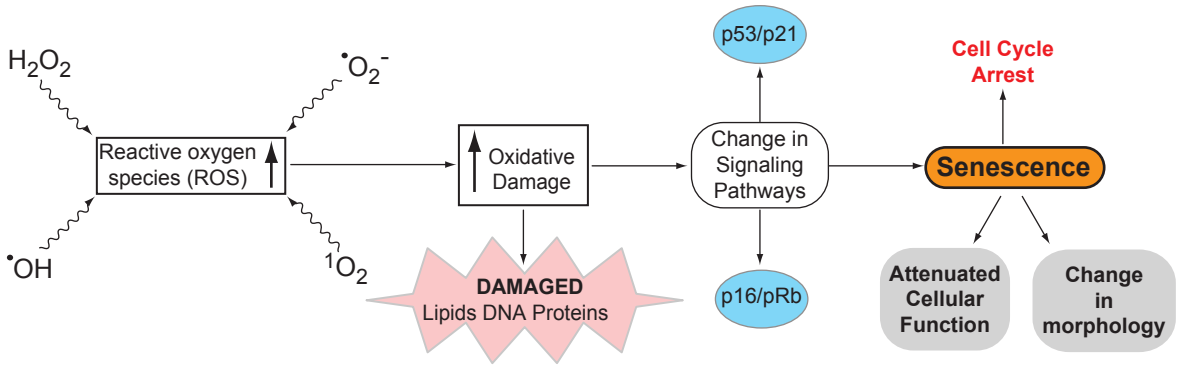

Fig. 1.1. *Overview of the major events leading to the senescent phenotype*.

Oxidative Stress. The relationship between oxidative stress and aging was first proposed by Harman in his Free Radical/Oxidative Stress Theory of Aging [25]. In the initial definition, oxidative stress referred to cellular damage caused by the sustained generation and accumulation of reactive oxygen species (ROS) during normal aerobic metabolism. Many of these species are produced as a byproduct of oxidative phosphorylation (ATP generation), essentially via the inefficient transport of electrons across the mitochondrial membrane. Types of ROS produced during this process include superoxide and hydroxyl free radicals as well as non-radicals such as hydrogen peroxide and singlet oxygen (Fig. 1.1) [26, 27]. While the generation of ROS has generally been considered detrimental to normal cell growth, there is a body of literature that suggests that ROS are an integral component of cellular signaling and essential to normal growth and metabolism [28-36]. This explains why cells exhibit a low level of oxidative stress; such levels are required for maintaining a balance between ROS production and scavenging [37, 38]. Unfortunately, ROS production can also lead to damaged proteins, membrane lipids, and DNA (both mitochondrial and nuclear). If this oxidative damage accumulates over time, normal cellular function can be attenuated. This can lead to abnormal cell behaviors such as cancer, or naturally preventative pathways such as apoptosis or senescence. Which event occurs and the timing of the event is ultimately controlled by activating or deactivating the appropriate cell signaling pathway (Fig. 1.2) [5, 33, 37, 39-41].

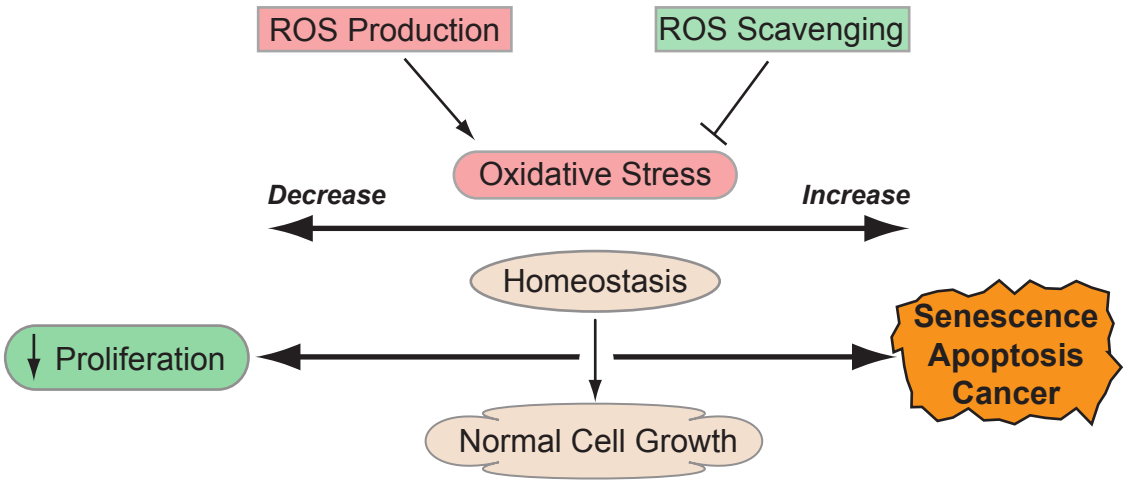

Fig. 1.2. *Diagram depicting the role of oxidative stress within the cell and how levels of oxidative stress leads to particular cell fates.*

Senescent Cell Signaling. The p16/pRb and p53/p21 pathways have been identified as the two major signaling pathways involved in replicative senescence (Fig. 1.3) [4, 5, 7, 42]. Both are activated with increased population doublings (PDs) in response to the accumulation of OD, mainly in the form of DNA damage. PDs are used as benchmarks to estimate the age of cells in culture. Other triggers include telomere shortening, chromatin perturbation, and oncogenes [19, 43-51]. The p16/pRb and p53/p21 pathways are known as tumor suppressor pathways because they can cause cell cycle arrest or apoptosis in response to pro-oncogenic stimuli [5-7, 52]. Therefore, they can be considered the first line of defense against cancer by protecting against mutations that could lead to uncontrolled cell growth. The senescent phenotype of irreversible proliferative arrest can be established and maintained by either of these pathways independently or by both cooperatively. This senescent cell cycle arrest is thought to predominantly occur during the G1 phase of the cell cycle (Fig. 1.4) [6, 7]. This arrest is distinct from the G0 phase known as quiescence as it is not reversible [53].

The p53/p21 pathway begins with the transcription factor p53. Under normal growth conditions, this protein exhibits a short half-life. Activation and stabilization occur through post-translational modifications such as phosphorylation [42]. This allows p53 to activate the transcription factor, p21, which is a cyclin dependent kinase (CDK) inhibitor that mediates cell

cycle arrest in the G1 phase by inhibiting the CyclinE-CDK2 complex (Fig. 1.4.) [6, 7, 53, 54]. CDKs are essential to cell division by forming activated complexes with cyclins, a family of proteins involved in cell cycle control, that enable cell cycle progression [53, 54]. p21 is also capable of mediating cell cycle arrest via the p16/pRb pathway by inhibiting the CyclinD-CDK4/6 complexes (Fig. 1.4) [4, 42].

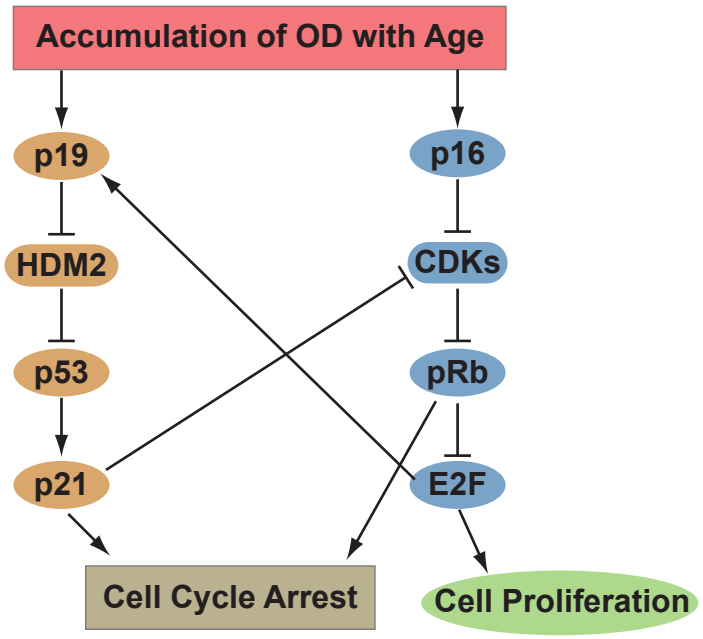

Fig. 1.3. *The major cell signaling pathways, p16/pRb and p19/p53, that are presently considered responsible for senescence.* Adapted from Campisi *et al.*, 2005 [14].

The p16/pRb pathway starts with p16; a CDK stoichiometric inhibitor that inactivates CyclinD-CDK4/6 complexes (Fig. 1.4) [6, 42]. CyclinD-CDK4/6 and CyclinE-CDK2 complexes mediate cell cycle progression by phosphorylating the retinoblastoma tumor suppressor protein (Rb). Rb in its unphosphorylated form associates with several transcription factors including E2F, effectively inactivating them. When Rb is phosphorylated, it releases E2F, permitting the expression of E2F-regluated genes that are responsible for DNA synthesis and cell cycle progression (Fig. 1.4). One of the genes is p19, a protein that suppresses the activity of human double minute (HDM2) oncogene, an E3 ubiquitin-protein ligase responsible for the degradation of p53. Increasing p53 half-life promotes cell cycle arrest via the p53/p21 pathway [4, 11, 42, 53,

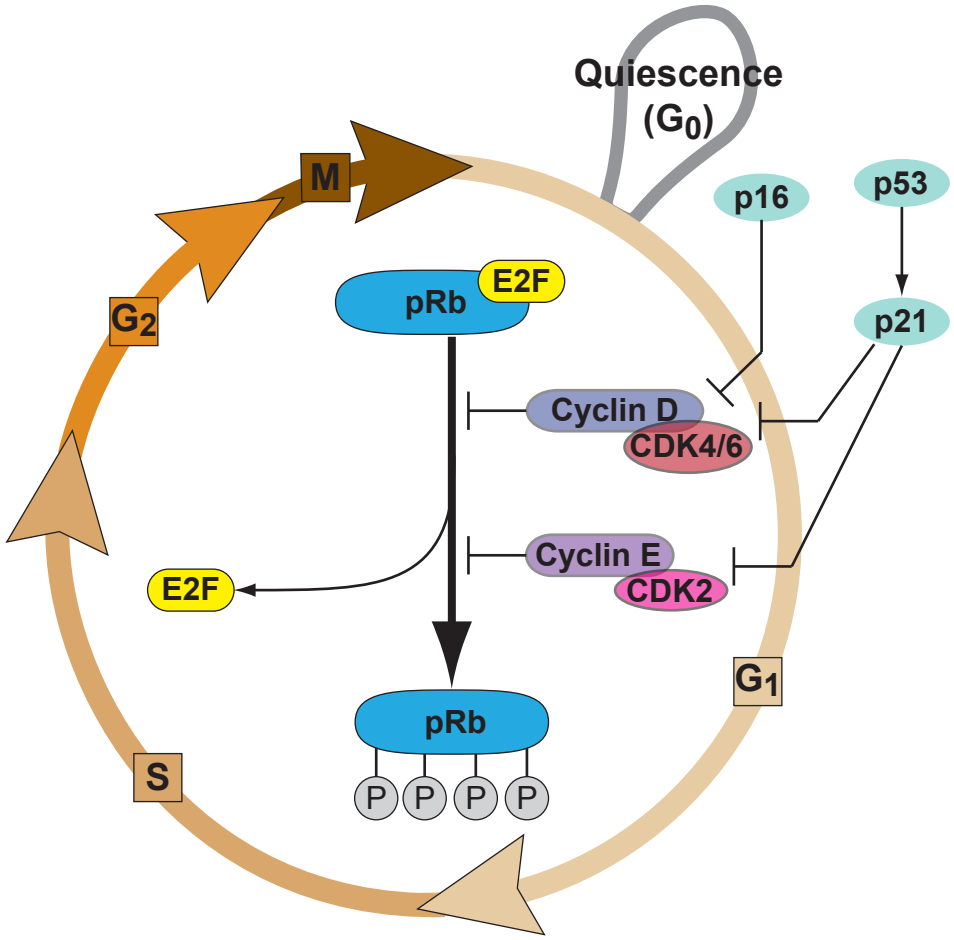

Fig. 1.4. *Diagram of the cell cycle and its regulation by the p16/pRb and p53/p21 cell signaling pathways*. Adapted from Coller *et al*., 2007 [53].

55]. These cooperative tumor suppressor pathways are presently thought to be the major cellular stress responses that control the cell cycle.

Antagonistic Pleiotropy. A pleiotropic gene is one that controls, or is involved in, several different processes or phenotypes. An antagonistic pleotropic gene is one where the different process or phenotypes under control are both advantageous and disadvantageous. In aging, one theory states that mechanisms that provide survival in younger organisms are selected through evolutionary pressure even if they are deleterious in older organisms [56]. This "escape from evolutionary pressure" is due to the declining force of natural selection with age accompanied

by a decrease in fertility [57]. This implies that senescent and apoptotic signaling pathways are beneficial to younger organisms because they prevent cancer by eliminating or arresting growth of precancerous cells. However, these pathways also drive aging phenotypes in older organisms via the decline of regenerative capacity as well as the loss of cellular function in response to the senescent phenotype [1, 4, 55, 58]. This domino effect stems from mitochondrial oxidative phosphorylation, a major source of ROS [26, 59]. It has been propagated by evolutionary pressure to intimately tie energy production with cancer and senescence. Electron transfer in oxidative phosphorylation used to generate ATP is leaky and can lead to free radicals escaping from the membrane. These free radicals are maintained in a delicate balance by scavenging mechanisms in order to promote normal physiological function [26, 33-35, 59]. Over time, free radical production leads to OD, either through excessive production or attenuation in scavenging, altering cellular signaling through two major pathways, p16/pRb and p53/p21 [4, 7, 42]. Changes in these pathways that act as a defense response mechanism against cancer lead to the senescent phenotype [7, 42, 55]. Thus, the mitochondria are both the primary source of high-energy compounds such as ATP as well as an important target and source of ROS [26, 60, 61]. Accordingly, mitochondria have been implicated as key players in the aging process [62-66].

Senescent Cell Metabolism. The tricarboxylic acid (TCA) cycle provides the majority of reducing power in the form of NADH to drive oxidative phosphorylation and hence ATP production. The TCA cycle is composed of a diverse set of enzymes and metabolites that act as a hub for many anabolic and catabolic pathways such as those for lipid and amino acid synthesis and degradation. For example, pyruvate, oxaloacetate, fumarate, and α-ketoglutarate are all involved in amino acid metabolism. The TCA cycle's amphibolic nature allows it to occupy a central position in intracellular metabolism. Mitochondrial metabolism is affected by age-associated dysfunction via OD leading to both metabolite and metabolic enzyme changes. This alters the energy status of the cell, modulating all downstream energy-requiring processes.

Several studies have aimed at characterizing changes in energy metabolism associated with aging and senescence. These studies have employed a variety of detection methods as well as types

of biological samples. Studies that have analyzed actual metabolite levels within cells were limited in focus (1 or 2 metabolites), derived from whole tissue (murine cerebella/kidneys) or primary cells (human fibroblasts), and determined enzymatically or by UV absorbency [67-70]. Studies that have focused on profiling the entire metabolome have utilized blood or urine from individuals (typically human), and metabolite levels were determined by mass spectrometry (GC/LC-MS) [71-73]. Reported changes in metabolite levels associated with aging and senescence include several metabolites such as ATP, AMP, citrate, isocitrate, malate, succinate, α-ketoglutarate, and lactate (Fig. 1.5) [60, 67-70, 74].

These metabolite changes are a result of oxidatively damaged metabolic components that typically result in increases in associated enzyme levels and decreases in their respective activities. For example, some TCA enzymes such as lactate dehydrogenase, pyruvate dehydrogenase, aconitase, malate dehydrogenase, fumarase, isocitrate dehydrogenase, and α-ketoglutarate dehydrogenase are especially sensitive to OD and as a result show a decline in activity with age in rat and murine models (Fig 1.5) [68, 75-80]. Other important metabolic enzymes that are also sensitive to OD and show decreases in activity with age include NAD/H dehydrogenase, NAD oxidase, and ATPase [80-81]. Metabolic enzymes that exhibit an increase in protein level with age and may be an indirect result of OD by attenuating protein turnover machinery include AMP kinase, glucose 6-phosphate dehydrogenase, phosphoglycerate kinase, phosphoglycerate mutase, and pyruvate kinase (Fig. 1.5) [60, 67-69, 75, 82]. Changes like these in energy metabolism have been implicated in modifying cell signaling pathways and driving the senescent phenotype instead of just being a consequence [67, 83]. Therefore, it is important to employ a universal detection method that is able to target metabolite changes in primary carbon metabolism in order to provide results that can be compared and related to changes seen in both the transcriptome and proteome.

Towards a More Complete Understanding of Senescence. Oxidative stress has been implicated in cellular senescence as well as in age-related diseases [84-93]. At the heart of this paradigm are the mitochondria—organelles providing the energy required to drive cellular processes, as well the primary source of ROS and the primary target for OD. Considering the main

function of mitochondria, relatively few studies have investigated the effects of aging and

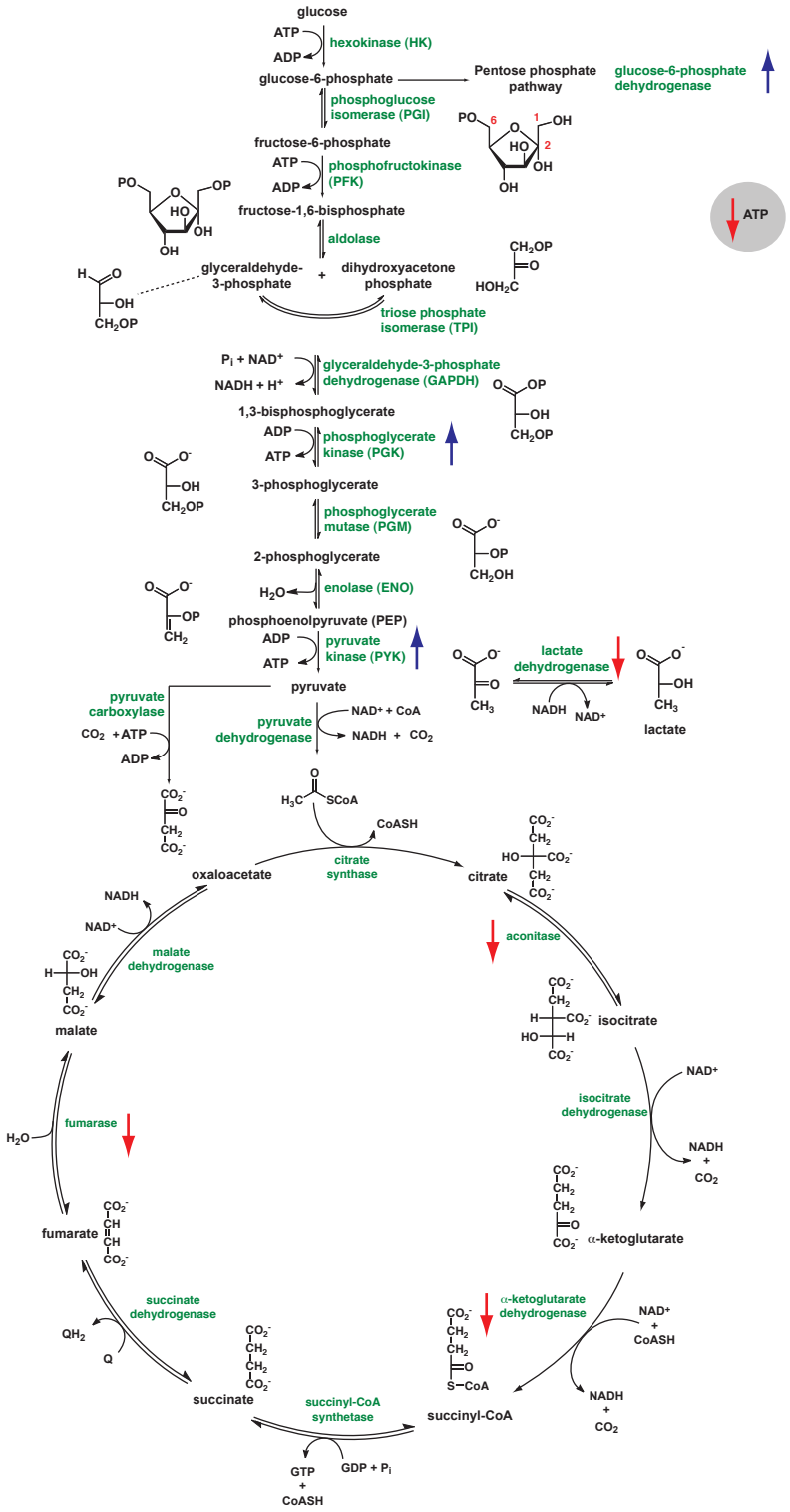

Fig. 1.5. *Central carbon metabolism and changes in metabolite and metabolic enzyme levels as reported in the literature.*

senescence on the metabolic profile of primary cells [60, 67-69, 72-74]. All studies published to date are limited in scope (1 or 2 metabolites), and no studies have targeted TCA metabolites. Since metabolite levels have been implicated in altering cellular signaling, the best example being lifespan extension through caloric restriction [67, 69, 83, 94], elucidating these metabolic changes may help more clearly define the relationships between metabolites, mitochondria and cell signaling as they pertain to replicative senescence [95-98].

In the studies presented here, human fibroblasts were grown in atmospheres of 3 and 20% O_2 to assess changes in the transcriptome, protein phosphorylation (by protein arrays), and metabolic profiling (by mass spectrometry). In addition, confocal microscopy was used to assess changes in mitochondrial volume, morphology, and orientation within the cell during the serial passaging process. The specific aims that were addressed during the course of this work are shown below:

Specific Aims

Specific Aim 1. *Assess global changes in protein and gene expression of human fibroblasts with age when cultured under 3 and 20 percent oxygen.*

Protein kinase and transcriptional microarrays were performed on IMR90 cells grown under 3 and 20% O_2. These experiments provided new insights into the cellular signaling pathways involved in senescence. Protein expression was measured using young and senescent cells under 20% O_2. Transcriptional profiling data were obtained under both 3 and 20% O_2.

Specific Aim 2. *Determine the morphological characteristics of primary human fibroblast mitochondria when serially passaged under 3 and 20% O_2 through senescence.*

Mitochondria were evaluated for changes in total volume, 3D morphology, and membrane potential using young, middle-aged, and senescent cells at 3 and 20% O_2. Visualizing change in the mitochondria not only provided a physiological perspective, but also permitted a quantitative measure of the volume of the cell allocated to this organelle. This measurement allowed an estimate

of metabolite concentrations (Aim 3, below) relative to mitochondrial volume.

Specific Aim 3. *Test the hypothesis that the metabolite profile of human fibroblasts changes with age.*

The testing of this hypothesis required the development of a reliable, reproducible, and robust method to assay metabolites within cultured primary human fibroblasts. This method focused specifically on the metabolites of central carbon metabolism. Method development proceeded with the use of faster growing MCF7 cells and was subsequently applied to serially passaged primary fibroblasts cultured under 3 and 20 percent oxygen.

The results obtained permitted the metabolism-based view of senescence, linking known senescent signaling pathways with primary metabolism, the energy status of the cell, and mitochondrial physiology.

References

1. Campisi, J., *Fragile fugue: p53 in aging, cancer and IGF signaling.* Nat Med, 2004. **10**(3): p. 231-2.
2. Campisi, J., *Senescent cells, tumor suppression, and organismal aging: good citizens, bad neighbors.* Cell, 2005. **120**(4): p. 513-22.
3. Cristofalo, V.J., A. Lorenzini, R.G. Allen, C. Torres, and M. Tresini, *Replicative senescence: a critical review.* Mech Ageing Dev, 2004. **125**(10-11): p. 827-48.
4. Campisi, J. and F. d'Adda di Fagagna, *Cellular senescence: when bad things happen to good cells.* Nat Rev Mol Cell Biol, 2007. **8**(9): p. 729-40.
5. Muller, M., *Cellular senescence: molecular mechanisms, in vivo significance, and redox considerations.* Antioxid Redox Signal, 2009. **11**(1): p. 59-98.
6. Ohtani, N., D.J. Mann, and E. Hara, *Cellular senescence: its role in tumor suppression and aging.* Cancer Sci, 2009. **100**(5): p. 792-7.
7. Ren, J.L., J.S. Pan, Y.P. Lu, P. Sun, and J. Han, *Inflammatory signaling and cellular senescence.* Cell Signal, 2009. **21**(3): p. 378-83.
8. Dimri, G.P., X. Lee, G. Basile, M. Acosta, G. Scott, C. Roskelley, E.E. Medrano, M. Linskens, I. Rubelj, O. Pereira-Smith, and et al., *A biomarker that identifies senescent human cells in culture and in aging skin in vivo.* Proc Natl Acad Sci U S A, 1995. **92**(20): p. 9363-7.
9. Yegorov, Y.E. and A.V. Zelenin, *Duration of senescent cell survival in vitro as a characteristic of organism longevity, an additional to the proliferative potential of fibroblasts.* FEBS Lett, 2003. **541**(1-3): p. 6-10.
10. Balin, A.K., A.J. Fisher, M. Anzelone, I. Leong, and R.G. Allen, *Effects of establishing cell cultures and cell culture conditions on the proliferative life span of human fibroblasts isolated from different tissues and donors of different ages.* Exp Cell Res, 2002. **274**(2): p. 275-87.
11. Patil, C.K., I.S. Mian, and J. Campisi, *The thorny path linking cellular senescence to organismal aging.* Mech Ageing Dev, 2005. **126**(10): p. 1040-5.
12. Cristofalo, V.J., J. Beck, and R.G. Allen, *Cell senescence: an evaluation of replicative senescence in culture as a model for cell aging in situ.* J Gerontol A Biol Sci Med Sci, 2003. **58**(9): p. B776-9; discussion 779-81.
13. Campisi, J., *Cellular senescence as a tumor-suppressor mechanism.* Trends Cell Biol, 2001. **11**(11): p. S27-31.
14. Cristofalo, V.J., R.G. Allen, R.J. Pignolo, B.G. Martin, and J.C. Beck, *Relationship between donor age and the replicative lifespan of human cells in culture: a reevaluation.* Proc Natl Acad Sci U S A, 1998. **95**(18): p. 10614-9.
15. Goldstein, S., E.J. Moerman, J.S. Soeldner, R.E. Gleason, and D.M. Barnett, *Chronologic and physiologic age affect replicative life-span of fibroblasts from diabetic, prediabetic, and normal donors.* Science, 1978. **199**(4330): p. 781-2.
16. Smith, J.R., S. Venable, T.W. Roberts, E.J. Metter, R. Monticone, and E.L. Schneider, *Relationship between in vivo age and in vitro aging: assessment of 669 cell cultures derived from members of the Baltimore Longitudinal Study of Aging.* J Gerontol A Biol Sci Med Sci, 2002. **57**(6): p. B239-46.
17. Balin, A.K., D.B. Goodman, H. Rasmussen, and V.J. Cristofalo, *The effect of oxygen and vitamin E on the lifespan of human diploid cells in vitro.* J Cell Biol, 1977. **74**(1): p. 58-67.
18. Vaupel, P., P. Okunieff, and L.J. Neuringer, *Blood flow, tissue oxygenation, pH distribution, and energy metabolism of murine mammary adenocarcinomas during growth.* Adv Exp Med Biol, 1989. **248**: p. 835-45.
19. Parrinello, S., E. Samper, A. Krtolica, J. Goldstein, S. Melov, and J. Campisi, *Oxygen sensitivity severely limits the replicative lifespan of murine fibroblasts.* Nat Cell Biol, 2003. **5**(8): p. 741-7.

20. Balin, A.K. and L. Pratt, *Oxygen modulates the growth of skin fibroblasts.* In Vitro Cell Dev Biol Anim, 2002. **38**(5): p. 305-10.
21. Balin, A.K., L. Pratt, and R.G. Allen, *Effects of ambient oxygen concentration on the growth and antioxidant defenses of of human cell cultures established from fetal and postnatal skin.* Free Radic Biol Med, 2002. **32**(3): p. 257-67.
22. Chen, Q., A. Fischer, J.D. Reagan, L.J. Yan, and B.N. Ames, *Oxidative DNA damage and senescence of human diploid fibroblast cells.* Proc Natl Acad Sci U S A, 1995. **92**(10): p. 4337-41.
23. Fehrer, C., R. Brunauer, G. Laschober, H. Unterluggauer, S. Reitinger, F. Kloss, C. Gully, R. Gassner, and G. Lepperdinger, *Reduced oxygen tension attenuates differentiation capacity of human mesenchymal stem cells and prolongs their lifespan.* Aging Cell, 2007. **6**(6): p. 745-57.
24. Herbig, U., M. Ferreira, L. Condel, D. Carey, and J.M. Sedivy, *Cellular senescence in aging primates.* Science, 2006. **311**(5765): p. 1257.
25. Harman, D., *Aging: a theory based on free radical and radiation chemistry.* J Gerontol, 1956. **11**(3): p. 298-300.
26. Andreyev, A.Y., Y.E. Kushnareva, and A.A. Starkov, *Mitochondrial metabolism of reactive oxygen species.* Biochemistry (Mosc), 2005. **70**(2): p. 200-14.
27. Stadtman, E.R., *Role of oxidant species in aging.* Curr Med Chem, 2004. **11**(9): p. 1105-12.
28. Genestra, M., *Oxyl radicals, redox-sensitive signalling cascades and antioxidants.* Cell Signal, 2007. **19**(9): p. 1807-19.
29. Nishikawa, T., D. Edelstein, X.L. Du, S. Yamagishi, T. Matsumura, Y. Kaneda, M.A. Yorek, D. Beebe, P.J. Oates, H.P. Hammes, I. Giardino, and M. Brownlee, *Normalizing mitochondrial superoxide production blocks three pathways of hyperglycaemic damage.* Nature, 2000. **404**(6779): p. 787-90.
30. Finkel, T., *Oxygen radicals and signaling.* Curr Opin Cell Biol, 1998. **10**(2): p. 248-53.
31. Nemoto, S., K. Takeda, Z.X. Yu, V.J. Ferrans, and T. Finkel, *Role for mitochondrial oxidants as regulators of cellular metabolism.* Mol Cell Biol, 2000. **20**(19): p. 7311-8.
32. Droge, W., *Free radicals in the physiological control of cell function.* Physiol Rev, 2002. **82**(1): p. 47-95.
33. Valko, M., D. Leibfritz, J. Moncol, M.T. Cronin, M. Mazur, and J. Telser, *Free radicals and antioxidants in normal physiological functions and human disease.* Int J Biochem Cell Biol, 2007. **39**(1): p. 44-84.
34. Camello-Almaraz, M.C., M.J. Pozo, M.P. Murphy, and P.J. Camello, *Mitochondrial production of oxidants is necessary for physiological calcium oscillations.* J Cell Physiol, 2006. **206**(2): p. 487-94.
35. Linnane, A.W., M. Kios, and L. Vitetta, *The essential requirement for superoxide radical and nitric oxide formation for normal physiological function and healthy aging.* Mitochondrion, 2007. **7**(1-2): p. 1-5.
36. Bashan, N., J. Kovsan, I. Kachko, H. Ovadia, and A. Rudich, *Positive and negative regulation of insulin signaling by reactive oxygen and nitrogen species.* Physiol Rev, 2009. **89**(1): p. 27-71.
37. Finkel, T. and N.J. Holbrook, *Oxidants, oxidative stress and the biology of ageing.* Nature, 2000. **408**(6809): p. 239-47.
38. Magder, S., *Reactive oxygen species: toxic molecules or spark of life?* Crit Care, 2006. **10**(1): p. 208.
39. Sohal, R.S., *Oxidative stress hypothesis of aging.* Free Radic Biol Med, 2002. **33**(5): p. 573-4.
40. Bokov, A., A. Chaudhuri, and A. Richardson, *The role of oxidative damage and stress in aging.* Mech Ageing Dev, 2004. **125**(10-11): p. 811-26.
41. Busuttil, R.A., M. Rubio, M.E. Dolle, J. Campisi, and J. Vijg, *Oxygen accelerates the accumulation of mutations during the senescence and immortalization of murine cells in culture.* Aging Cell, 2003. **2**(6): p. 287-94.

42. Bringold, F. and M. Serrano, *Tumor suppressors and oncogenes in cellular senescence.* Exp Gerontol, 2000. **35**(3): p. 317-29.
43. Zhu, J., D. Woods, M. McMahon, and J.M. Bishop, *Senescence of human fibroblasts induced by oncogenic Raf.* Genes Dev, 1998. **12**(19): p. 2997-3007.
44. Ogryzko, V.V., T.H. Hirai, V.R. Russanova, D.A. Barbie, and B.H. Howard, *Human fibroblast commitment to a senescence-like state in response to histone deacetylase inhibitors is cell cycle dependent.* Mol Cell Biol, 1996. **16**(9): p. 5210-8.
45. Di Leonardo, A., S.P. Linke, K. Clarkin, and G.M. Wahl, *DNA damage triggers a prolonged p53-dependent G1 arrest and long-term induction of Cip1 in normal human fibroblasts.* Genes Dev, 1994. **8**(21): p. 2540-51.
46. d'Adda di Fagagna, F., P.M. Reaper, L. Clay-Farrace, H. Fiegler, P. Carr, T. Von Zglinicki, G. Saretzki, N.P. Carter, and S.P. Jackson, *A DNA damage checkpoint response in telomere-initiated senescence.* Nature, 2003. **426**(6963): p. 194-8.
47. Hemann, M.T., M.A. Strong, L.Y. Hao, and C.W. Greider, *The shortest telomere, not average telomere length, is critical for cell viability and chromosome stability.* Cell, 2001. **107**(1): p. 67-77.
48. Herbig, U., W.A. Jobling, B.P. Chen, D.J. Chen, and J.M. Sedivy, *Telomere shortening triggers senescence of human cells through a pathway involving ATM, p53, and p21(CIP1), but not p16(INK4a).* Mol Cell, 2004. **14**(4): p. 501-13.
49. Martens, U.M., E.A. Chavez, S.S. Poon, C. Schmoor, and P.M. Lansdorp, *Accumulation of short telomeres in human fibroblasts prior to replicative senescence.* Exp Cell Res, 2000. **256**(1): p. 291-9.
50. Munro, J., N.I. Barr, H. Ireland, V. Morrison, and E.K. Parkinson, *Histone deacetylase inhibitors induce a senescence-like state in human cells by a p16-dependent mechanism that is independent of a mitotic clock.* Exp Cell Res, 2004. **295**(2): p. 525-38.
51. Lin, A.W., M. Barradas, J.C. Stone, L. van Aelst, M. Serrano, and S.W. Lowe, *Premature senescence involving p53 and p16 is activated in response to constitutive MEK/MAPK mitogenic signaling.* Genes Dev, 1998. **12**(19): p. 3008-19.
52. Ohtani, N., K. Yamakoshi, A. Takahashi, and E. Hara, *The p16INK4a-RB pathway: molecular link between cellular senescence and tumor suppression.* J Med Invest, 2004. **51**(3-4): p. 146-53.
53. Coller, H.A., *What's taking so long? S-phase entry from quiescence versus proliferation.* Nat Rev Mol Cell Biol, 2007. **8**(8): p. 667-70.
54. Harbour, J.W., R.X. Luo, A. Dei Santi, A.A. Postigo, and D.C. Dean, *Cdk phosphorylation triggers sequential intramolecular interactions that progressively block Rb functions as cells move through G1.* Cell, 1999. **98**(6): p. 859-69.
55. Campisi, J., *Aging, tumor suppression and cancer: high wire-act!* Mech Ageing Dev, 2005. **126**(1): p. 51-8.
56. Williams, G.C., *Pleiotropy, natural selection, and the evolution of senescence.* Evolution, 1957. **11**: p. 398-411.
57. Kirkwood, T.B. and S.N. Austad, *Why do we age?* Nature, 2000. **408**(6809): p. 233-8.
58. Ungewitter, E. and H. Scrable, *Antagonistic pleiotropy and p53.* Mech Ageing Dev, 2009. **130**(1-2): p. 10-7.
59. Lambeth, J.D., *Nox enzymes, ROS, and chronic disease: an example of antagonistic pleiotropy.* Free Radic Biol Med, 2007. **43**(3): p. 332-47.
60. Mansouri, A., F.L. Muller, Y. Liu, R. Ng, J. Faulkner, M. Hamilton, A. Richardson, T.T. Huang, C.J. Epstein, and H. Van Remmen, *Alterations in mitochondrial function, hydrogen peroxide release and oxidative damage in mouse hind-limb skeletal muscle during aging.* Mech Ageing Dev, 2006. **127**(3): p. 298-306.

61. Sastre, J., F.V. Pallardo, J. Garcia de la Asuncion, and J. Vina, *Mitochondria, oxidative stress and aging.* Free Radic Res, 2000. **32**(3): p. 189-98.
62. Morrow, G. and R.M. Tanguay, *Mitochondria and ageing in Drosophila.* Biotechnol J, 2008. **3**(6): p. 728-39.
63. Reddy, P.H., *Mitochondrial medicine for aging and neurodegenerative diseases.* Neuromolecular Med, 2008. **10**(4): p. 291-315.
64. Lopez-Lluch, G., P.M. Irusta, P. Navas, and R. de Cabo, *Mitochondrial biogenesis and healthy aging.* Exp Gerontol, 2008. **43**(9): p. 813-9.
65. Vila, M., D. Ramonet, and C. Perier, *Mitochondrial alterations in Parkinson's disease: new clues.* J Neurochem, 2008. **107**(2): p. 317-28.
66. Terzioglu, M. and N.G. Larsson, *Mitochondrial dysfunction in mammalian ageing.* Novartis Found Symp, 2007. **287**: p. 197-208; discussion 208-13.
67. Wang, W., X. Yang, I. Lopez de Silanes, D. Carling, and M. Gorospe, *Increased AMP:ATP ratio and AMP-activated protein kinase activity during cellular senescence linked to reduced HuR function.* J Biol Chem, 2003. **278**(29): p. 27016-23.
68. Yarian, C.S., D. Toroser, and R.S. Sohal, *Aconitase is the main functional target of aging in the citric acid cycle of kidney mitochondria from mice.* Mech Ageing Dev, 2006. **127**(1): p. 79-84.
69. Zwerschke, W., S. Mazurek, P. Stockl, E. Hutter, E. Eigenbrodt, and P. Jansen-Durr, *Metabolic analysis of senescent human fibroblasts reveals a role for AMP in cellular senescence.* Biochem J, 2003. **376**(Pt 2): p. 403-11.
70. Sastre, J., F.V. Pallardo, R. Pla, A. Pellin, G. Juan, J.E. O'Connor, J.M. Estrela, J. Miquel, and J. Vina, *Aging of the liver: age-associated mitochondrial damage in intact hepatocytes.* Hepatology, 1996. **24**(5): p. 1199-205.
71. Lawton, K.A., A. Berger, M. Mitchell, K.E. Milgram, A.M. Evans, L. Guo, R.W. Hanson, S.C. Kalhan, J.A. Ryals, and M.V. Milburn, *Analysis of the adult human plasma metabolome.* Pharmacogenomics, 2008. **9**(4): p. 383-97.
72. Jiang, H., S. Zhang, Q. Guan, C. Chen, F. Gao, and Y. Zhang, *1H NMR investigations of inclusion complexes between beta-cyclodextrin and 1-hexadecanol.* Curr Drug Discov Technol, 2007. **4**(4): p. 295-7.
73. Gu, H., Z. Pan, B. Xi, B.E. Hainline, N. Shanaiah, V. Asiago, G.A. Gowda, and D. Raftery, *(1)H NMR metabolomics study of age profiling in children.* NMR Biomed, 2009.
74. Zhang, X., H. Liu, J. Wu, M. Liu, and Y. Wang, *Metabonomic alterations in hippocampus, temporal and prefrontal cortex with age in rats.* Neurochem Int, 2009. **54**(8): p. 481-7.
75. Yarian, C.S., I. Rebrin, and R.S. Sohal, *Aconitase and ATP synthase are targets of malondialdehyde modification and undergo an age-related decrease in activity in mouse heart mitochondria.* Biochem Biophys Res Commun, 2005. **330**(1): p. 151-6.
76. Kanski, J., A. Behring, J. Pelling, and C. Schoneich, *Proteomic identification of 3-nitrotyrosine-containing rat cardiac proteins: effects of biological aging.* Am J Physiol Heart Circ Physiol, 2005. **288**(1): p. H371-81.
77. Ji, L.L., D. Dillon, and E. Wu, *Myocardial aging: antioxidant enzyme systems and related biochemical properties.* Am J Physiol, 1991. **261**(2 Pt 2): p. R386-92.
78. Yan, L.J., R.L. Levine, and R.S. Sohal, *Oxidative damage during aging targets mitochondrial aconitase.* Proc Natl Acad Sci U S A, 1997. **94**(21): p. 11168-72.
79. Kil, I.S., J.H. Lee, A.H. Shin, and J.W. Park, *Glycation-induced inactivation of NADP(+)-dependent isocitrate dehydrogenase: implications for diabetes and aging.* Free Radic Biol Med, 2004. **37**(11): p. 1765-78.
80. Chakravarti, B., M. Oseguera, N. Dalal, P. Fathy, B. Mallik, A. Raval, and D.N. Chakravarti, *Proteomic profiling of aging in the mouse heart: Altered expression of mitochondrial proteins.* Arch Biochem Biophys, 2008. **474**(1): p. 22-31.

81. Takeyama, N., N. Matsuo, and T. Tanaka, *Oxidative damage to mitochondria is mediated by the Ca(2+)-dependent inner-membrane permeability transition.* Biochem J, 1993. **294 (Pt 3)**: p. 719-25.
82. Yarian, C.S. and R.S. Sohal, *In the aging housefly aconitase is the only citric acid cycle enzyme to decline significantly.* J Bioenerg Biomembr, 2005. **37**(2): p. 91-6.
83. Jazwinski, S.M., *Metabolic control and ageing.* Trends Genet, 2000. **16**(11): p. 506-11.
84. Pratico, D., *Evidence of oxidative stress in Alzheimer's disease brain and antioxidant therapy: lights and shadows.* Ann N Y Acad Sci, 2008. **1147**: p. 70-8.
85. Beal, M.F., *Energy, oxidative damage, and Alzheimer's disease: clues to the underlying puzzle.* Neurobiol Aging, 1994. **15 Suppl 2**: p. S171-4.
86. Browne, S.E. and M.F. Beal, *Oxidative damage and mitochondrial dysfunction in neurodegenerative diseases.* Biochem Soc Trans, 1994. **22**(4): p. 1002-6.
87. Bubber, P., V. Haroutunian, G. Fisch, J.P. Blass, and G.E. Gibson, *Mitochondrial abnormalities in Alzheimer brain: mechanistic implications.* Ann Neurol, 2005. **57**(5): p. 695-703.
88. Gibson, G.E., A.E. Kingsbury, H. Xu, J.G. Lindsay, S. Daniel, O.J. Foster, A.J. Lees, and J.P. Blass, *Deficits in a tricarboxylic acid cycle enzyme in brains from patients with Parkinson's disease.* Neurochem Int, 2003. **43**(2): p. 129-35.
89. Koutsilieri, E., C. Scheller, E. Grunblatt, K. Nara, J. Li, and P. Riederer, *Free radicals in Parkinson's disease.* J Neurol, 2002. **249 Suppl 2**: p. II1-5.
90. Perry, G., R.J. Castellani, K. Hirai, and M.A. Smith, *Reactive Oxygen Species Mediate Cellular Damage in Alzheimer Disease.* J Alzheimers Dis, 1998. **1**(1): p. 45-55.
91. Mecocci, P., U. MacGarvey, and M.F. Beal, *Oxidative damage to mitochondrial DNA is increased in Alzheimer's disease.* Ann Neurol, 1994. **36**(5): p. 747-51.
92. Pallas, M., A. Camins, M.A. Smith, G. Perry, H.G. Lee, and G. Casadesus, *From aging to Alzheimer's disease: unveiling "the switch" with the senescence-accelerated mouse model (SAMP8).* J Alzheimers Dis, 2008. **15**(4): p. 615-24.
93. Ding, X., M. Patel, and C.C. Chan, *Molecular pathology of age-related macular degeneration.* Prog Retin Eye Res, 2009. **28**(1): p. 1-18.
94. Lane, M.A., A. Black, A. Handy, E.M. Tilmont, D.K. Ingram, and G.S. Roth, *Caloric restriction in primates.* Ann N Y Acad Sci, 2001. **928**: p. 287-95.
95. Schwarzer, R., S. Dames, D. Tondera, A. Klippel, and J. Kaufmann, *TRB3 is a PI 3-kinase dependent indicator for nutrient starvation.* Cell Signal, 2006. **18**(6): p. 899-909.
96. Jones, R.G., D.R. Plas, S. Kubek, M. Buzzai, J. Mu, Y. Xu, M.J. Birnbaum, and C.B. Thompson, *AMP-activated protein kinase induces a p53-dependent metabolic checkpoint.* Mol Cell, 2005. **18**(3): p. 283-93.
97. Wilson, W.A. and P.J. Roach, *Nutrient-regulated protein kinases in budding yeast.* Cell, 2002. **111**(2): p. 155-8.
98. Dechant, R. and M. Peter, *Nutrient signals driving cell growth.* Curr Opin Cell Biol, 2008. **20**(6): p. 678-87.

Chapter 2

Method Development for Targeted Metabolite Analyses of Primary Fibroblasts by LC-tandem Mass Spectrometry

Abstract

Due to the complex mixture of metabolites in eukaryotic cells and low cell population densities of primary fibroblast monolayers, a tailored approach must be designed for proper metabolic analysis of selected pathways. Since there are no data available at this time on the best available procedure for metabolite extraction and analysis in primary fibroblasts, extensive method development was performed in order to target the compounds of interest and provide quantifiable samples. The purpose of the work described here was to develop specific metabolomic methodologies that could be directly applied to primary adherent fibroblasts at low cell population densities. The LC-MS/MS platform was chosen as the most appropriate mass spectrometry method due to its high sensitivity and specificity for the small polar metabolites involved in glycolysis and the TCA cycle. Various LC-MS/MS and extraction methods were compared, including new methods developed independently during the course of the project. An electrospray LC-MS/MS method that utilized an extended HILIC gradient and a trypsinization method that incorporated a phosphate wash step proved to be the most suitable method for the isolation and detection of the aforementioned metabolites.

Introduction

Targeted metabolomics aims to quantify a set of pre-defined molecules within the cell or organism that belong to a particular group of compounds or are a part of a particular pathway of interest. By targeting a specific class of compounds, one can improve the sensitivity of the instrument performing the analysis and increase the level of measurement accuracy by minimizing the total metabolite pool through selective sample preparation and instrument methodology steps [1]. The term "metabolomics" was coined in 1999 by Nicholson and describes the quantitation and detection of all the low molecular weight metabolites within a biological sample [2, 3]. Since it is assumed that there are roughly 3000 [1, 4] or more metabolites in eukaryotic cells, complete metabolic profiling is an extremely arduous task [1, 5]. However, combined with proteomic and genomic approaches, metabolomics can provide a more comprehensive picture of cellular processes with emphasis on the relationship of these processes with environmental conditions and energy status. In fact, the argument has been made that the metabolome is a more accurate snapshot of the cellular phenotype than either the transcriptome or proteome because metabolite changes can occur very rapidly in response to perturbations in the environment [1, 2, 6-11].

Techniques for profiling metabolites have evolved very rapidly over the past several years. The two main criteria in accurately profiling a particular group of metabolites are choosing an appropriate extraction protocol and instrument(s) for analysis. Several accepted and popular chromatographic separation and mass spectral (MS) methods are routinely being employed to characterize the metabolome. Separation methodologies include gas chromatography (GC), liquid chromatography (LC), and capillary electrophoresis (CE). GC is an older technology that has been used to identify hundreds of metabolites but requires that the metabolites be volatile either innately or through derivatization [8, 12-15]. LC is a newer technology that is not hampered by the necessity of molecules to be volatile and therefore can detect a broader range of metabolites [8]. CE is a very recently developed technology that provides excellent separation and sensitivity and can be used to detect low abundant metabolites [8, 16-19].

The low levels of metabolites encountered in life science research often require detectors

that are more sensitive than UV or refractive index (RI); mass spectrometers can often provide the detection limit required for this work. The sensitivity of mass spectrometers has increased greatly over the past decade, with three major technologies employed for detection and quantification: quadrupoles, ion traps, and time-of-flight (TOF) instruments. These detectors are generally arranged in tandem in order to permit a MS/MS configuration (ion fragmentation). In this format, ions can be filtered to allow only specific ions or mass ranges to pass through. These selected ions can then be fragmented to gain structural information. In quantitative work, ions and their key fragments can be detected and quantified by multiple reaction monitoring (MRM). While the triple quad and ion trap configurations offer excellent sensitivity, they lack the higher resolving power of the TOF/TOF configuration [1, 8, 20]. Nonetheless, the triple quadrupole and ion trap MS/MS configurations have been the standard workhorses for metabolite analysis, offering good sensitivity and reproducibility over a broad range of small molecules.

Multiple reaction monitoring provides increased sensitivity because it allows the targeting of specific parent ion masses rather than scanning an ion mass range. This permits MS parameter optimization for each metabolite of interest, thereby generating the best signal-to-noise ratio possible [20], increasing the limits of detection. Nuclear magnetic resonance (NMR) and matrix assisted laser desorption ionization (MALDI) TOF/TOF are also technologies that have been employed to detect metabolites. However, NMR suffers from a lack of sensitivity when compared to LC and GC methods and MALDI TOF/TOF, despite its high though-put and good sensitivity, suffers from background interference due to the matrix when detecting low molecular weight metabolites [8, 20-24].

Recent targeted metabolomics studies utilized different LC-MS/MS configurations for the detection of small polar metabolites (nucleotides, sugar phosphates, and carboxylic acids). These include ion-pairing reverse phase liquid chromatography (IPRP-LC MS/MS) and hydrophilic interaction liquid chromatography (HILIC-LC MS/MS) [4, 20, 25-32]. The IPRP-LC MS/MS configuration provides better sensitivity and separation than the HILIC-LC MS/MS but the use of alkylamine cationic-pairing reagents results in contamination of the mass spectrometers, leading to

loss of signal in the positive ion mode due to ion suppression [20, 33]. Return to normal signal-to-noise ratios in the positive ion mode requires rather vigorous cleaning regimes.

While there are a relatively limited number of LC-MS protocols available for metabolite work, many extraction methods have been developed for obtaining metabolites from a wide variety of biological materials. These methods vary based upon factors such as the metabolites of interest (solubility is specific solvents) and whether or not the biological sample will be tissue or cells grown in culture [7, 25, 27, 34, 35]. Metabolite extractions must accomplish two essential objectives. First, all metabolic and enzymatic activity must cease as soon as the extraction begins; this is often referred to as 'quenching'. Second, sample complexity must be reduced by selectively and quantitatively extracting the metabolites of interest as quickly as possible. Both objectives attempt to provide metabolites that are as close to the physiological concentrations as possible [7].

Our efforts with replicative senescence necessitate the quenching of adherent monolayer cells. This is typically performed using methanol, methanol/water, acetonitrile, methanol, or water at relatively low temperatures (around -20 °C for organic-based extraction solvents) [25, 27, 34]. Cells can be washed with phosphate buffered saline (PBS) prior to quenching in order to remove any metabolites present in the growth medium that may be the same or interfere with intracellular metabolites, or they can be quenched in the growth medium. The actual extraction of metabolites is often simply accomplished by the quenching solution itself followed by a centrifugation step. However other additional steps have been employed such as brief incubations and mixing periods at either cold or hot temperatures, the addition of chloroform to separate hydrophilic and hydrophobic compounds, or the removal of the quenching solution followed by the addition an extraction solution such as perchloric acid, potassium hydroxide, or 100% methanol. The analysis of small sample sizes often necessitates an additional drying (Speed vac) and resuspension step, usually in water or 50% methanol, in order to concentrate the extracted sample [25, 31, 34, 35]. While there are limited data available on primary fibroblast metabolites [30], there are no data available on the best available procedure for metabolite extraction and analysis [4].

Due to the lack of information available for human cell culture metabolite extractions,

different extraction methods such as flash freezing, trypsinization, scraping, media removal, and sample concentration (speed vac) were evaluated for their effects on the metabolic profile. An optimal extraction and LC-MS/MS method was obtained for adherent human cells in monolayer using human breast adenocarcinoma cells (MCF7). This protocol can be applied directly to Imr90 and BJ cells (Chapter 4).

Experimental Procedures

Cell Growth. MCF7 cells were obtained from ATCC. Cells were cultured as monolayers in Dubelco's modified medium (DMEM; ATCC) supplemented with 10% (v/v) fetal bovine serum (FBS; Atlanta Biologicals) and 5% CO_2 humidified air at 37 °C. Monolayers were grown to 80% confluency in T-150 flasks with the growth medium (25 ml) changed every 2-3 days. Cells were passaged by the removing the DMEM, washing with phosphate-buffered saline (PBS, 10 ml; Gibco), and treating the cultures with 2 ml of 1× trypsin-EDTA (Gibco) for 5 minutes in the incubator. The released cells were then resuspended in supplemented DMEM (8 ml) and 2 ml aliquots were removed for the seeding of new flasks for continued cell growth containing supplemented DMEM (30 ml). For the creation of frozen stocks, dimethyl sulfoxide (DMSO; Sigma) was added to the remaining cell suspension in order to provide a 10% DMSO and DMEM cocktail. Aliquots (2 ml each) were then frozen at -80 °C for 4 hrs using cryotube vials (Nunc). These vials were then transferred to a Biocane (Thermolyne) for storage in liquid nitrogen.

LC-MS/MS Method Development. A standard mixture of metabolites (Sigma-Aldrich), each at 1 μg/ml, was used for all assays: nicotinamide adenine dinucleotide phosphate (NADPH, NADP+), nicotinamide adenine dinucleotide (NADH, NAD+), adenosine triphosphate (ATP), adenosine diphosphate (ADP), adenosine monophosphate (AMP), fructose bisphosphate (FBP), glucose/fructose-6-phosphate (G/F6P), citrate (CIT), isocitrate (ISO), N-acetylglutamine (NAG), 3-phosphoglycerate (3PG), dihydroxyacetone phosphate (DHAP), glyceraldehyde-3-phosphate (G3P), phosphoenolpyruvate (PEP), α-ketoglutarate (αKG), malate (MAL), oxaloacetate (OAA), succinate (SUC), fumarate (FUM), lactate (LAC), pyruvate (PYR). Metabolite standards were

analyzed by nanospray/electospray (NSI/ESI)-LC-MS/MS on a 4000 QTrap (Applied Biosystems) interfaced with a TEMPO nanoLC system for NSI and an LC Packings Ultimate microLC system for ESI. Liquid chromatography (LC) separation for both ESI and NSI LC-MS/MS used an aminopropyl column (Luna, Phenomenex) at pH 9.4 in hydrophilic interaction chromatography (HILIC) mode. For ESI mode, the column came prepackaged from Phenomenex with dimensions of 50 mm x 2 mm. Packing material averaged 5 μm in diameter with a pore size of 100 angstroms. For NSI mode, a column was packed using the aminopropyl packing material and a PicoFrit (New Objective) giving a column with the dimensions of 15 cm x 100 μm. The LC solvents were Solvent A: 20 mM ammonium acetate + 20 mM ammonium hydroxide in 95:5 water:acetonitrile, pH 9.45; Solvent B: acetonitrile. All solutions were HPLC grade. Multiple reaction monitoring (MRM) parameters were determined by direct infusion (DI) of standards on the 4000QTrap using standards for each individual metabolite of interest. The MRM parameters are listed in Table 2.1. These MRMs were used to detect metabolites of interest during all of the LC-MS/MS runs.

A volume of 10 μl of standard mix was used to compare four LC-MS/MS methods (3 in ESI mode and one in NSI mode). Two of the ESI methods were based upon previous work [29, 31]. The third ESI and the one NSI methods were optimized during the course of this work and were named Stab-ESI and Stab-NSI respectively. The MRMs in Table 2.1 were used for all methods, with a dwell time of 40 msec for each product ion. The MS/MS parameters were optimized for each method. LC separation was performed on a Luna NH_2 aminopropyl column (Phenomenex) at pH 9.4 in HILIC mode. The column dimensions were 50 mm x 2 mm. The packing material was 5 μm in diameter, 100 angstrom pore size. The LC solvents were Solvent A: 20 mM ammonium acetate + 20 mM ammonium hydroxide in 95:5 water:acetonitrile, pH 9.45; Solvent B: acetonitrile.

Table 2.1. *List of MRMs for each metabolite quantified*. Major and minor product ions are shown when applicable for each. Only one product ion was observed for several of the metabolite standards used and have only a major product ion listed.

Metabolite	$[M-H]^-$	Product ions	Product Ion type	Declustering potential	Entrance potential	Collision energy	Collision cell exit potential
NADPH	744.12	78.8	Major	-135	-10	-54	-5
		408	Minor	-135	-10	-54	-5
NADP	742.18	620.3	Major	-55	-10	-20	-11
		78.7	Minor	-55	-10	-126	-1
NADH	664.22	79	Major	-70	-10	-124	-1
		158.6	Minor	-70	-10	-60	-7
NAD	662.21	540	Major	-50	-10	-16	-53
		78.8	Minor	-50	-10	-114	-11
ATP	506.01	78.8	Major	-60	-10	-120	-11
		158.5	Minor	-60	-10	-40	-9
ADP	426.05	78.9	Major	-65	-10	-98	-1
		133.9	Minor	-65	-10	-32	-1
AMP	346.05	78.8	Major	-65	-10	-64	-9
		134	Minor	-65	-10	-40	-7
FBP	338.99	240.9	Major	-50	-10	-20	-11
fructose bisphosphate		97	Minor	-50	-10	-28	-5
G/F6P	258.94	168.8	Major	-55	-10	-16	-11
glucose/fructose 6-phosphate		96.7	Minor	-55	-10	-56	-9
Iso/Cit	190.95	110.8	Major	-45	-10	-18	-5
CIT (citrate)	190.96	86.8	Major	-45	-10	-24	-13
ISOCIT (isocitrate)	190.95	172.8	Major	-40	-10	-14	-25
NAG	187.02	124.8	Major	-60	-10	-20	-9
N-acetylglutamine		57.8	Minor	-60	-10	-28	-9
3PG	184.93	96.9	Major	-40	-10	-22	-9
3-phosphoglycerate		62.9	Minor	-40	-10	-112	-1
DHAP/GAP	168.84	96.9	Major	-50	-10	-12	-15
dihydroxyacetone phosphate		78.8	Minor	-50	-10	-94	-3
PEP	166.88	78.8	Major	-35	-10	-14	-7
phosphoenolpyruvate		62.8	Minor	-35	-10	-106	-11
AKG	144.91	100.9	Major	-30	-10	-12	-15
α-ketoglutarate		57.1	Minor	-30	-10	-18	-3
MAL	132.94	115	Major	-40	-10	-16	-7
malate		70.9	Minor	-40	-10	-20	-9
OAA (oxaloacetate)	130.92	86.8	Major	-30	-10	-14	-7
SUC	116.97	73	Major	-50	-10	-16	-11
succinate		98.9	Minor	-50	-10	-16	-5
FUM (fumarate)	114.94	70.9	Major	-25	-10	-12	-5
LAC (lactate)	89.02	70.9	Major	-35	-10	-16	-5
PYR	86.92	43.1	Major	-30	-10	-12	-1
pyruvate		58.9	Minor	-30	-10	-12	-1

Method A [29]. The ESI spray voltage was -4500 V in negative mode. Nitrogen was used as sheath gas at 20 psi, as gas 1 at 35psi, as gas 2 at 50 psi, and as the collision gas set to high. The interface heater was on and the temperature was set to 325 °C. The flow rate was 150 µl/min. The solvent gradient was t = 0 min, 85% B; t = 15 min, 100% A; t = 38 min, 100% A; t = 40 min, 85% A; t = 50 min, 85% B [29].

Method B [31]. The ESI spray voltage was -4500 V (negative ion mode). Nitrogen was used as sheath gas at 20 psi, as gas 1 at 35psi, as gas 2 at 50 psi, and as the collision gas set to high. The interface heater was on and the temperature was set to 325 °C. The flow rate was 100 µl/min from t = 0 min through t = 16 min and t = 26 min through t = 27 min and 200 ul/min from t = 18 min through t = 25 min. The solvent gradient was t = 0 min, 85% B, 100 ul/min; t = 3 min, 40% B; t = 10 min, 100% A; t = 16 min, 100% A, 100 µl/min; t = 18 min, 100% A, 200 µl/min; t = 20 min, 100% A; t = 21 min, 85% B; t = 25 min, 85% B, 200 µl/min; t = 26 min, 85% B, 100 µl/min; t = 27 min, 85% B, 100 µl/min [31].

Method C (this work). ESI spray voltage was -4500 V in negative mode. Nitrogen was used as sheath gas at 20 psi, as gas 1 at 25 psi, as gas 2 at 50 psi, and as the collision gas set to high. The interface heater was on and the temperature was set to 200 °C. The flow rate was 70 µl/min for the actual MS/MS run (0-125 min) and then was increased to 150 µl/min for column re-equilibration (125-150 min). The solvent gradient was t = 0 min, 100% B, 70 µl/min; t = 15 min, 100% B; t = 30 min, 100% A; t = 125 min, 100% A, 70 µl/min; t = 135 min, 100% A, 150 µl/min; t = 140 min, 100% B; t = 148 min, 100% B, 150 µl/min; t = 150 min, 100% B, 70 µl/min.

Method D (this work). NSI spray voltage was -1900 V in negative mode. Nitrogen was used as sheath gas at 20 psi, as gas 1 at 30psi, as gas 2 at 0 psi, and as the collision gas set to high. The interface heater was on and the temperature was set to 125 °C. LC separation was performed on a Luna NH_2 aminopropyl column (Phenomenex) at pH 9.4 in HILIC mode. Material was packed in-house using the aminopropyl material and a PicoFrit column. Final column dimensions: 15 cm length x 100 µm ID. The flow rate was 300 nl/min. The solvent gradient was t = 0 min, 100% B; t = 15 min, 100% B; t = 30 min, 100% A; t = 65 min, 100% A; t = 80 min, 100% B; t = 120 min,

100% B.

Quantitation. Averaging of peak area spectra for each metabolite (technical triplicates) normalized to the internal standard NAG was performed using the Analyst software that accompanies the 4000 QTrap. The data were subsequently summarized using Microsoft Excel.

Metabolite Extraction Method Development for LC-MS/MS. MCF-7 (human breast adeninocarcinoma) cells were used for all metabolite extractions in the method development phase of this work due to their high cell density and unlimited proliferative capacity. In order to detect all the metabolites of interest, 3×10^7 cells were needed in 500 μl of extraction solvent. This cell number was achieved at 100% confluency in one T-150 flask. Four sample preparation methods were evaluated to determine the effects of cell scraping, PBS washing, trypsinization, and flash freezing (3×10^8; 6 ml) on the metabolite profile. The effects of residual extracellular media and sample concentration were also analyzed. A schematic representation of the methods is shown in Figure 2.1.

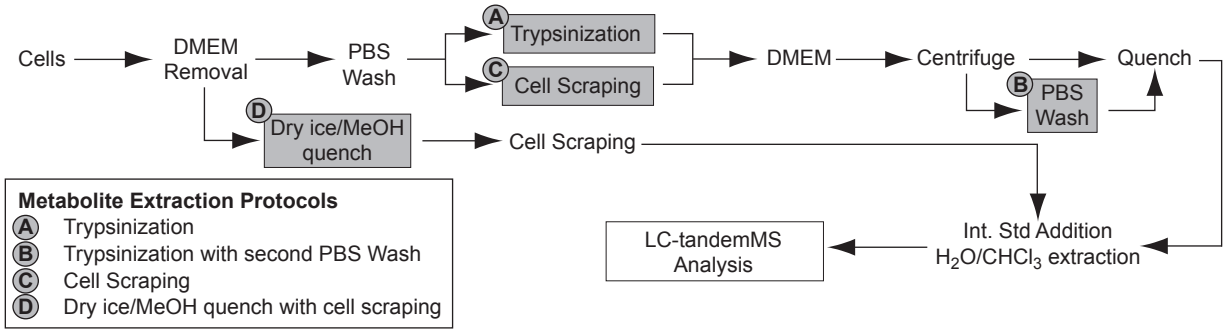

Fig. 2.1. *Diagram of the trypsinization (A), PBS wash (B), cell scraping (C), and flash freezing (D) extraction methods for LC MS/MS.*

Method A. Trypsinization. Media was changed 2 hours before extraction. DMEM was removed by decantation and washed once with PBS (10 ml). Cells were then treated with 1× trypsin-EDTA (2 ml; 10 min) in the incubator to release them from the flask surface. Cells were then resuspended in supplemented DMEM (23 ml) with 500 μl of the suspension removed for cell counting. The remaining suspension was incubated at 37 °C (10 min), and subsequently centrifuged (750 ×g; 2 min). The media was then decanted and the cells were resuspended in ice-

cold methanol (250 μl), vortexed, and flash frozen in liquid nitrogen. The cell suspension was then allowed to thaw in an ice bath (5 min) and kept on ice while adding H_2O (250 μl), chloroform (500 μl), and N-acetyl glutamine (NAG) (1 μl, internal standard, final concentration of 1 μg/ml) (Fig. 6). NAG degrades over time at -20 °C; therefore, standard aliquots must be kept at -80 °C prior to use at -20 °C. The suspension was then vortexed, mixed in a rotator (10 min) at 4 °C, vortexed again, and centrifuged (14000 ×g; 5 min) at 4 °C. The aqueous layer (450 ul) was carefully removed, flash frozen in liquid nitrogen, and stored at -80 °C (Fig. 2.1).

Method B. PBS Washing. The trypsinization method was modified where the cells were washed once with PBS and centrifuged (750 ×g; 2 min) again following the first centrifugation and decant step (prior to the addition of methanol; Fig. 2.1).

Method C. Cell Scraping. Cells were scraped in supplemented DMEM (25 ml) instead of being trypsinized (Fig. 2.1).

Method D. Flash Freezing. Ten T-150 flasks were required to achieve the same concentration per volume as the other methods. The supplemented DMEM was removed from the first flask, the flask was put on dry ice and methanol (2.5 ml) at -20 °C was added immediately to flash freeze/ quench the cells. The cells were then scraped while the flask was kept on dry ice and the suspension was removed and used to flash freeze the remaining 9 flasks by repeating the method above. Aliquots of the cell suspensions (200 μl) were removed and the remainder was then flash frozen in liquid nitrogen. Density measurements were performed on a UV/Vis spectrophotometer (650 nm; DU520/Beckman-Coulter). A standard cell density curve was prepared for determining cell numbers in methanol so that the cell density could be converted to cell number for normalization with the methods being evaluated (Fig. 2.2). The cell suspension was then allowed to thaw in an ice bath (5 min) and kept on ice while adding H_2O (2.5 ml) and chloroform (5 ml). The standard protocol was performed for the rest of this method except that 4.5 ml of the aqueous layer was removed instead of 450 μl (Fig. 2.1).

Analysis of the Media. Analysis of the metabolite profile of the media was carried out by removing 250 μl of residual DMEM from the cells, adding that to 1 ml of extraction solution, and

then performing the regular extraction procedure. The 250 μl amount was determined by visual color matching of the mock extraction to the regular extractions. The following provided an estimate of competing metabolites found within the residual media.

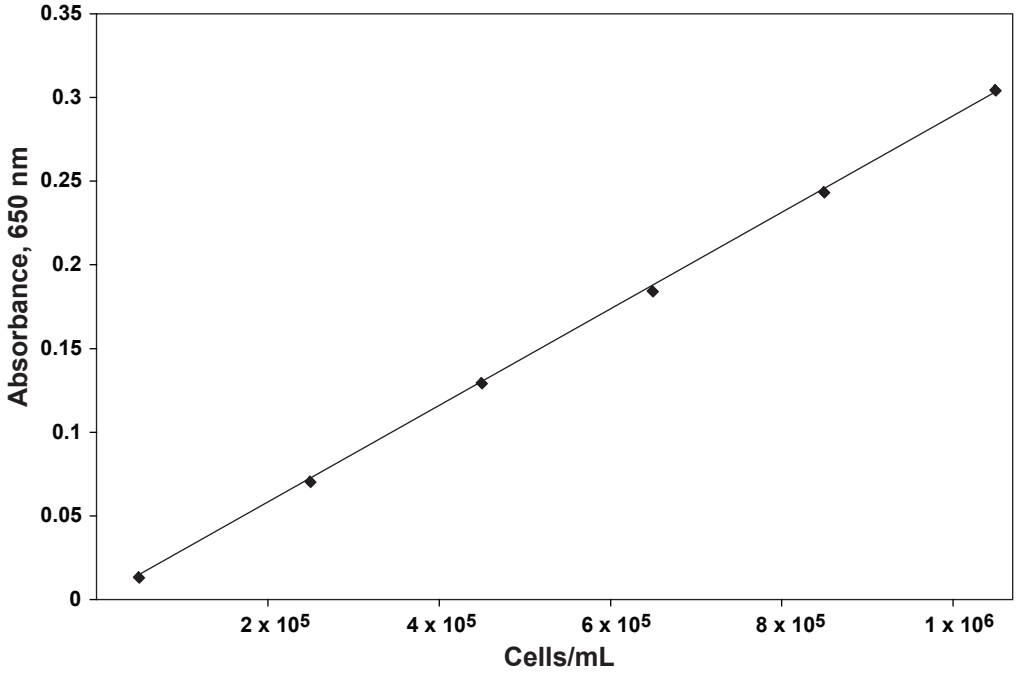

Fig. 2.2. *Standard curve of the optical density measurement at 650 nm and its corresponding cell density measurement in 10e5 cells/ml.*

Effects of Sample Concentration. The effects of drying/concentration on the metabolite profile was determined by drying three flash frozen biological replicates of 3 $\times 10^7$ MCF-7 cells in a centrivap concentrator (LabConco). After the samples were completely dried they were then resuspended in 450 μl of 50% methanol to match both the starting sample solution's original composition and volume. These samples were flash frozen and stored at -80 °C prior to analysis. Samples were thawed in an ice-bath for 5 minutes and aliquots (50 μl) were put in 250 μl test tubes, flash frozen, and stored at -80 °C. The aliquots were then thawed as needed in an ice-bath for 5 minutes and used for sample analysis.

Results and Discussion

LC MS/MS and Extraction Method Development. The two ESI LC MS/MS methods

using a hydrophilic interaction chromatography (HILIC) column, were originally published by Bajad and coworkers [29, 31]. These methods have been employed for the analysis of metabolites in yeast, bacteria, and human cells [29-31]. However, these methods performed poorly (decreased sensitivity and reproducibility) on human primary fibroblasts with low cell population densities, and especially senescent fibroblasts, where cell numbers are extremely low. This necessitated the development of a more robust and sensitive LC MS/MS method. As a nanospray MS/MS technique had not been previously developed for analysis of small polar metabolites, but has the capability of increasing sensitivity as well as reducing the sample size required for analyses, both electropray and nanospray LC MS/MS methodologies were explored.

The results of the comparative analyses are shown in Table 2.2. Empty boxes represent undetectable metabolite levels. All methods were conducted using a standard metabolite mix where each metabolite was present at a concentration of (5 μg/ml). Average peak area ion intensity (purple) of metabolites of interest in technical triplicate are shown for the method of Bajad *et al*., (Method A) [29]. Increases and decreases in average peak area ion intensities for each metabolite between methods are represented by positive or negative multipliers (green or red, respectively) in the other recently reported method of Rabinowitz *et. al*. (Method B) [31], and the methods developed in this work (Method C, ESI; Method D, NSI) using Method A as the baseline for comparison. For those metabolites that were not detectable by Method A, Method C was used for baseline comparison of ESI-based methods, with ion intensities (purple) listed for Method C. For metabolites only detected in the NSI mode, ion intensities (purple) are listed in Method D. For example, the major product ion peak of ADP has an average ion intensity of 9100 in Method A, and its intensity is 5.1 times less in Method B, 315.4 times greater in Method C, and 2186.8 times greater in Method D. Standard deviation for all metabolites did not exceed 20 percent.

Each method had its advantages and disadvantages. Both NSI and ESI LC MS/MS have the advantage of HILIC chromatography, which provided increased column retention times relative to reverse-phase. However, in order to optimize the separation characteristics, the HILIC column must be run at a relatively high pH (9.4). Under these conditions, the packing material solid

Table 2.2. *Comparison of the two published ESI LC MS/MS methods to those generated in this work (ESI and NSI LC MS/MS).* See text for details.

				Peak Area/Relative Peak Area (ESI)			Peak Area (NSI)
Metabolites	Parent Ion	Product Ions		Method A [29]	Method B [31]	Method C (this work)	Method D (this work)
NADPH	744.12	Major	78.8			2.34E+04	91.9
NADP	742.18	Major	620.3			1.06E+05	138
		Minor	78.7			4.27E+05	13.8
NADH	664.22	Major	79	2.19E+04		12.76	58.3
		Minor	158.6	3.99E+03		16.82	59.7
NAD	662.21	Major	540			5.49E+05	4.50
		Minor	78.8			6.08E+05	3.26
ATP	506.01	Major	78.8				4.75E+06
		Minor	158.5				3.02E+06
ADP	426.05	Major	78.9	9.10E+03	0.19	315	2190
		Minor	133.9	9.57E+03	0.17	107	652
AMP	346.05	Major	78.8	1.76E+05	0.16	8.28	16.8
		Minor	97	6.72E+04	0.10	9.31	20.2
FBP	338.98	Major	97	6.67E+05	0.40	1.98	7.67
		Minor	78.8	8.72E+05	0.50	1.71	6.03
cAMP	327.97	Major	133.9	2.17E+07	0.01	0.18	0.47
		Minor	78.7	5.20E+06	0.01	0.27	0.49
G/F6P	258.94	Major	96.7	2.64E+06	1.68	0.94	3.74
		Minor	78.8	2.54E+06	1.55	0.94	2.85
Iso/Cit	190.95	Major	110.8	3.88E+07	0.25	0.27	0.28
CIT	190.96	Major	86.8	1.02E+07	0.25	0.24	0.22
ISOCIT	190.95	Major	172.8	1.43E+07	0.21	0.26	0.28
NAG	187.02	Major	124.8	2.71E+07	0.36	0.06	0.15
		Minor	57.8	2.15E+07	0.41	0.07	0.10
2/3PG	184.93	Major	96.9	4.16E+06	0.39	0.52	1.55
		Minor	78.9	4.31E+06	0.41	0.52	1.42
DHAP/GAP	168.84	Major	96.9	1.52E+06	0.86	0.22	0.23
		Minor	78.8	8.49E+05	1.13	0.22	0.21
PEP	166.88	Major	78.8	1.06E+07	0.30	0.30	0.17
		Minor	62.8	6.46E+05	0.32	0.34	0.16
AKG	144.91	Major	100.9	7.75E+06		1.02	1.38
		Minor	57.1	1.11E+06		0.69	1.78
MAL	132.94	Major	115	1.27E+07	1.15	1.27	0.71
		Minor	70.9	5.60E+06	1.13	1.28	0.63
OAA	130.92	Major	86.8			2.03E+5	6.35
SUC	116.97	Major	73	2.53E+06	0.81	2.45	11.3
		Minor	98.9	2.64E+05	0.73	3.39	13.4
FUM	114.94	Major	70.9	2.17E+05	1.10		4.13
PYR	86.92	Major	43.1				1.05E+06
		Minor	58.9				7.69E+04

support slowly dissolved, depositing the packing material on the mass spectrometer. While this is not a tremendous problem in ESI mode (orthogonal sample spray), in NSI mode the sample is directly sprayed into the mass spectrometer. Hence, while the NSI LC MS/MS proved to be the most robust and sensitive method for the analysis of metabolites in central carbon metabolism (Table 2.2), the HILIC column routinely clogged at the nanospray tip followed by contamination of the mass spectrometer.

The ESI LC MS/MS Method C developed in this work was determined to be the best overall method since it provided good sensitivity and reproducible LC retention times without contamination of the mass spectrometer (Method D). Although lifetime of the column is somewhat limited due to the used of an alkaline mobile phase, at this point in time there are no alternatives for LC-MS analyses. Clearly the development of alternative stationary phases that are capable of separating small negatively-charged metabolites would improve the analysis of core metabolites. Nonetheless, the methodology described here, which utilized an extended gradient relative to that described in Method A [29] permitted the detection of 3 additional metabolites and provided higher sensitivity for 6 metabolites that exhibit low ion intensities in the other two ESI-based methods.

Evaluation of "Speed Vac" Concentration. The ideal extraction method needs to: (1) quench metabolic events immediately in order to preserve the endogenous levels of metabolites within the cell, (2) extract the materials of interest quantitatively, (3) minimize processing times in order to decrease the possibility of compound degradation. For analysis of adherent human fibroblasts, a confounding factor is obtaining the appropriate cell population densities, especially when they are in the senescent, non-dividing state, where low cell densities limit the number of cells that can be conveniently extracted. To obtain the appropriate cell density and sample volume from fibroblasts, one must either process the monolayer prior to quenching or concentrate the sample after extraction.

A traditional approach described in the literature for dealing with low levels of metabolites in extracts has been to concentrate the extract using a refrigerated centrifugal concentrator (Speed vac) [7, 25, 31, 34]. In an effort to assess concentrating the samples to permit analysis of limited

cell numbers, it was found that the approach leads to dramatic changes in the metabolite profile and significantly less overall metabolite recovery (Table 2.3).

Starting with flash-frozen MCF-7 cells (3 x 10^7 cells), average peak area ion intensities of the metabolites of interest were determined in biological triplicate, both with and without speed vac concentration. The concentration method consisted of evaporating the sample to completion via the Speed vac with no heat and subsequently resuspending the sample to the same starting volume using the ice cold extraction solution on ice with vortexing. Decreases in average peak area ion intensities for each metabolite are represented by negative values in the concentration method. Most of the metabolites were not detectable after the drying and resuspension of the samples. In addition, the error associated with the measurement increased for those metabolites that could be monitored after concentration. In summary, concentration is not a viable approach to adherent monolayer metabolite profiling.

Optimization of the quenching and extraction methodologies. With a mass spectral analysis method in place, the next step was to determine the best overall method to extract metabolites from cells grown as monolayers. High cell population density MCF-7 cells were utilized to perform this experiment due to the slow growth characteristics of primary fibroblasts. MCF-7 cells can reach a cell population of 3 $\times 10^7$ cells in one flask, ten times more than what can be obtained with BJ or Imr90 cells. Trypsinization, scraping, washing, and flash-frozen extractions were compared to determine the effects of these extraction methods on the metabolite profile. The trypsinization and scraping methods were methods where release by protease activity or manual scraping permitted concentrating the sample before quenching (Fig. 2.1). The wash method was simply the trypsinization method with an additional PBS wash to remove any residual DMEM prior to quenching and extraction. This was performed along with a mock sample (data not shown), which simply consisted of residual DMEM, to address if there were any metabolites in the DMEM that contribute to intracellular metabolite levels. The wash method also addressed if there was any leakage of metabolites during the wash process. The results are summarized in Fig. 2.3.

Table 2.3. *Comparison of flash-frozen samples before and after being concentrated and resuspended.* Parent and characteristic product ion peaks are shown. Empty boxes (---) represent metabolite present in levels below the detection limit.

				Flash Frozen Method		Speed vac Concentration	
Metabolite	$[M-H]^-$	Product ion	Ion Type	Avg. Peak Area	Error (%)	Relative Peak Area*	Error (%)
NADP	742.179	620.3	Major	8.70E+5	6.46	0.0034	64.94
		78.7	Minor	3.75E+5	1.49	---	---
NADH	664.22	79	Major	3.52E+5	4.35	---	---
		158.6	Minor	6.46E+4	6.53	---	---
NAD	662.211	540	Major	2.41E+6	9.72	0.0016	34.71
		78.8	Minor	1.52E+6	3.33	0.0027	18.46
ADP	426.046	78.9	Major	7.22E+5	10.68	---	---
		133.9	Minor	3.51E+5	13.81	---	---
AMP	346.05	78.8	Major	3.75E+4	10.96	0.083	20.20
		97	Minor	1.02E+4	6.61	0.33	85.92
FBP	338.984	97	Major	1.42E+5	3.10	0.11	2.23
		78.8	Minor	8.33E+4	0.33	---	---
G/F6P	258.941	96.7	Major	1.01E+6	2.07	0.008	0.44
		78.8	Minor	4.05E+4	4.50	0.038	2.69
Iso/Cit	190.95	110.8	Major	2.31E+6	4.42	---	---
CIT	190.96	86.8	Major	9.85E+5	1.07	---	---
ISOCIT	190.95	172.8	Major	1.58E+5	9.20	---	---
2/3PG	184.93	96.9	Major	2.86E+5	5.47	---	---
		78.9	Minor	1.50E+4	0.95	---	---
DHAP/GAP	168.838	96.9	Major	5.46E+4	2.54	0.2	4.52
		78.8	Minor	3.03E+4	5.60	---	---
PEP	166.882	78.8	Major	9.72E+4	6.79	---	---
		62.8	Minor	4.09E+3	2.28	---	---
AKG	144.913	100.9	Major	1.39E+6	4.43	0.03	0.33
		57.1	Minor	1.97E+5	6.83	0.028	30.51
MAL	132.943	115	Major	7.26E+6	5.52	0.022	38.73
		70.9	Minor	3.93E+6	6.39	0.02	17.77
OAA	130.915	86.8	Major	9.27E+5	3.52	0.021	17.68
SUC	116.969	73	Major	1.73E+6	6.62	0.026	22.68
		98.9	Minor	1.75E+5	8.00	---	---
FUM	114.943	70.9	Major	6.91E+5	0.62	0.14	3.56
LAC	88.9	70.9	Major	2.35E+6	1.83	---	---

*Relative peak area was determined by dividing the averaged peak areas for the concentrated sample by that of the flash frozen. Peak areas were determined in triplicate.

Fig. 2.3. *The impact of the various extraction methods on the resulting metabolic profile.* Metabolite levels represent the average area in biological triplicate of the major product ion peak for each metabolite of interest normalized to the internal standard NAG and are shown as relative ion intensity. The changes were confirmed by minor product ion peaks for most of the metabolites listed. A list of all of the averaged area major and minor product ion peaks for each metabolite can be found in the appendix. NADPH, ATP, and PYR could not be detected in the samples. The average percent errors for each method tested are also shown (bottom panel).

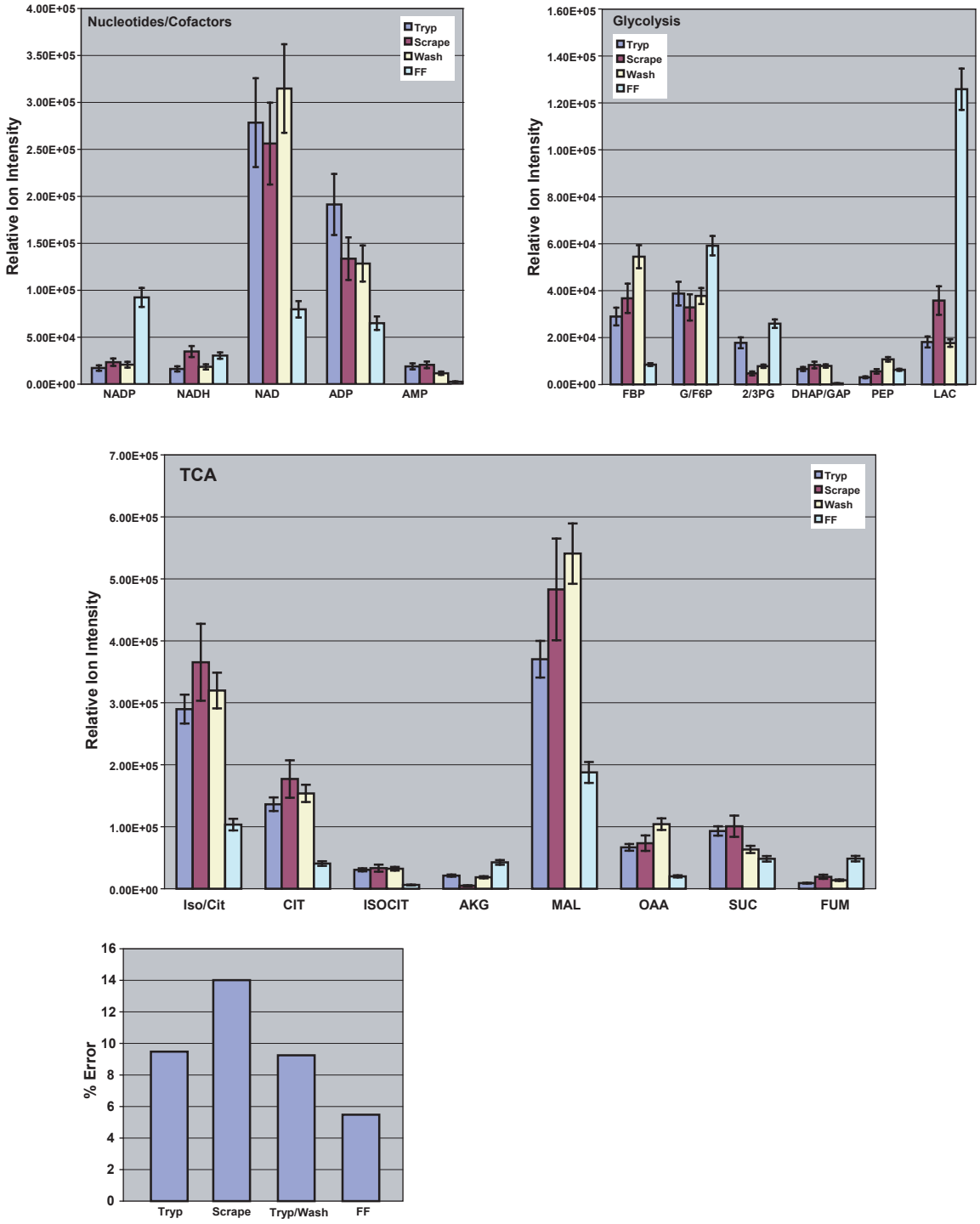

Significant changes in almost all of the metabolites were seen among the processing methods. Some of the more dramatic differences observed across methods were increases in the levels of NAD, AMP, FBP, citrate, isocitrate, and malate along with decreases in the levels of NADP and lactate when the flash freeze method was compared to trypsinization, washing or scraping. Changes in the metabolite profile between trypsinization, washing, and scraping were relatively small (2-fold or less) and included the following metabolites: ADP, NADH, FBP, 2/3 PG, PEP, MAL, OAA, SUC, FUM. Metabolite levels that changed as a result of the additional wash included increases in the levels of PEP, FUM, OAA, MAL, and FBP along with decreases in the level of AMP, SUC, and ADP. Increased metabolite levels are presumably due to the preparation of "cleaner" samples, leading to reduced ion suppression and increased metabolite signals.

Decreased ion intensities could be due to loss of materials by the additional wash. This scenario seems somewhat probable considering AMP, ADP, LAC, and SUC were found in the mock sample that consisted of residual DMEM only (data not shown). This suggests that intracellular metabolites are also found in the extracellular media and therefore the media does contribute to the metabolite levels found within the cells. Metabolite levels that changed as a result of the scraping method when compared to the trypsinization method included increases in the levels of PEP, NADH, FUM, and LAC, and decreases in the levels of AKG, ADP, 2/3 PG. AKG was extremely difficult to detect in this method because of its very low levels.

The PBS wash method was shown to be the best method for preparing the sample prior to quenching and extraction. This method is less cumbersome than the scraping method and provides a lower overall percent error while removing any contributing metabolites found in the residual DMEM of the trypsinization method (Fig. 2.3). Even though the addition of a sample concentration step prior to quenching results in a significant change on the metabolic profile, it is a better option than drying the sample and provides a relatively fast and reproducible method of analyzing the metabolite changes under various conditions when source materials (monolayer cells) are used for analysis.

Summary/Conclusions

The objective of the work described in this Chapter was to develop cell quenching, metabolite extraction, and LC-tandem MS analysis methodologies that could be directly applied to primary adherent fibroblasts, where low cell population densities provide limit the amount of sample available for analysis. Using MCF-7 cell extracts, several LC-MS/MS methods were compared to determine the best overall method for quantifying metabolites on the mass spectrometer. A series of MRMs were developed for quantifying a set of nucleotides, cofactors, and glycolytic/TCA metabolites, and an electrospray LC-MS/MS method that utilized an extended HILIC-based gradient was shown to be the best method for the detection of metabolites at low cell population densities. An investigation of several published quenching and extraction methods revealed that the fast quenching of cells followed by concentration via a Speed vac is inadequate. A trypsinization method that incorporates a phosphate wash step proved to be the most suitable (Method B, Table 2.2) for the isolation of core metabolites for LC-mass spectral analyses.

References

1. Oldiges, M., S. Lutz, S. Pflug, K. Schroer, N. Stein, and C. Wiendahl, *Metabolomics: current state and evolving methodologies and tools.* Appl Microbiol Biotechnol, 2007. **76**(3): p. 495-511.
2. Griffin, J.L., *The Cinderella story of metabolic profiling: does metabolomics get to go to the functional genomics ball?* Philos Trans R Soc Lond B Biol Sci, 2006. **361**(1465): p. 147-61.
3. Nicholson, J.K., J.C. Lindon, and E. Holmes, *'Metabonomics': understanding the metabolic responses of living systems to pathophysiological stimuli via multivariate statistical analysis of biological NMR spectroscopic data.* Xenobiotica, 1999. **29**(11): p. 1181-9.
4. Buscher, J.M., D. Czernik, J.C. Ewald, U. Sauer, and N. Zamboni, *Cross-Platform Comparison of Methods for Quantitative Metabolomics of Primary Metabolism.* Anal Chem, 2009. **81**(6): p. 2135-2143.
5. Mungur, R., A.D. Glass, D.B. Goodenow, and D.A. Lightfoot, *Metabolite fingerprinting in transgenic Nicotiana tabacum altered by the Escherichia coli glutamate dehydrogenase gene.* J Biomed Biotechnol, 2005. **2005**(2): p. 198-214.
6. Whitfield, P.D., A.J. German, and P.J. Noble, *Metabolomics: an emerging post-genomic tool for nutrition.* Br J Nutr, 2004. **92**(4): p. 549-55.
7. Sellick, C.A., R. Hansen, A.R. Maqsood, W.B. Dunn, G.M. Stephens, R. Goodacre, and A.J. Dickson, *Effective quenching processes for physiologically valid metabolite profiling of suspension cultured Mammalian cells.* Anal Chem, 2009. **81**(1): p. 174-83.
8. Fernie, A.R., R.N. Trethewey, A.J. Krotzky, and L. Willmitzer, *Metabolite profiling: from diagnostics to systems biology.* Nat Rev Mol Cell Biol, 2004. **5**(9): p. 763-9.
9. Dunn, W.B., N.J. Bailey, and H.E. Johnson, *Measuring the metabolome: current analytical technologies.* Analyst, 2005. **130**(5): p. 606-25.
10. Raamsdonk, L.M., B. Teusink, D. Broadhurst, N. Zhang, A. Hayes, M.C. Walsh, J.A. Berden, K.M. Brindle, D.B. Kell, J.J. Rowland, H.V. Westerhoff, K. van Dam, and S.G. Oliver, *A functional genomics strategy that uses metabolome data to reveal the phenotype of silent mutations.* Nat Biotechnol, 2001. **19**(1): p. 45-50.
11. Weckwerth, W. and K. Morgenthal, *Metabolomics: from pattern recognition to biological interpretation.* Drug Discov Today, 2005. **10**(22): p. 1551-8.
12. Fiehn, O., J. Kopka, P. Dormann, T. Altmann, R.N. Trethewey, and L. Willmitzer, *Metabolite profiling for plant functional genomics.* Nat Biotechnol, 2000. **18**(11): p. 1157-61.
13. Roessner, U., A. Luedemann, D. Brust, O. Fiehn, T. Linke, L. Willmitzer, and A. Fernie, *Metabolic profiling allows comprehensive phenotyping of genetically or environmentally modified plant systems.* Plant Cell, 2001. **13**(1): p. 11-29.
14. Halket, J.M., A. Przyborowska, S.E. Stein, W.G. Mallard, S. Down, and R.A. Chalmers, *Deconvolution gas chromatography/mass spectrometry of urinary organic acids--potential for pattern recognition and automated identification of metabolic disorders.* Rapid Commun Mass Spectrom, 1999. **13**(4): p. 279-84.
15. Lisec, J., N. Schauer, J. Kopka, L. Willmitzer, and A.R. Fernie, *Gas chromatography mass spectrometry-based metabolite profiling in plants.* Nat Protoc, 2006. **1**(1): p. 387-96.
16. Tolstikov, V.V., O. Fiehn, and N. Tanaka, *Application of liquid chromatography-mass spectrometry analysis in metabolomics: reversed-phase monolithic capillary chromatography and hydrophilic chromatography coupled to electrospray ionization-mass spectrometry.* Methods Mol Biol, 2007. **358**: p. 141-55.
17. Soga, T., Y. Ohashi, Y. Ueno, H. Naraoka, M. Tomita, and T. Nishioka, *Quantitative metabolome analysis using capillary electrophoresis mass spectrometry.* J Proteome Res, 2003. **2**(5): p. 488-94.

18. Horie, K., T. Ikegami, K. Hosoya, N. Saad, O. Fiehn, and N. Tanaka, *Highly efficient monolithic silica capillary columns modified with poly(acrylic acid) for hydrophilic interaction chromatography.* J Chromatogr A, 2007. **1164**(1-2): p. 198-205.
19. Horie, M., F. Ishikawa, M. Oishi, T. Shindo, A. Yasui, and K. Ito, *Rapid determination of cyclamate in foods by solid-phase extraction and capillary electrophoresis.* J Chromatogr A, 2007. **1154**(1-2): p. 423-8.
20. Lu, W., B.D. Bennett, and J.D. Rabinowitz, *Analytical strategies for LC-MS-based targeted metabolomics.* J Chromatogr B Analyt Technol Biomed Life Sci, 2008. **871**(2): p. 236-42.
21. Sun, G., K. Yang, Z. Zhao, S. Guan, X. Han, and R.W. Gross, *Shotgun metabolomics approach for the analysis of negatively charged water-soluble cellular metabolites from mouse heart tissue.* Anal Chem, 2007. **79**(17): p. 6629-40.
22. Vaidyanathan, S., S. Gaskell, and R. Goodacre, *Matrix-suppressed laser desorption/ionisation mass spectrometry and its suitability for metabolome analyses.* Rapid Commun Mass Spectrom, 2006. **20**(8): p. 1192-8.
23. Shroff, R., A. Muck, and A. Svatos, *Analysis of low molecular weight acids by negative mode matrix-assisted laser desorption/ionization time-of-flight mass spectrometry.* Rapid Commun Mass Spectrom, 2007. **21**(20): p. 3295-300.
24. Want, E.J., B.F. Cravatt, and G. Siuzdak, *The expanding role of mass spectrometry in metabolite profiling and characterization.* Chembiochem, 2005. **6**(11): p. 1941-51.
25. Cordell, R.L., S.J. Hill, C.A. Ortori, and D.A. Barrett, *Quantitative profiling of nucleotides and related phosphate-containing metabolites in cultured mammalian cells by liquid chromatography tandem electrospray mass spectrometry.* J Chromatogr B Analyt Technol Biomed Life Sci, 2008. **871**(1): p. 115-24.
26. Luo, B., K. Groenke, R. Takors, C. Wandrey, and M. Oldiges, *Simultaneous determination of multiple intracellular metabolites in glycolysis, pentose phosphate pathway and tricarboxylic acid cycle by liquid chromatography-mass spectrometry.* J Chromatogr A, 2007. **1147**(2): p. 153-64.
27. Bennett, B.D., J. Yuan, E.H. Kimball, and J.D. Rabinowitz, *Absolute quantitation of intracellular metabolite concentrations by an isotope ratio-based approach.* Nat Protoc, 2008. **3**(8): p. 1299-311.
28. Yuan, J., B.D. Bennett, and J.D. Rabinowitz, *Kinetic flux profiling for quantitation of cellular metabolic fluxes.* Nat Protoc, 2008. **3**(8): p. 1328-40.
29. Bajad, S.U., W. Lu, E.H. Kimball, J. Yuan, C. Peterson, and J.D. Rabinowitz, *Separation and quantitation of water soluble cellular metabolites by hydrophilic interaction chromatography-tandem mass spectrometry.* J Chromatogr A, 2006. **1125**(1): p. 76-88.
30. Munger, J., S.U. Bajad, H.A. Coller, T. Shenk, and J.D. Rabinowitz, *Dynamics of the cellular metabolome during human cytomegalovirus infection.* PLoS Pathog, 2006. **2**(12): p. e132.
31. Rabinowitz, J.D. and E. Kimball, *Acidic acetonitrile for cellular metabolome extraction from Escherichia coli.* Anal Chem, 2007. **79**(16): p. 6167-73.
32. Brauer, M.J., J. Yuan, B.D. Bennett, W. Lu, E. Kimball, D. Botstein, and J.D. Rabinowitz, *Conservation of the metabolomic response to starvation across two divergent microbes.* Proc Natl Acad Sci U S A, 2006. **103**(51): p. 19302-7.
33. Socher, G., R. Nussbaum, K. Rissler, and E. Lankmayr, *Analysis of sulfonated compounds by ion-exchange high-performance liquid chromatography-mass spectrometry.* J Chromatogr A, 2001. **912**(1): p. 53-60.
34. Ritter, J.B., Y. Genzel, and U. Reichl, *Simultaneous extraction of several metabolites of energy metabolism and related substances in mammalian cells: optimization using experimental design.* Anal Biochem, 2008. **373**(2): p. 349-69.

35. Villas-Boas, S.G., J. Hojer-Pedersen, M. Akesson, J. Smedsgaard, and J. Nielsen, *Global metabolite analysis of yeast: evaluation of sample preparation methods.* Yeast, 2005. **22**(14): p. 1155-69.

Chapter 3

The Mitochondrial Life Cycle Dynamics of Primary Fibroblasts

Abstract

Mitochondrial dynamics such as size, shape, and changes in membrane potential are extremely useful biomarkers for cellular processes. In particular, the mitochondrial dynamics associated with senescence provide unique insights into metabolic processes. This work focuses on mitochondrial dynamics in both BJ and Imr90 cells with age and senescence under conditions of 3% and 20% O_2. Changes in mitochondrial membrane potential (MMP) with age and oxidative stress suggest a loss in mitochondrial membrane structure and function. These changes were cell type specific, with the oxidative-susceptible Imr90 cells reacting more prominently to oxidative stress and oxidative-resistant BJ cells reacting more prominently to cellular age. In addition, there were decreases in the overall percent of mitochondria volume per cell volume with senescence, despite an overall increase in both mitochondria and cell volumes. This suggests hypertrophic mitochondria due to lack of fission and attenuated metabolic function with senescence. These changes in morphology were uniform across both BJ and Imr90 cell types and suggest that mitochondrial morphological changes with senescence are uniform for most cell types and may be the same for both in vivo and in vitro conditions. These findings confirm the importance of mitochondria dynamics in oxidative stress and cellular aging.

Introduction

Human lung and skin fibroblasts exhibit a limited proliferative capacity when grown in culture. When such cultures are maintained under atmospheric oxygen levels (20%), fibroblasts generally reach replicative senescence between 50-60 population doublings (PD) [1-3]. Atmospheric oxygen levels, while convenient for cell culturing, can be considered hyperoxic relative to physiological oxygen concentrations in humans, which are on the order of 3% O_2. Indeed, when fibroblasts are cultured under normal physiological conditions (3% O_2), PDs increase about 30% relative to atmospheric levels [1-6]. Hence, while oxygen is a requirement for normal aerobic respiration, in high concentrations it can contribute to the total amount of oxidative stress to which cells are exposed, leading to a long-term adverse effect *in vitro*. Despite some controversies over *in vitro/ in vivo* life spans and donor age [6-14], replicative senescence *in vitro* can be considered a model for human aging. Inasmuch, cultures maintained under hyperoxic and hypoxic conditions provide a convenient model system for assessing the relationship between oxygen/oxidative stress and senescence.

Senescent cells adopt a distinctive flattened morphology along with other characteristic molecular and cytological markers such as proliferative arrest, senescence-associated β-galactosidase (SA β-Gal) staining, and senescence-associated heterochromatin formation (SAHF) visualized by 4', 6-diamidino-2-phenylindole (DAPI) staining [15-17]. The widely used SA β-Gal was first proposed as a biomarker for *in vivo* and *in vitro* aging by Dimri *et al*. in 1995 [17]. The protocol utilizes a β-galactosidase (β-Gal) staining procedure at pH 6 with 5-bromo-4-chloro-3-indolyl-β-galactopyranoside (X-Gal) as the substrate [18]. Under these conditions the assay is selective for the non-lysosomal form of β-Gal (optimal pH for lysosomal β-Gal is 4.5). These enzymes normally cleave D-galactose residues from non-reducing β-D-galactosides, structures that are found in a wide range of naturally occurring substrates (lactose for example). Despite some controversy over *in vivo* and *in vitro* staining [18, 19], SA β-Gal provides reliable supporting evidence for senescence in culture [17, 20-22].

Heterochromatin is a condensed form of transcriptionally silent DNA. Recently, senescence-

associated heterochromatic foci (SAHF) have been observed with the senescent phenotype in various lung, and to a lesser extent foreskin, human fibroblasts. During senescence, the chromatin structure is extensively remodeled, and multiple heterochromatic regions appear. This phenomenon is easily seen via DAPI staining as irregularly shaped structures containing dense DNA foci throughout the nuclear region. SAHF, an Rb dependent process, is thought to recruit histone deacetylases (HDACs) to E2F-dependent promoters resulting in heterochromatin formation and stable repression of genes involved in proliferation [15, 23-25]. A combination of senescent markers can provide a reliable methodology to validate senescence *in vitro* for analyzing the cytological changes that occur during the aging process.

Mitochondria are multi-functional organelles that have unique roles in modulating energy metabolism, apoptosis, and senescence [26]. Despite these central roles, research into the life cycle of mitochondria, *i.e.*, biogenesis, migration, and changes in morphology are just beginning to be explored. Mitochondria are dynamic organelles that regularly exhibit changes in orientation, number, and/or size within individual cells as a result of mitochondrial fission and fusion processes. It is believed that such processes are tightly regulated and allow for the constant remodeling of mitochondrial structure in response to a cell's bioenergetic state [27-32]. Conditions such as hypoxia, stress, and aging have been reported to impact mitochondrial life cycle dynamics, leading to cellular dysfunction and age related diseases such as Huntington's, Alzheimer's, Parkinson's, and stroke [33-38]. Recently, mitochondrial fission has been correlated with the replicative senescent processes in mammalian cell culture as well as several senescent characteristics such as SA β-Gal staining, and the enlarged/flattened cellular morphology typical of senescent cells [39]. It was shown that inhibition of hFis1, a key regulator of fission processes, decreased mitochondrial fission rates and resulted in changes of both mitochondrial and cellular morphology. The mitochondria became elongated and the cell adopted an enlarged and flattened morphology. Decreased fission also resulted in increased SA β-Gal staining, decreased membrane potential, and increased levels of reactive oxygen species (ROS) [39]. Other studies performed on rat/monkey cerebella and human epithelial cells have also shown changes in mitochondrial morphology associated with the

aging phenotype, including decreases in mitochondrial number and increases in mitochondrial volume and density. These changes are often correlated with a decrease in overall mitochondrial function as measured by decreases in mitochondrial membrane potential (MMP). Decreases in MMP are caused by both damage and concomitant decreases in the activities of Complexes I and IV of the electron transport chain, as well as succinate dehydrogenase (Complex II, a part of both the electron transport chain and the TCA cycle; Fig. 3.1) [40-47]. Studies that have focused on mitochondrial membrane potential and permeability under normal *in vitro* growth conditions have shown changes that accumulate with increased population doublings (PDs). Decreases in mitochondrial membrane potential along with increases in membrane permeability were seen in liver, heart, brain, and endothelial cells [48-57]. These changes have been associated with changes in the mitochondrial membrane composition and have been shown to impact mitochondrial metabolism [57-59].

Recent literature strongly suggests that the mitochondria's life cycle dynamics and its associated factors play an important role in replicative senescence. Further work is needed to explore the changes in this dynamic life cycle as they occur with age under different levels of oxidative stress, and explore the connections between these changes and primary metabolism. In this Chapter, the senescence process is characterized in both Imr90 and BJ cell lines through evaluation of cell growth, SAHF formation, β-Gal staining, and the behavior of primary fibroblast mitochondria during their serial passaging into senescence during exposure to both 3% and 20% O_2. This is an important study, as we are not aware of any efforts undertaken to explore changes in the life cycle of mitochondria, *i.e.*, biogenesis, migration, MMP, and morphology with age, using primary human fibroblasts grown under different levels of oxygen.

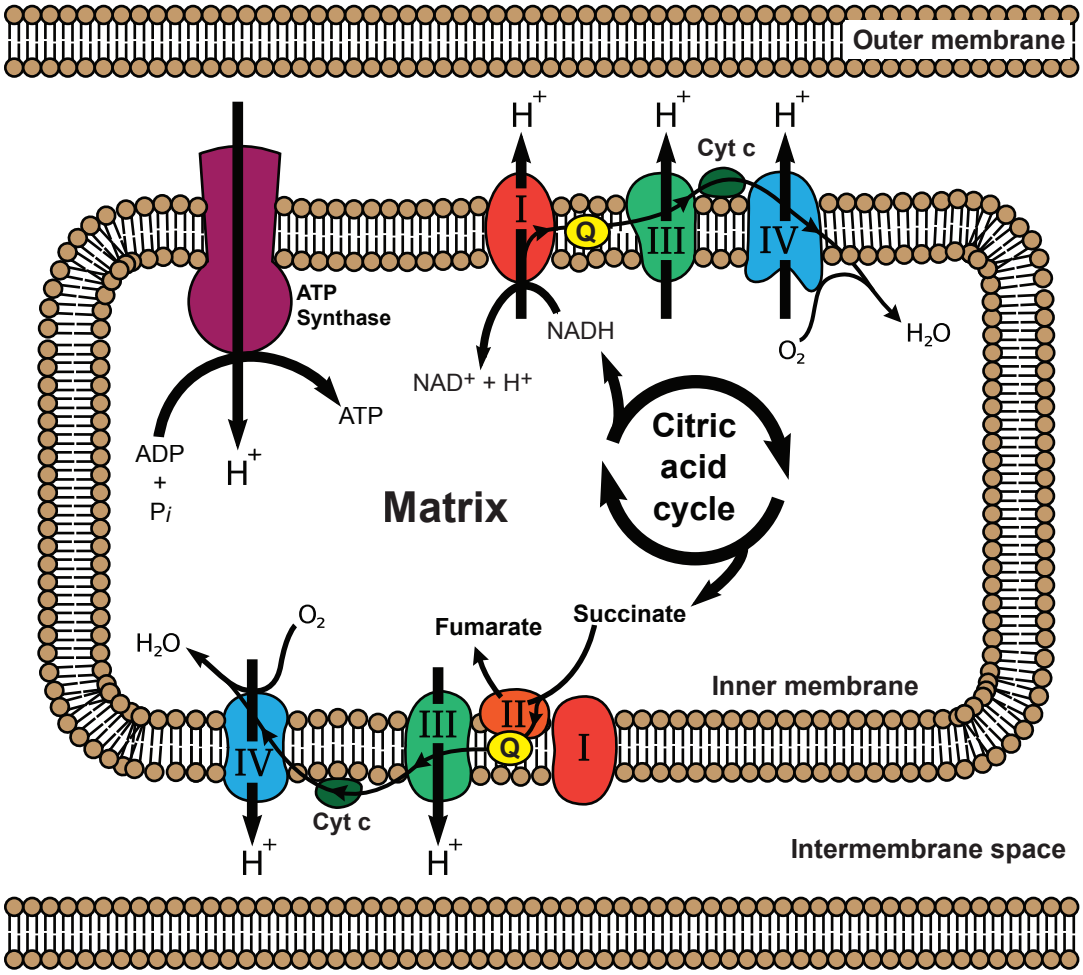

Fig. 3.1. *Diagram of the electron transport chain and its synergy with metabolism.* Complexes I, II, and IV of the electron transport chain are often damaged during the aging process, resulting in decreased MMP. Adapted from http://en.wikipedia.org/wiki/Electron_transport_chain.

Experimental Procedures

Cell Growth. BJ (human foreskin fibroblast) and Imr90 (human lung fibroblast) cells were obtained from ATCC at population doublings (PD) 21 and 27, respectively. Cells were cultured as monolayers in Dubelco's modified medium (DMEM; ATCC) supplemented with 10% (v/v) fetal bovine serum (FBS; Atlanta Biologicals) and 5% CO_2 humidified air at 37 °C. Monolayers were grown to 80% confluency in T-150 flasks with the growth medium (25 ml) changed every 2-3 days. Separate incubators were used for both the 3% and 20% oxygen growth conditions, with nitrogen gas used to maintain levels of oxygen in the 3% incubator. Cells were passaged by the removing the DMEM, washing with phosphate-buffered saline (PBS, 10 ml; Gibco), and treating the cultures with 2 ml of 1× trypsin-EDTA (Gibco) for 5 minutes in the incubator. The released cells were then resuspended in supplemented DMEM (8 ml), with 200 μl aliquots removed for cell counting and 2 ml aliquots removed for the seeding of new flasks for cell growth containing supplemented DMEM (30 ml). Population doublings were calculated using the formula: log (N/Ni) ×3.33 (N = number of cells, Ni = initial seeded number of cells). Dimethyl sulfoxide (DMSO; Sigma) was added to the remaining cell suspension in order to provide a 10% DMSO and DMEM cocktail. Five aliquots (2 ml each) were frozen at -80 °C for 4 hrs using cryotube vials (Nunc). These vials were then transferred to a Biocane (Thermolyne) for storage in liquid nitrogen.

β-Gal and DAPI Staining. Cells were collected at 80% confluency by removing the DMEM, washing with PBS (10 ml), and treating the cells with 1× trypsin-EDTA (2 ml; 5 min). The released cells were resuspended in supplemented DMEM (8 ml), and an aliquot (200 μl) was removed for cell counting. Staining was then performed using 35 mm glass bottom culture dishes, each containing a 14 mm microwell (MatTek), and seeded with 1 $\times 10^4$ cells. The newly seeded cells were allowed to adhere and grow overnight for both β-galactosidase (β-Gal) and 4', 6-diamidino-2-phenylindole (DAPI) staining. Invitrogen's β-Gal staining kit was used following the directions of the manufacturer. The β-Gal staining was allowed to proceed for 8-12 hrs at room temperature before images were taken using light microscopy (Nikon, 2× phase 1 objective). DAPI (Invitrogen) staining was carried out at 37 °C for 10 minutes in 5 ml of DAPI (800 μM) in

supplemented DMEM. Cells were then washed with PBS (5 ml) and resuspended in supplemented DMEM (5 ml). Confocal microscopy was performed on live cells using a Zeiss LSM-510 laser-scanning microscope (40× water immersion DIC 3,4 objective) and 3D images of nuclei were collected using excitation and emission wavelengths of 375 and 470 nm, respectively.

FACS Analysis. Fluorescence activated cell sorting (FACS) analysis was carried out using Mitotracker Green FM (Invitrogen). Cells were collected at 80% confluency by removing the DMEM, washing with PBS (10 ml), treating the cells with 1× trypsin-EDTA (2 ml; 5 min), and resuspending the released cells in supplemented DMEM (8 ml). Following resuspension, cells (5×10^5) were placed in a 15 ml tube and supplemented DMEM was added to a final volume of 10 ml. Mitotracker Green FM (1 μl of a 1 mM stock solution prepared in DMSO) was added to the 10 ml cell suspension giving a working solution of 100 nM. The cells were then incubated for 10 minutes with the stain at 37 °C, centrifuged (750 ×g; 2 min), washed twice with ice-cold PBS (10 ml; with an intermediate centrifugation step at 750 ×g for 2 min), centrifuged (750 ×g; 2 min), then resuspended in ice-cold PBS (1 ml) and put on ice. Mitochondrial staining intensity was analyzed by using excitation and emission wavelengths of 490 and 519 nm, respectively.

3D Cellular Imaging and Volume Analysis. Cells were grown, collected, and seeded in culture dishes as described in the above β-Gal and DAPI staining procedure. The cells were allowed to grow for 2-3 days in the confocal dishes before staining. All staining solutions were prewarmed to 37 °C and staining was performed under conditions of 5% CO_2 humidified air at 37 °C. Cells were incubated for 30 minutes with Mitotracker Green FM (3 ml, 80 nM) in supplemented DMEM, followed by a 15 minute incubation in CellTracker Orange CMRA (3 ml, 5 μM; Invitrogen) in DMEM without FBS, followed by a 10 minute incubation with DAPI (2 ml, 800 μM) in supplemented DMEM. The cells were then washed twice with DMEM (1 ml) and resuspended in supplemented DMEM for 5 minutes before imaging. Cells remained viable for at least 2 hours and imaging was completed within an hour of staining. 3D images were collected by confocal microscopy (40× water immersion DIC 3,4 objective, multichannel, Z-stack) using the following excitation and emission wavelengths: 375/470 nm for DAPI, 490/519 nm for Mitotracker

Green FM, and 548/576 nm for CellTracker Orange CMRA. Z-stack parameters were as follows: 8-15 z-axis slices were taken at 0.53 μm intervals with a final Z-stack thickness of 4.27-7.45 μm. Z-stacks of cells were than imported and processed using the DAIME (digital image analysis in microbial ecology) program for computation of nuclear, mitochondrial, and cellular volumes [60, 61]. Measurements of mitochondrial and cellular volumes were determined by analysis of ten replicates. Individual slices were saved as tiff files and converted to digital movies using Adobe Flash CS4 and presented in the thesis as embedded QuickTime movies (Fig. 3.6A-H).

Results and Discussion

Lifespan and Heterochromatin Foci. Lifespan extension of cells grown under 3% O_2 conditions is well documented for both murine and human fibroblasts [2, 4, 62]. We observed the same behavior with two types of human primary fibroblasts, Imr90 (lung) and BJ (foreskin) cells. At 20% O_2 levels, Imr90 and BJ cells senesced at approximately 45 and 55 PD, respectively (Fig. 3.2). Senescence by both senescence-associated (SA) β-Gal staining [17] and the appearance of senescence-associated heterochromatin foci [15] (SAHF) (Fig. 3.3) supported the conclusion that both BJ and Imr90 cells were senescent.

SAHF in the BJ cells (Fig. 3.3A) is less prominent than in the Imr90 cells (Fig. 3.3B). This phenomenon has been observed previously [24] and is thought to be a result of the senescent cell signaling pathways involved. Imr90 cells are currently thought to senescence predominantly through a pRb/p16 pathway, whereas the BJ cells senescence predominantly through a p53/p21 pathway [23-25]. At conditions of 3% oxygen, lifespan was extended by 10 and 20 PDs for BJ and Imr90 cells, respectively. That the age-matched 3% old cells are not senescent is supported by the lack of prominent SA β-Gal staining and SAHF as well as the extension in lifespan. The shorter extension in lifespan observed in the BJ cells compared to the Imr90 cells may be explained by the BJ cells innate resistance to oxidative stress; therefore, lower oxygen growth conditions would be expected to have a greater impact on the Imr90 cells [2, 63].

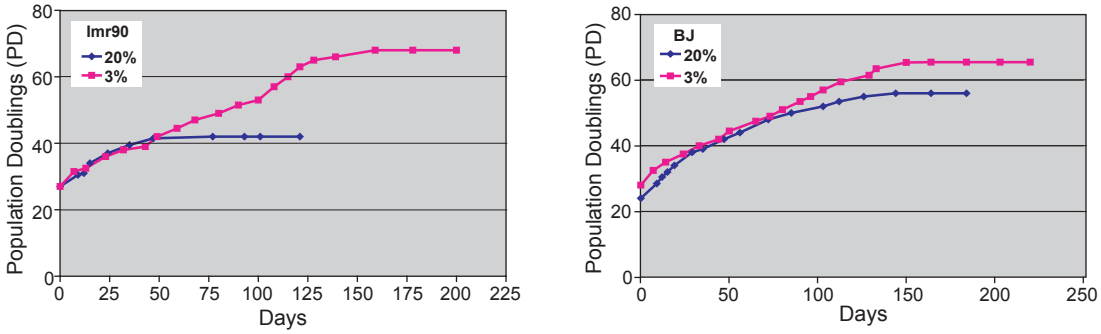

Fig. 3.2. *Lifespan assays of both BJ and Imr90 cells at 3 and 20% oxygen growth conditions.* Imr90 cells senesced at PD 43 under 20% oxygen and at PD 65 under 3% oxygen. BJ cells senesced at PD 55 under 20% oxygen and at PD 65 under 3% oxygen.

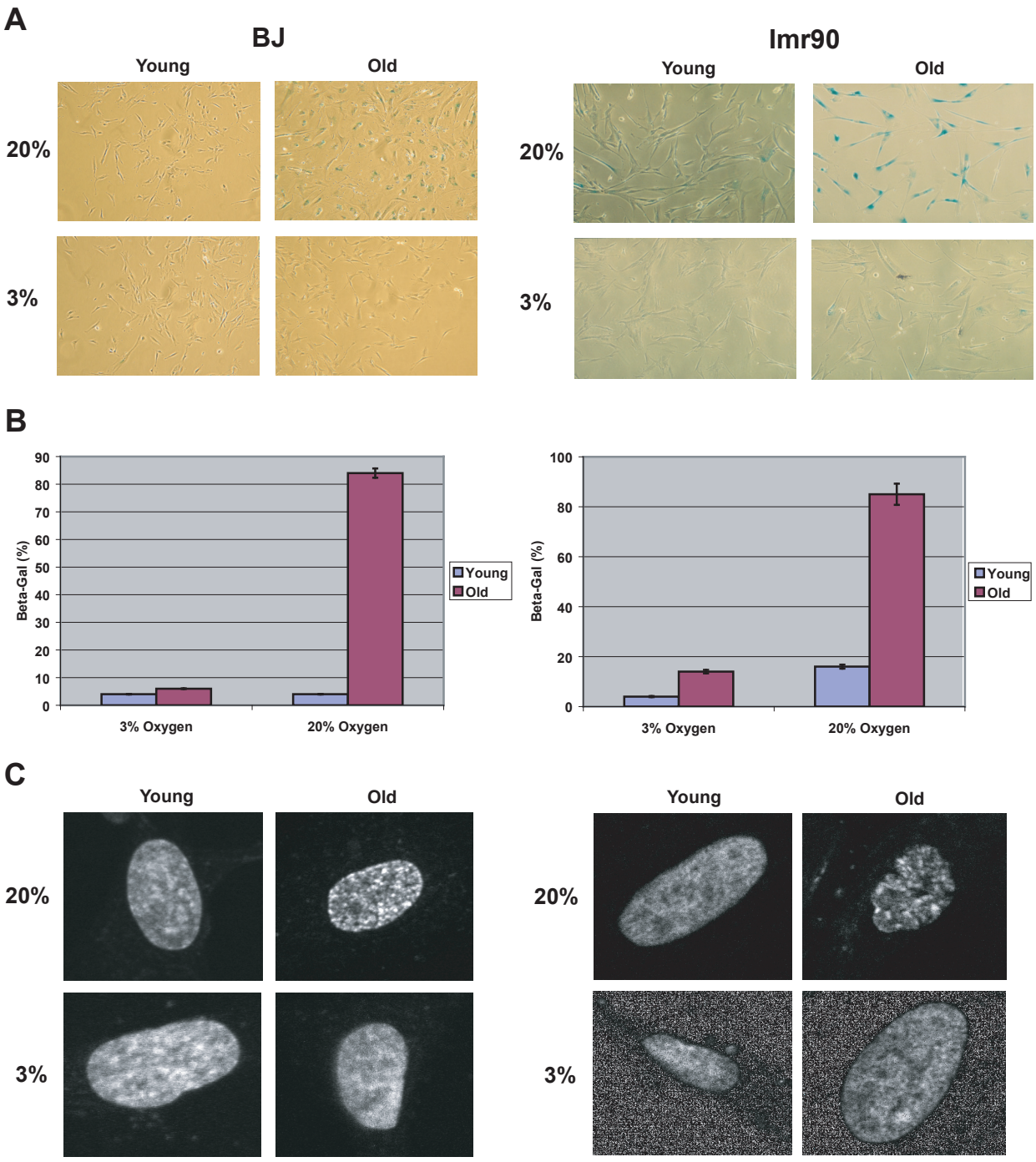

Fig. 3.3. *Representative SA β-Gal and DAPI staining images of BJ and Imr90 cells the average number of SA β-Gal positive cells.* **A**, β-Gal staining for young and old BJ and Imr90 cells. **B**, Numerical estimate of senescence via *SA β-Gal staining*. Note that both cell lines were senescent at the 20% oxygen/old condition. **C**, DAPI staining to evaluate SAHF formation. All results confirm that the 20% oxygen "old" cells were senescent. BJ cells: 20% young cells were at PD 30 and senescent cells were at PD 55. The 3% young cells were at PD 30 and the age matched old cells were at PD 57. Imr90 cells: 20% young cells were at PD 30 and senescent cells were at PD 45. The Imr90 3% young cells were at PD 30 and the age matched old cells were at PD 49.

Mitochondrial Membrane Potential and Permeability. MitoTracker Green FM can be utilized to measure mitochondrial membrane potential [64]. The dye behaves similarly to Rh123, a stain that has also been utilized to measure membrane potential [65, 66]. These cationic and lipophilic dyes accumulate within the mitochondria by binding to mitochondrial membrane constituents. However, Green FM exhibits higher mitochondrial retention relative to Rh123, with stain uptake dependent upon actively respiring mitochondria. The relative changes in membrane potential are shown via FACS analysis (Fig. 3.4). The Imr90 cells grown under 20% O_2 exhibited a lower membrane potential than those grown under 3% O_2, with no change observed in mitochondrial membrane potential with increased PDs and senescence. In contrast, the BJ cells exhibited no change in membrane potential between 3% and 20% O_2 growth conditions and exhibited an increase in membrane potential with increased PDs and senescence (Fig. 3.4).

The decrease in membrane potential of Imr90 cells at 20 percent oxygen could be due to the increase in oxidative stress and damage at the high, non-native level of oxygen [2-4, 59, 67, 68]. The absence of change in membrane potential of Imr90 cells with age and senescence is not a complete surprise as this behavior was reported previously [50]. The lack of change in membrane potential of BJ cells under 3% and 20% O_2 may be explained by the innate resistance to oxidative stress that these cells exhibit [2, 63]. This resistance in BJ cells is reflected by their higher number of PDs relative to Imr90 cells (Fig. 3.2). Our results are in alignment with the studies of Campisi and co-workers, where it was shown that murine fibroblasts have shorter replicative lifespans relative to human fibroblasts due to higher sensitivity to oxidative stress [4, 67, 69]. It can be inferred from these results that changes in membrane potential are cell type specific, suggesting that Imr90 and BJ cells respond differently to oxidative stress and aging.

The increase in membrane potential of BJ cells with age seems to be counterintuitive. However, membrane composition and permeability may also be affected in addition to membrane potential as a result of the aging process [51, 68, 70]. Dye uptake into the mitochondria may no longer be completely dependent on membrane potential, and an observed increase in uptake may be reflecting permeability/membrane composition changes rather than a true increase in MMP.

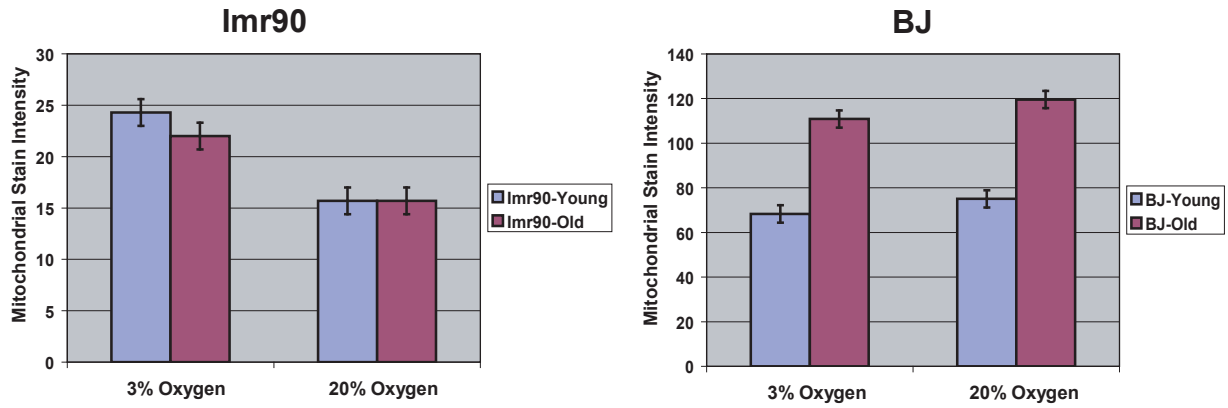

Fig. 3.4. *Average mitochondrial stain intensities of Imr90 and BJ cells with age under 3% and 20% oxygen levels.* 20% BJ young cells were at PD31 and senescent cells at PD 54. Age matched 3% BJ young cells were at PD33 and old cells at PD56. 20% Imr90 young cells were at PD33 and senescent cells at PD44. Age matched 3% Imr90 young cells were at PD31 and old cells at PD51. Mitochondrial stain intensity was determined based on relative fluorescence per cell of MitoTracker Green FM dye by FACS analysis at 516nm. Error bars are for measurements of 10 replicates.

These changes may result in mitochondrial swelling [68], a phenotype observed in neuronal cells in rats and hepatocytes in mice [51, 70]. This was also further supported by BJ mitochondrial volume measurements which were shown to increase significantly with senescence at 20% oxygen conditions as discussed below (Fig. 3.5).

Mitochondria and cell volume experiments were performed using 3D confocal images of both BJ and Imr90 cells. Nuclear, mitochondrial, and cellular stains were utilized and the resulting 3D images were processed using the DAIME program [60]. In essence, digital images were captured at specified "slices" through individual cells (Table 3.1) and these stacked images were used to calculate both volume and morphology. Extracted numerical data are shown in Fig. 3.5 with compiled example slices in Fig. 3.6A-H.

Both mitochondria and cell volumes increased significantly with senescence at 20% oxygen conditions for both BJ and Imr90 cells (Fig. 3.5). This phenomenon has been shown to occur in monkey and rat cerebella as well as in human epithelial cells and is thought to be a result of attenuated fission processes that induce mitochondrial hypertrophy or enlargement [39, 41-43, 45, 46]. These increases, along with the typical flattened morphology, can be seen when comparing young 20% or 3% BJ and Imr90 cells to those that have undergone senescence (Fig. 3.4). Despite the increases in volume with senescence the actual percent of mitochondrial volume per cell volume decreased significantly (Fig. 3.5).

Only one other study to date has analyzed the percent of mitochondrial volume versus cell volume. This study was performed on rabbit cerebella and similar results were obtained [71]. The next closest study was performed on mitochondria volume per tissue density in rat cerebella and no significant changes were reported with age [41, 46]. Our results with both BJ and Imr90 cells under 3% O_2 conditions, typical of *in vivo* oxygen conditions, also showed no significant changes in the percent of mitochondria volume per cell volume. The fact that no significant changes in both mitochondria and cell volumes were seen with age under 3% O_2 conditions along with a significant decrease in mitochondria and cell volumes when compared to 20% O_2 conditions suggests that the increases in both mitochondria and cell volumes are a result of senescence under conditions

of high oxidative stress. Interestingly, the percent of mitochondria volume per cell volume under conditions of 3% O_2 were shown to be relatively the same as the senescent cells. This can be attributed to the fact that under conditions of 3% O_2, cells produce less energy by mitochondrial oxidative phosphorylation, resulting in a decrease of the percent of mitochondrial volume per cell volume.

Also of note were clear pockets in the perinuclear cytoplasm outlined by mitochondria (Fig. 3.7). These were observed only in senescent Imr90 cells in about 30% of the population. This phenomenon was initially thought to be multi-nucleated cells; however, after utilizing a nuclear stain, it was shown that these pockets were not nuclei. Instead these pockets are presumed to be enlarged vacuoles as described by previous reports on senescent keratinocytes [72, 73].

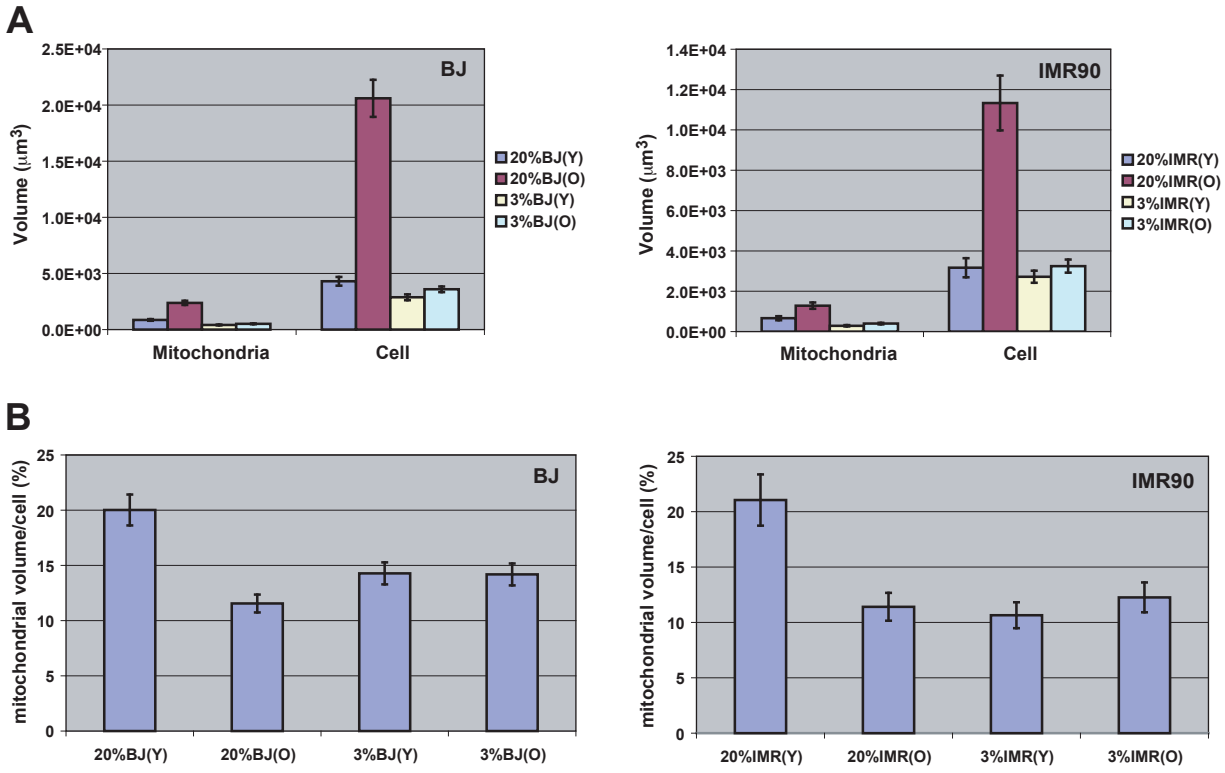

Fig. 3.5. *Changes in mitochondrial volume, cell volume, and percent of mitochondrial volume per cell volume of Imr90 and BJ cells at young, old, and senescent time-points.* **A**, Mitochondrial and cell volumes; **B**, mitochondrial volume/cell. 20% BJ young cells were at PD 31 and senescent cells at PD 54. Age matched 3% BJ young cells were at PD 33 and old cells at PD 56. 20% Imr90 young cells were at PD33 and senescent cells at PD 44. Age-matched 3% Imr90 young cells were at PD 31 and old cells at PD 51. Mitochondria and cell volumes were measured from 3-D confocal images of cells stained with MitoTracker Green FM and CellTracker Orange CMRA using the DAIME program.

Table 3.1. *Summary of Mitochondrial Images Displayed in Figures 3.6.*[a]

Cell Lines	Dimensions (μm^3) x	y	z[b]	PD	Senescent	Figure
20%BJ (Y)	54.7	116.9	7.4	31	No	A
20% BJ (O)	100.8	82.3	4.8	54	Yes	B
3% BJ (Y)	77.4	25.1	5.3	33	No	C
3% BJ(O)	80.1	50.2	5.3	56	No	D
20% Imr (Y)	131.4	30.4	5.3	33	No	E
20% Imr(O)	74.7	144.7	4.2	46	Yes	F
3% Imr (Y)	82.7	61.1	5.3	31	No	G
3% Imr (O)	46.4	77.4	6.3	51	No	H

[a]Fig. 3.6A-H are embedded QuickTime movies and require Adobe Acrobat 6.0/PDF1.5 or higher to visualize. If they cannot be seen with your present configuration, update to the newest versions of QuickTime and Adobe Acrobat.
[b]z-dimension represents the step size (slices) through the cell.

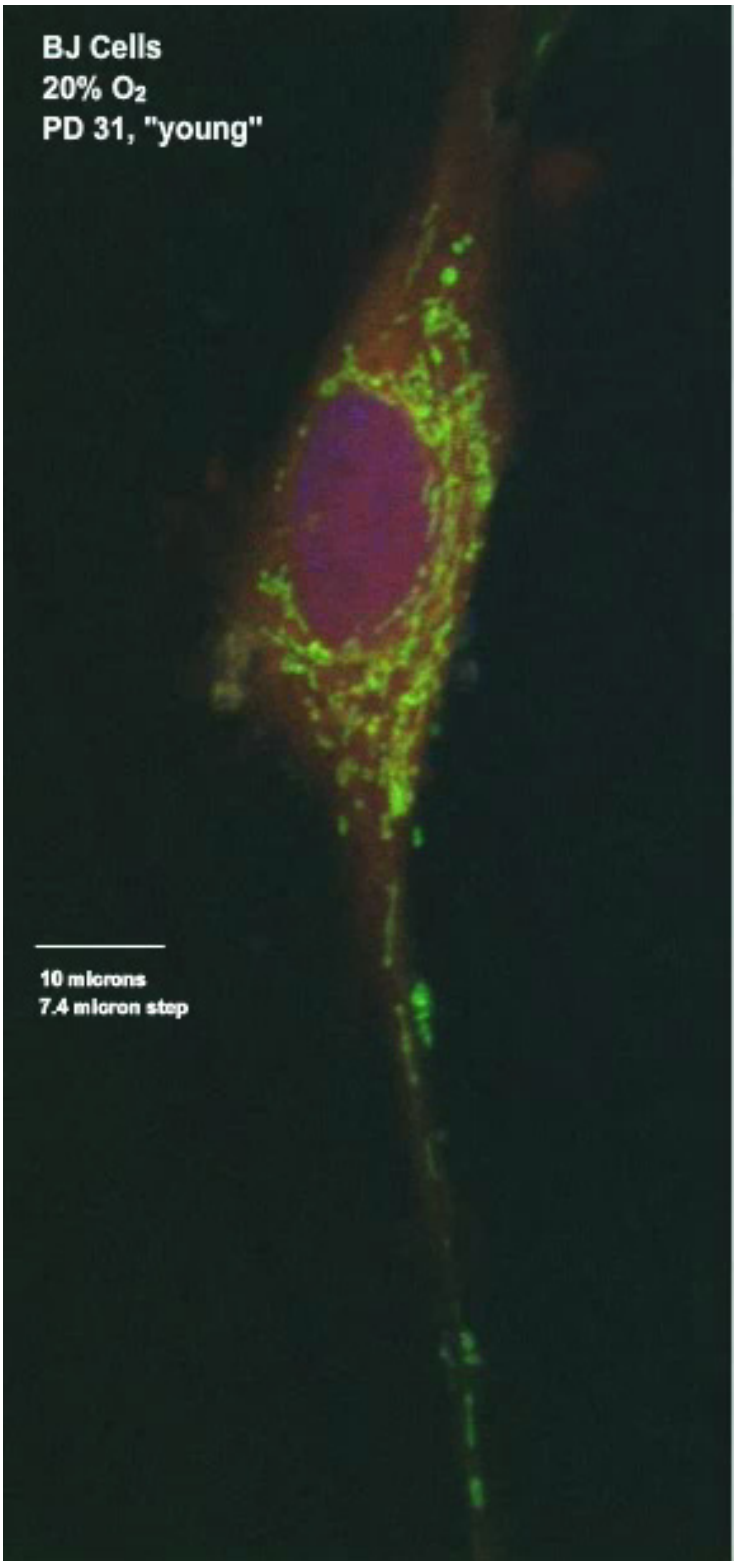

Figure 3.6A. *BJ Cells at PD 31 ("young") grown in 20% oxygen.*

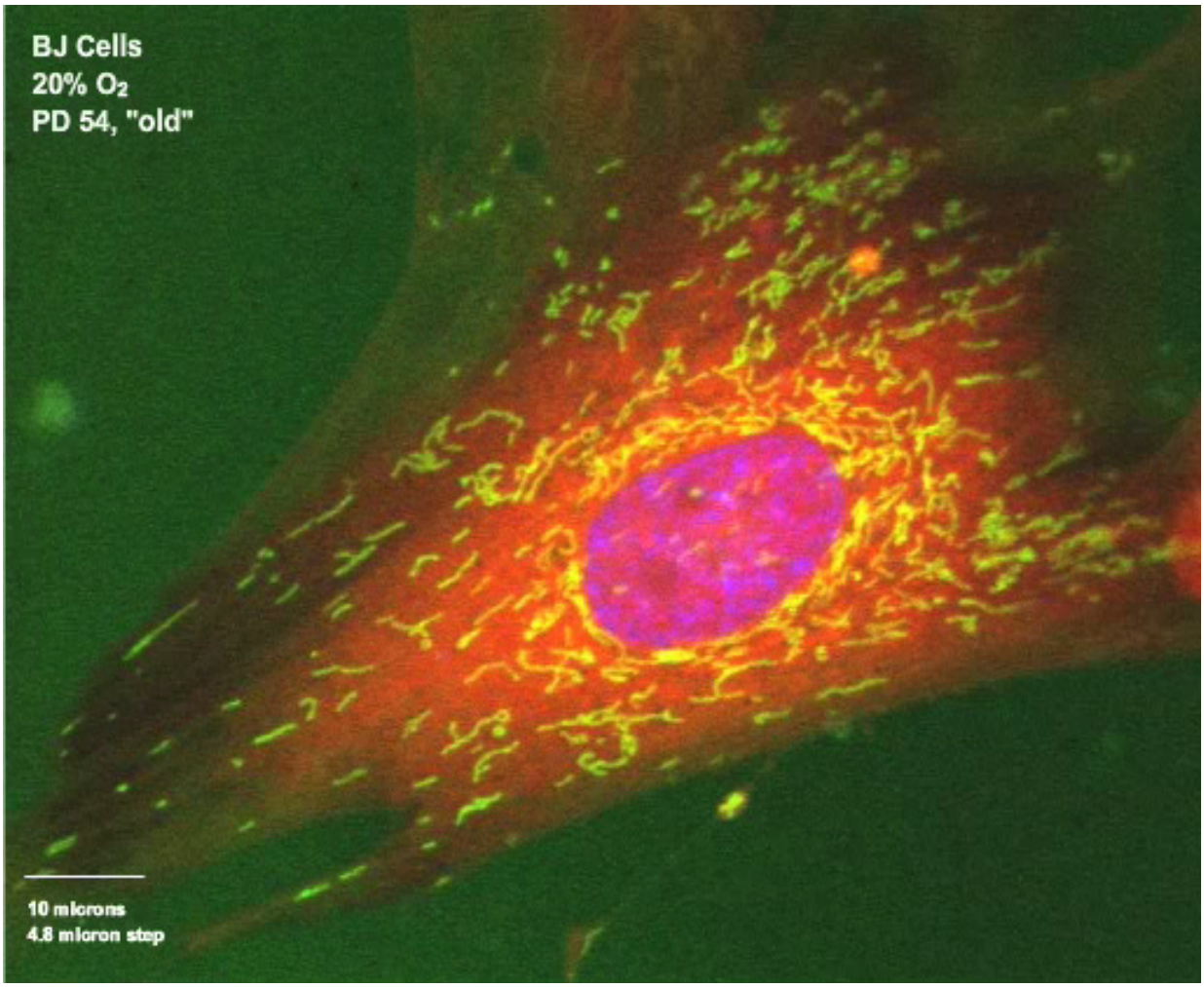

Figure 3.6B. *BJ Cells at PD 54 ("old") grown in 20% oxygen.* Cells are in the senescent state (note the flattened morphology).

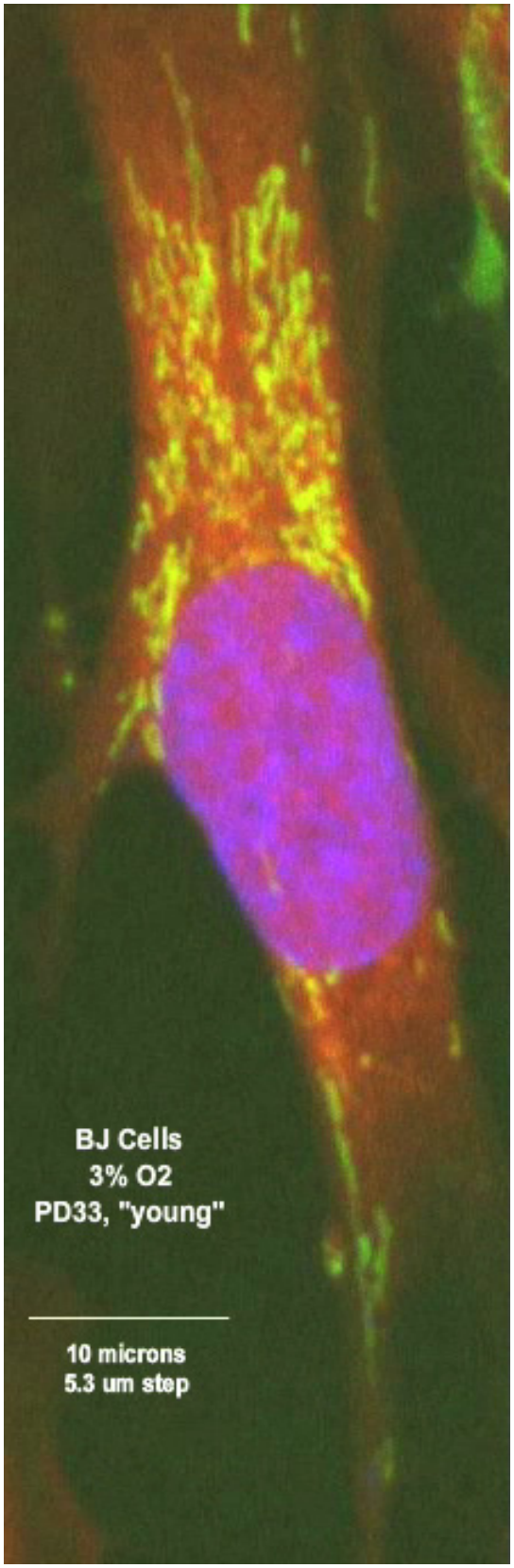

Figure 3.6C. *BJ Cells at PD 33 ("young") grown in 3% oxygen.*

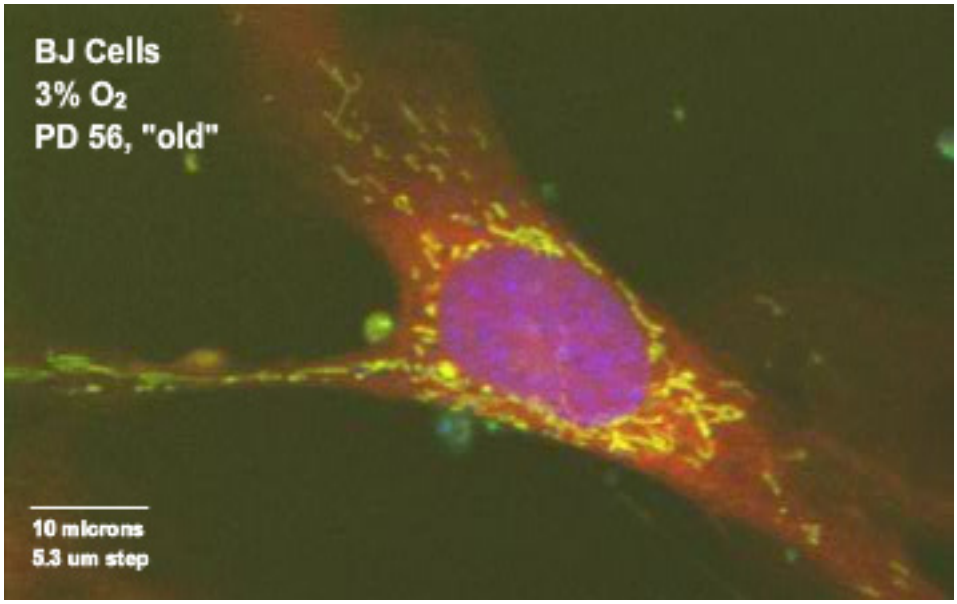

Figure 3.6D. *BJ Cells at PD 56 ("old") grown in 3% oxygen.* Cells are not senescent.

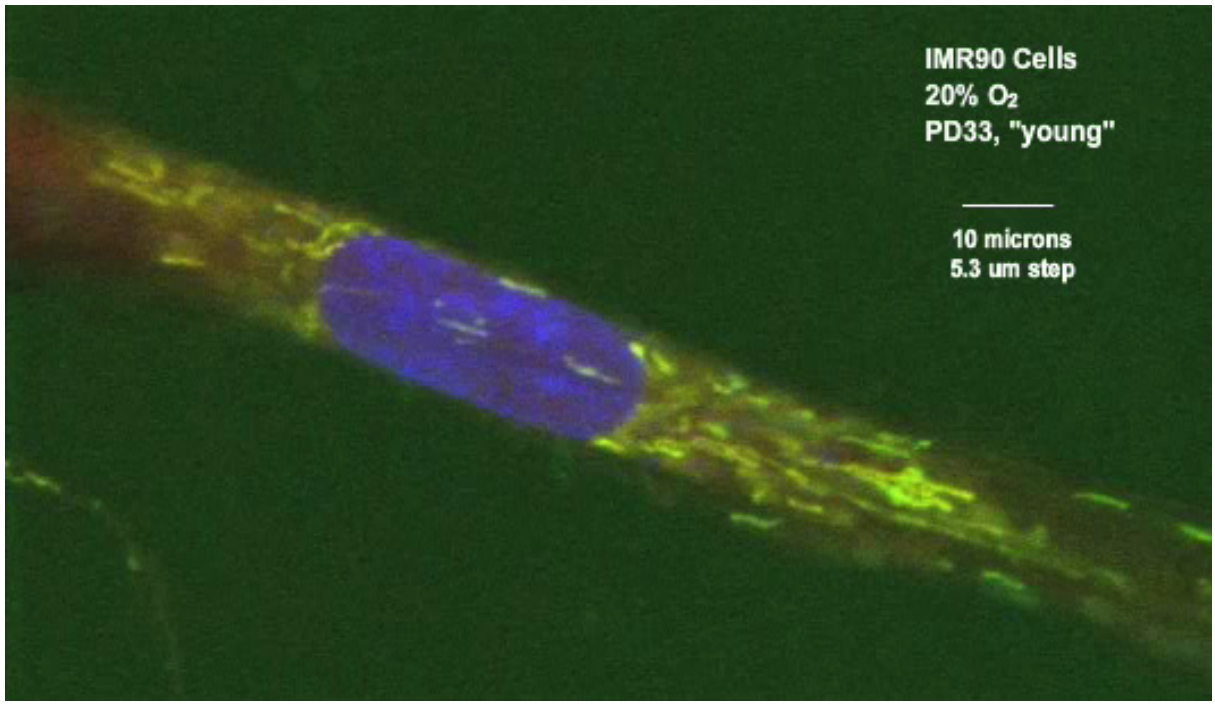

Figure 3.6E. *Imr90 Cells at PD 33 ("young") grown in 20% oxygen.*

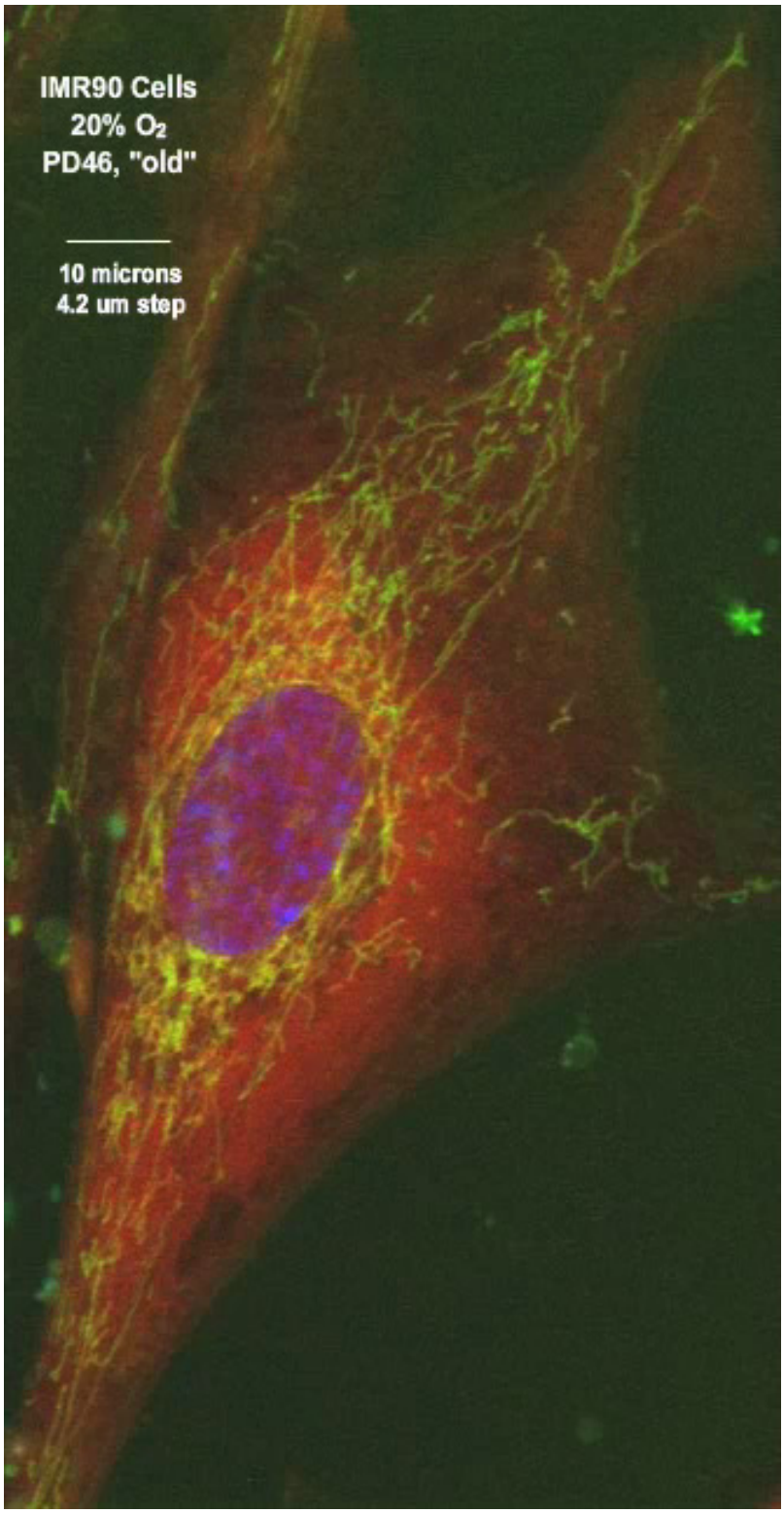

Figure 3.6F. *Imr90 Cells at PD46 ("old") grown in 20% oxygen.* Cells are in the sensecent state (note flattened morphology).

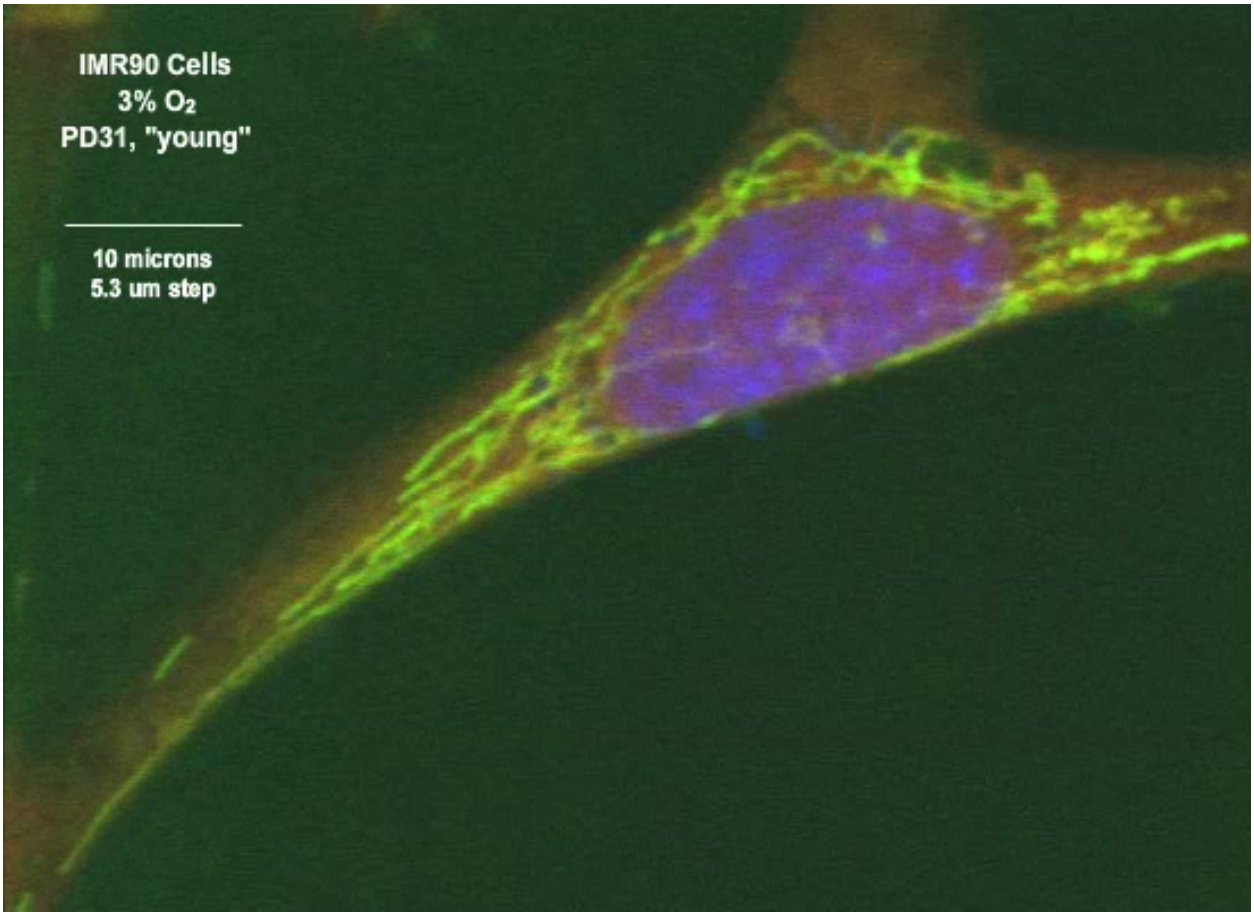

Figure 3.6G. *Imr90 Cells at PD 31 ("young") grown in 3% oxygen.*

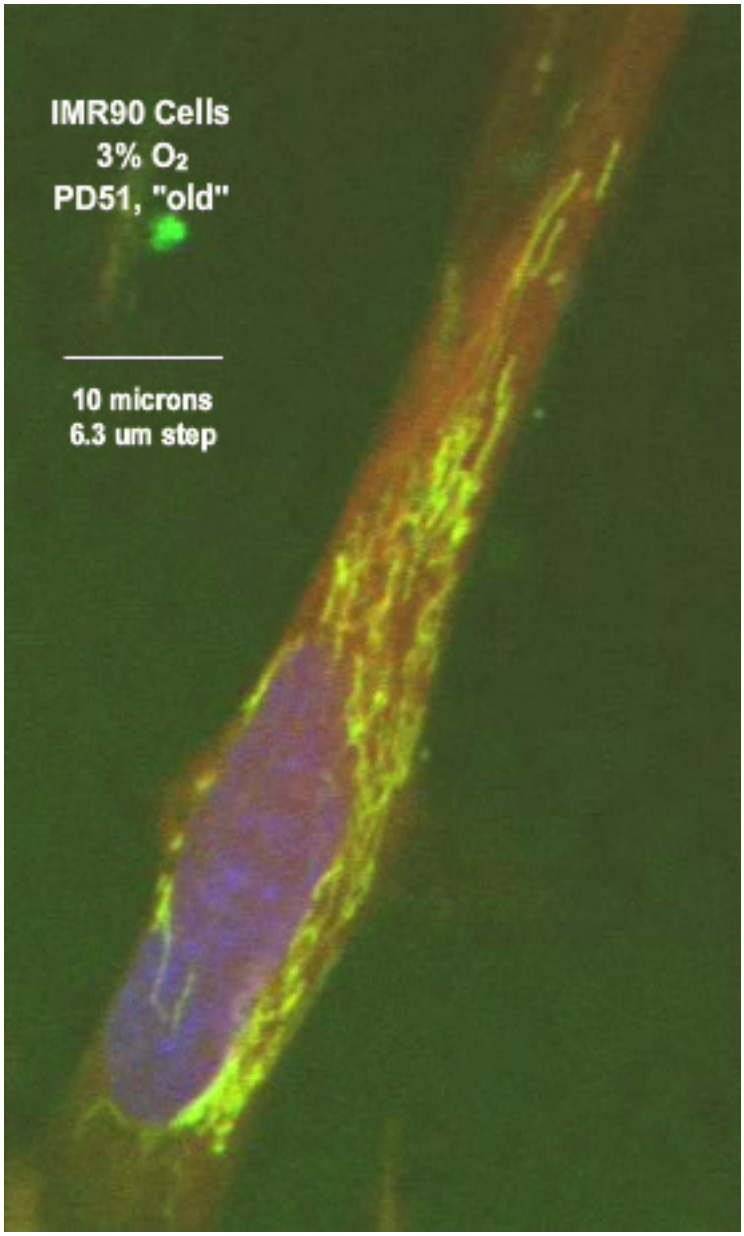

Figure 3.6H. *Imr90 Cells at PD 51 ("old") grown in 3% oxygen.* Cells are not senescent.

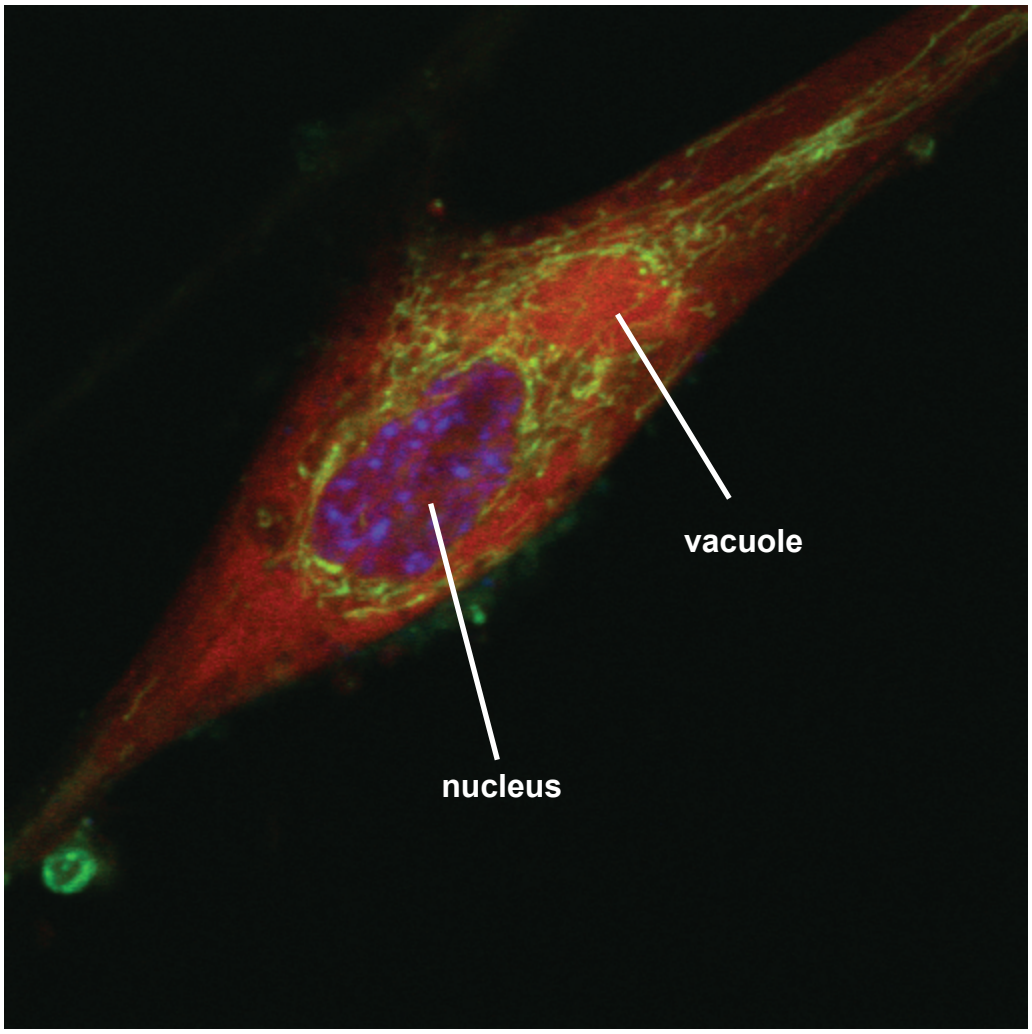

Fig. 3.7. *A senescent Imr90 cell exhibiting an enlarged vacuole.* Approximately 30% of the senescent Imr90 cells contained such structures. The assignment of the organelle to a vacuole is based upon its staining characteristics.

Summary/Conclusions

The purpose of the work described in this Chapter was to define senescence in both BJ and Imr90 cells and characterize mitochondrial life cycle dynamics in these cells as a result of *in vitro* aging under conditions of 3% and 20% O_2. Changes in the mitochondria's life cycle dynamics such as mitochondrial hypertrophy have been shown to be a result of both the aging process and oxidative damage. These changes have been associated with the attenuation of mitochondrial function such as decreases in mitochondrial metabolism and energy production [68]. A loss in mitochondrial membrane structure and function was suggested by changes in MMP with age and under different oxygen conditions. Mitochondrial membrane potential was shown to decrease significantly under high oxidative stress conditions in cells that are sensitive to oxidative stress (Imr90), and membrane potential and/or permeability was shown to change with age in more oxidative-resistant BJ cells. Significant changes in mitochondrial and cellular morphology were also seen with senescence and under different oxygen conditions. Despite increases in both mitochondria and cell volumes with senescence, the overall percent of mitochondria volume per cell volume was shown to decrease. This suggests an attenuation of mitochondrial function and a lack of mitochondrial fission resulting in hypertrophic mitochondria as a compensatory mechanism. This trend is not seen under conditions of 3% oxygen with age suggesting that degradation of mitochondrial morphology is in part a result of oxidative stress. These changes in morphology were uniform across both BJ and Imr90 cells types. When combined with previous reports in the literature, the results suggest that mitochondrial morphological changes with age are uniform for all cell types and may be the same for both *in vivo* and *in vitro* conditions [41-46]. Overall these results stress the importance of the mitochondria in the replicative senescence process.

References

1. Balin, A.K., L. Pratt, and R.G. Allen, *Effects of ambient oxygen concentration on the growth and antioxidant defenses of of human cell cultures established from fetal and postnatal skin.* Free Radic Biol Med, 2002. **32**(3): p. 257-67.
2. Chen, Q., A. Fischer, J.D. Reagan, L.J. Yan, and B.N. Ames, *Oxidative DNA damage and senescence of human diploid fibroblast cells.* Proc Natl Acad Sci U S A, 1995. **92**(10): p. 4337-41.
3. Balin, A.K., D.B. Goodman, H. Rasmussen, and V.J. Cristofalo, *The effect of oxygen and vitamin E on the lifespan of human diploid cells in vitro.* J Cell Biol, 1977. **74**(1): p. 58-67.
4. Parrinello, S., E. Samper, A. Krtolica, J. Goldstein, S. Melov, and J. Campisi, *Oxygen sensitivity severely limits the replicative lifespan of murine fibroblasts.* Nat Cell Biol, 2003. **5**(8): p. 741-7.
5. Balin, A.K. and L. Pratt, *Oxygen modulates the growth of skin fibroblasts.* In Vitro Cell Dev Biol Anim, 2002. **38**(5): p. 305-10.
6. Balin, A.K., A.J. Fisher, M. Anzelone, I. Leong, and R.G. Allen, *Effects of establishing cell cultures and cell culture conditions on the proliferative life span of human fibroblasts isolated from different tissues and donors of different ages.* Exp Cell Res, 2002. **274**(2): p. 275-87.
7. Cristofalo, V.J., R.G. Allen, R.J. Pignolo, B.G. Martin, and J.C. Beck, *Relationship between donor age and the replicative lifespan of human cells in culture: a reevaluation.* Proc Natl Acad Sci U S A, 1998. **95**(18): p. 10614-9.
8. Rohme, D., *Evidence for a relationship between longevity of mammalian species and life spans of normal fibroblasts in vitro and erythrocytes in vivo.* Proc Natl Acad Sci U S A, 1981. **78**(8): p. 5009-13.
9. Goldstein, S., *Biological aging. An essentially normal process.* JAMA, 1974. **230**(12): p. 1651-2.
10. Goldstein, S., *Replicative senescence: the human fibroblast comes of age.* Science, 1990. **249**(4973): p. 1129-33.
11. Peacocke, M. and J. Campisi, *Cellular senescence: a reflection of normal growth control, differentiation, or aging?* J Cell Biochem, 1991. **45**(2): p. 147-55.
12. Campisi, J., *Cellular senescence as a tumor-suppressor mechanism.* Trends Cell Biol, 2001. **11**(11): p. S27-31.
13. Schneider, E.L. and Y. Mitsui, *The relationship between in vitro cellular aging and in vivo human age.* Proc Natl Acad Sci U S A, 1976. **73**(10): p. 3584-8.
14. Yegorov, Y.E. and A.V. Zelenin, *Duration of senescent cell survival in vitro as a characteristic of organism longevity, an additional to the proliferative potential of fibroblasts.* FEBS Lett, 2003. **541**(1-3): p. 6-10.
15. Zhang, R., M.V. Poustovoitov, X. Ye, H.A. Santos, W. Chen, S.M. Daganzo, J.P. Erzberger, I.G. Serebriiskii, A.A. Canutescu, R.L. Dunbrack, J.R. Pehrson, J.M. Berger, P.D. Kaufman, and P.D. Adams, *Formation of MacroH2A-containing senescence-associated heterochromatin foci and senescence driven by ASF1a and HIRA.* Dev Cell, 2005. **8**(1): p. 19-30.
16. Ohtani, N., D.J. Mann, and E. Hara, *Cellular senescence: its role in tumor suppression and aging.* Cancer Sci, 2009. **100**(5): p. 792-7.

17. Dimri, G.P., X. Lee, G. Basile, M. Acosta, G. Scott, C. Roskelley, E.E. Medrano, M. Linskens, I. Rubelj, O. Pereira-Smith, and et al., *A biomarker that identifies senescent human cells in culture and in aging skin in vivo.* Proc Natl Acad Sci U S A, 1995. **92**(20): p. 9363-7.
18. Krishna, D.R., B. Sperker, P. Fritz, and U. Klotz, *Does pH 6 beta-galactosidase activity indicate cell senescence?* Mech Ageing Dev, 1999. **109**(2): p. 113-23.
19. Yegorov, Y.E., S.S. Akimov, R. Hass, A.V. Zelenin, and I.A. Prudovsky, *Endogenous beta-galactosidase activity in continuously nonproliferating cells.* Exp Cell Res, 1998. **243**(1): p. 207-11.
20. Cristofalo, V.J., *SA beta Gal staining: biomarker or delusion.* Exp Gerontol, 2005. **40**(10): p. 836-8.
21. Braig, M., S. Lee, C. Loddenkemper, C. Rudolph, A.H. Peters, B. Schlegelberger, H. Stein, B. Dorken, T. Jenuwein, and C.A. Schmitt, *Oncogene-induced senescence as an initial barrier in lymphoma development.* Nature, 2005. **436**(7051): p. 660-5.
22. Michaloglou, C., L.C. Vredeveld, M.S. Soengas, C. Denoyelle, T. Kuilman, C.M. van der Horst, D.M. Majoor, J.W. Shay, W.J. Mooi, and D.S. Peeper, *BRAFE600-associated senescence-like cell cycle arrest of human naevi.* Nature, 2005. **436**(7051): p. 720-4.
23. Ye, X., B. Zerlanko, R. Zhang, N. Somaiah, M. Lipinski, P. Salomoni, and P.D. Adams, *Definition of pRB- and p53-dependent and -independent steps in HIRA/ASF1a-mediated formation of senescence-associated heterochromatin foci.* Mol Cell Biol, 2007. **27**(7): p. 2452-65.
24. Narita, M., S. Nunez, E. Heard, A.W. Lin, S.A. Hearn, D.L. Spector, G.J. Hannon, and S.W. Lowe, *Rb-mediated heterochromatin formation and silencing of E2F target genes during cellular senescence.* Cell, 2003. **113**(6): p. 703-16.
25. Dirac, A.M. and R. Bernards, *Reversal of senescence in mouse fibroblasts through lentiviral suppression of p53.* J Biol Chem, 2003. **278**(14): p. 11731-4.
26. Bertoni-Freddari, C., P. Fattoretti, B. Giorgetti, M. Solazzi, M. Balietti, and W. Meier-Ruge, *Role of mitochondrial deterioration in physiological and pathological brain aging.* Gerontology, 2004. **50**(3): p. 187-92.
27. Annex, B.H., W.E. Kraus, G.L. Dohm, and R.S. Williams, *Mitochondrial biogenesis in striated muscles: rapid induction of citrate synthase mRNA by nerve stimulation.* Am J Physiol, 1991. **260**(2 Pt 1): p. C266-70.
28. Song, W., B. Bossy, O.J. Martin, A. Hicks, S. Lubitz, A.B. Knott, and E. Bossy-Wetzel, *Assessing mitochondrial morphology and dynamics using fluorescence wide-field microscopy and 3D image processing.* Methods, 2008. **46**(4): p. 295-303.
29. Lopez-Lluch, G., P.M. Irusta, P. Navas, and R. de Cabo, *Mitochondrial biogenesis and healthy aging.* Exp Gerontol, 2008. **43**(9): p. 813-9.
30. Hoppins, S., L. Lackner, and J. Nunnari, *The machines that divide and fuse mitochondria.* Annu Rev Biochem, 2007. **76**: p. 751-80.
31. Nagino, M., M. Tanaka, M. Nishikimi, Y. Nimura, H. Kubota, M. Kanai, T. Kato, and T. Ozawa, *Stimulated rat liver mitochondrial biogenesis after partial hepatectomy.* Cancer Res, 1989. **49**(17): p. 4913-8.
32. Freyssenet, D., P. Berthon, and C. Denis, *Mitochondrial biogenesis in skeletal muscle in response to endurance exercises.* Arch Physiol Biochem, 1996. **104**(2): p. 129-41.

33. Lee, H.C., P.H. Yin, C.W. Chi, and Y.H. Wei, *Increase in mitochondrial mass in human fibroblasts under oxidative stress and during replicative cell senescence.* J Biomed Sci, 2002. **9**(6 Pt 1): p. 517-26.
34. Baloh, R.H., R.E. Schmidt, A. Pestronk, and J. Milbrandt, *Altered axonal mitochondrial transport in the pathogenesis of Charcot-Marie-Tooth disease from mitofusin 2 mutations.* J Neurosci, 2007. **27**(2): p. 422-30.
35. Wu, C.W., Y.H. Ping, J.C. Yen, C.Y. Chang, S.F. Wang, C.L. Yeh, C.W. Chi, and H.C. Lee, *Enhanced oxidative stress and aberrant mitochondrial biogenesis in human neuroblastoma SH-SY5Y cells during methamphetamine induced apoptosis.* Toxicol Appl Pharmacol, 2007. **220**(3): p. 243-51.
36. Barsoum, M.J., H. Yuan, A.A. Gerencser, G. Liot, Y. Kushnareva, S. Graber, I. Kovacs, W.D. Lee, J. Waggoner, J. Cui, A.D. White, B. Bossy, J.C. Martinou, R.J. Youle, S.A. Lipton, M.H. Ellisman, G.A. Perkins, and E. Bossy-Wetzel, *Nitric oxide-induced mitochondrial fission is regulated by dynamin-related GTPases in neurons.* EMBO J, 2006. **25**(16): p. 3900-11.
37. Chang, D.T., G.L. Rintoul, S. Pandipati, and I.J. Reynolds, *Mutant huntingtin aggregates impair mitochondrial movement and trafficking in cortical neurons.* Neurobiol Dis, 2006. **22**(2): p. 388-400.
38. Lee, H.C. and Y.H. Wei, *Mitochondrial biogenesis and mitochondrial DNA maintenance of mammalian cells under oxidative stress.* Int J Biochem Cell Biol, 2005. **37**(4): p. 822-34.
39. Lee, S., S.Y. Jeong, W.C. Lim, S. Kim, Y.Y. Park, X. Sun, R.J. Youle, and H. Cho, *Mitochondrial fission and fusion mediators, hFis1 and OPA1, modulate cellular senescence.* J Biol Chem, 2007. **282**(31): p. 22977-83.
40. Bertoni-Freddari, C., P. Fattoretti, B. Giorgetti, Y. Grossi, M. Balietti, T. Casoli, G. Di Stefano, and G. Perretta, *Synaptic and mitochondrial morphometry provides structural correlates of successful brain aging.* Ann N Y Acad Sci, 2007. **1097**: p. 51-3.
41. Bertoni-Freddari, C., P. Fattoretti, T. Casoli, C. Spagna, W. Meier-Ruge, and J. Ulrich, *Morphological plasticity of synaptic mitochondria during aging.* Brain Res, 1993. **628**(1-2): p. 193-200.
42. Bertoni-Freddari, C., P. Fattoretti, B. Giorgetti, M. Solazzi, M. Balietti, G. Di Stefano, and T. Casoli, *Decay of mitochondrial metabolic competence in the aging cerebellum.* Ann N Y Acad Sci, 2004. **1019**: p. 29-32.
43. Bertoni-Freddari, C., P. Fattoretti, T. Casoli, G. Di Stefano, M. Solazzi, and W. Meier-Ruge, *Quantitative cytochemical mapping of mitochondrial enzymes in rat cerebella.* Micron, 2001. **32**(4): p. 405-10.
44. Boveris, A. and A. Navarro, *Brain mitochondrial dysfunction in aging.* IUBMB Life, 2008. **60**(5): p. 308-14.
45. Soroka, Y., Z. Ma'or, Y. Leshem, L. Verochovsky, R. Neuman, F.M. Bregegere, and Y. Milner, *Aged keratinocyte phenotyping: morphology, biochemical markers and effects of Dead Sea minerals.* Exp Gerontol, 2008. **43**(10): p. 947-57.
46. Bertoni-Freddari, C., P. Fattoretti, B. Giorgetti, M. Solazzi, M. Balietti, T. Casoli, and G. Di Stefano, *Cytochrome oxidase activity in hippocampal synaptic mitochondria during aging: a quantitative cytochemical investigation.* Ann N Y Acad Sci, 2004. **1019**: p. 33-6.

47. Bertoni-Freddari, C., P. Fattoretti, R. Paoloni, U. Caselli, B. Giorgetti, and M. Solazzi, *Inverse correlation between mitochondrial size and metabolic competence: a quantitative cytochemical study of cytochrome oxidase activity.* Naturwissenschaften, 2003. **90**(2): p. 68-71.
48. Sastre, J., A. Millan, J. Garcia de la Asuncion, R. Pla, G. Juan, Pallardo, E. O'Connor, J.A. Martin, M.T. Droy-Lefaix, and J. Vina, *A Ginkgo biloba extract (EGb 761) prevents mitochondrial aging by protecting against oxidative stress.* Free Radic Biol Med, 1998. **24**(2): p. 298-304.
49. Hagen, T.M., D.L. Yowe, J.C. Bartholomew, C.M. Wehr, K.L. Do, J.Y. Park, and B.N. Ames, *Mitochondrial decay in hepatocytes from old rats: membrane potential declines, heterogeneity and oxidants increase.* Proc Natl Acad Sci U S A, 1997. **94**(7): p. 3064-9.
50. Cavazzoni, M., S. Barogi, A. Baracca, G. Parenti Castelli, and G. Lenaz, *The effect of aging and an oxidative stress on peroxide levels and the mitochondrial membrane potential in isolated rat hepatocytes.* FEBS Lett, 1999. **449**(1): p. 53-6.
51. Goodell, S. and G. Cortopassi, *Analysis of oxygen consumption and mitochondrial permeability with age in mice.* Mech Ageing Dev, 1998. **101**(3): p. 245-56.
52. Lin, D.T., J. Wu, D. Holstein, G. Upadhyay, W. Rourk, E. Muller, and J.D. Lechleiter, *Ca2+ signaling, mitochondria and sensitivity to oxidative stress in aging astrocytes.* Neurobiol Aging, 2007. **28**(1): p. 99-111.
53. LaFrance, R., N. Brustovetsky, C. Sherburne, D. Delong, and J.M. Dubinsky, *Age-related changes in regional brain mitochondria from Fischer 344 rats.* Aging Cell, 2005. **4**(3): p. 139-45.
54. Savitha, S. and C. Panneerselvam, *Mitochondrial membrane damage during aging process in rat heart: potential efficacy of L-carnitine and DL alpha lipoic acid.* Mech Ageing Dev, 2006. **127**(4): p. 349-55.
55. Jendrach, M., S. Pohl, M. Voth, A. Kowald, P. Hammerstein, and J. Bereiter-Hahn, *Morpho-dynamic changes of mitochondria during ageing of human endothelial cells.* Mech Ageing Dev, 2005. **126**(6-7): p. 813-21.
56. Takeyama, N., N. Matsuo, and T. Tanaka, *Oxidative damage to mitochondria is mediated by the Ca(2+)-dependent inner-membrane permeability transition.* Biochem J, 1993. **294 (Pt 3)**: p. 719-25.
57. Sastre, J., F.V. Pallardo, R. Pla, A. Pellin, G. Juan, J.E. O'Connor, J.M. Estrela, J. Miquel, and J. Vina, *Aging of the liver: age-associated mitochondrial damage in intact hepatocytes.* Hepatology, 1996. **24**(5): p. 1199-205.
58. Pepe, S., *Effect of dietary polyunsaturated fatty acids on age-related changes in cardiac mitochondrial membranes.* Exp Gerontol, 2005. **40**(8-9): p. 751-8.
59. Shigenaga, M.K., T.M. Hagen, and B.N. Ames, *Oxidative damage and mitochondrial decay in aging.* Proc Natl Acad Sci U S A, 1994. **91**(23): p. 10771-8.
60. Daims, H., S. Lucker, and M. Wagner, *daime, a novel image analysis program for microbial ecology and biofilm research.* Environ Microbiol, 2006. **8**(2): p. 200-13.
61. Kara, D., S.B. Luppens, J. van Marle, R. Ozok, and J.M. ten Cate, *Microstructural differences between single-species and dual-species biofilms of Streptococcus mutans and Veillonella parvula, before and after exposure to chlorhexidine.* FEMS Microbiol Lett, 2007. **271**(1): p. 90-7.

62. Cristofalo, V.J., *Biological Gerontology.* Science, 1977. **198**(4319): p. 818-819.
63. Lorenz, M., G. Saretzki, N. Sitte, S. Metzkow, and T. von Zglinicki, *BJ fibroblasts display high antioxidant capacity and slow telomere shortening independent of hTERT transfection.* Free Radic Biol Med, 2001. **31**(6): p. 824-31.
64. Juan, G., M. Cavazzoni, G.T. Saez, and J.E. O'Connor, *A fast kinetic method for assessing mitochondrial membrane potential in isolated hepatocytes with rhodamine 123 and flow cytometry.* Cytometry, 1994. **15**(4): p. 335-42.
65. Juan, G., R. Gil-Benso, J.E. O'Connor, and R.C. Callaghan, *Oxidative metabolism in a rat hepatoma (N13) and isolated rat hepatocytes: a flow cytometric comparative study.* Hepatology, 1996. **24**(2): p. 385-90.
66. Busuttil, R.A., M. Rubio, M.E. Dolle, J. Campisi, and J. Vijg, *Oxygen accelerates the accumulation of mutations during the senescence and immortalization of murine cells in culture.* Aging Cell, 2003. **2**(6): p. 287-94.
67. Sastre, J., F.V. Pallardo, J. Garcia de la Asuncion, and J. Vina, *Mitochondria, oxidative stress and aging.* Free Radic Res, 2000. **32**(3): p. 189-98.
68. Patil, C.K., I.S. Mian, and J. Campisi, *The thorny path linking cellular senescence to organismal aging.* Mech Ageing Dev, 2005. **126**(10): p. 1040-5.
69. Alba, C., L. Vidal, F. Diaz, A. Villena, and I.P. de Vargas, *Ultrastructural and quantitative age-related changes in capillaries of the dorsal lateral geniculate nucleus.* Brain Res Bull, 2004. **64**(2): p. 145-53.
70. Cavallaro, U., V. Castelli, U. Del Monte, and M.R. Soria, *Phenotypic alterations in senescent large-vessel and microvascular endothelial cells.* Mol Cell Biol Res Commun, 2000. **4**(2): p. 117-21.
71. Martinelli, C., P. Sartori, M. Ledda, and E. Pannese, *Mitochondria in perineuronal satellite cell sheaths of rabbit spinal ganglia: quantitative changes during life.* Cells Tissues Organs, 2007. **186**(2): p. 141-6.
72. Rheinwald, J.G., W.C. Hahn, M.R. Ramsey, J.Y. Wu, Z. Guo, H. Tsao, M. De Luca, C. Catricala, and K.M. O'Toole, *A two-stage, p16(INK4A)- and p53-dependent keratinocyte senescence mechanism that limits replicative potential independent of telomere status.* Mol Cell Biol, 2002. **22**(14): p. 5157-72.
73. Kang, M.K., C. Bibb, M.A. Baluda, O. Rey, and N.H. Park, *In vitro replication and differentiation of normal human oral keratinocytes.* Exp Cell Res, 2000. **258**(2): p. 288-97.

Chapter 4

Changes in Central Carbon Metabolism Upon Senescence of Primary Fibroblasts at 3% and 20% Oxygen Levels

Abstract

The metabolic profile of cells undergoing senescence and oxidative damage can reflect changes in cell energy metabolism and enzyme function. Previous studies have provided only limited information as to metabolite levels; in this work, multiple metabolites and pathways were targeted. Numerous central carbon metabolites of primary human fibroblasts (BJ and Imr90) were analyzed as the cells aged and senesced under conditions of 3% and 20% oxygen. In both cell types, there was an overall increase in metabolite levels with senescence, compared to a decrease or no change in these metabolite levels with aged 3% oxygen cells. This difference in the metabolic profile suggests that the attenuation of energy production with senescence is partly a result of oxidative damage (OD), since replicative senescence under hyperoxic conditions (20% O_2) is thought to occur predominantly through OD. Cell type specific differences, likely related to cell type specific OD resistances, were also seen in certain metabolite levels. It was determined that senscence and oxidative damage cause a "pooling effect" of glycolytic/TCA metabolites in the cell and may be a result of attenuated enzyme function.

Introduction

Mitochondrial metabolism is affected by age-associated dysfunction through the accumulation of oxidatively damaged cell constituents. Attenuation of function [1-8] and increase in levels [1, 2, 9-12] of metabolic enzymes should ultimately result in changes in the metabolic profile of the cell. Only a few studies have explored this sequence of events in cell culture or whole tissues [2, 9, 10, 12-14], and are limited with respect to the metabolites quantified. Reported metabolite changes include decreases in ATP levels and increases in AMP levels as determined by HPLC analysis of senescent human diploid fibroblasts [12]; increases in AMP:ATP ratios via enzymatic assay in three human fibroblast cell lines (WI-38, IDH4, Imr90) [10]; decreases in ATP levels via HPLC of aged murine skeletal muscle [9]; and increases in NADPH:NADP ratios via enzymatic assay in aged murine kidneys [2] (Fig. 1.5). With respect to glycolytic and TCA intermediates, reported metabolite changes included increases in FBP levels via enzymatic assay in senescent human diploid fibroblasts [12], increases in malate levels via enzymatic assay in aged rat livers [13], and increases in lactate levels via NMR in aged rat cerebella [14] (Fig. 1.5). Other changes in metabolite levels within cells grown in culture are to be expected as several studies have reported changes in primary carbon metabolites such as malate, fumarate, succinate, etc. in blood and urine of aged humans [15-17] (Fig. 1.5).

While these reported changes in metabolites provide some insight into metabolism with respect to aging and senescence, they suffer from a lack of completeness (1 or 2 metabolites) and the various methods used for detection. A more universal method capable of targeting multiple metabolites involved in primary carbon metabolism simultaneously will provide a more complete picture. In this Chapter, the LC-MS/MS method previously developed (Chapter 2) is used to determine the changes that occur in the primary carbon metabolite pool with age and senescence in both Imr90 and BJ cell lines. Oxygen conditions of 3% and 20% were employed as ambient sources of two levels of oxidative stress to elucidate metabolite changes in the senescence process that may be sensitive to OD. During performance of this work, the use of MALDI-TOF/TOF mass spectrometry was also evaluated for its ability to detect and quantify the primary metabolites

identified previously by LC-MS/MS.

Experimental Procedures

Cell Growth. BJ (human foreskin fibroblast) and Imr90 (human lung fibroblast) cells were obtained from ATCC at population doubling's (PD) 21 and 27 respectively. Cells were cultured as monolayers in Dubelco's modified medium (DMEM; ATCC) supplemented with 10% (v/v) fetal bovine serum (FBS; Atlanta Biologicals) and 5% CO_2 humidified air at 37 °C. Monolayers were grown to 80% confluency in T-150 flasks with the growth medium (25 ml) changed every 2-3 days. Separate incubators were used for both the 3% and 20% oxygen growth conditions. Nitrogen gas was used to maintain steady levels of 3% oxygen in the 3% oxygen incubator. Cells were passaged by removing the DMEM, washing with phosphate-buffered saline (PBS, 10 ml; Gibco), and treating the cultures with 2 ml of 1× trypsin-EDTA (Gibco) for 5 minutes in the incubator. The released cells were then resuspended in supplemented DMEM (8 ml), with 200 ul aliquots removed for cell counting and 2 ml aliquots removed for the seeding of new flasks for cell growth containing supplemented DMEM (30ml). Population doublings were calculated by the following formula: log (N/Ni) ×3.33 (N = number of cells, Ni = initial seeded number of cells). Dimethyl sulfoxide (DMSO; Sigma) was added to the remaining cell suspension in order to provide a 10% DMSO and DMEM cocktail. Five aliquots (2 ml each) were frozen at -80 °C for 4 hrs using cryotube vials (Nunc). These vials were then transferred to a Biocane (Thermolyne) for storage in liquid nitrogen.

Metabolite Extraction for MALDI Mass Spectrometry Analysis. Cells were collected at 80% confluency by removing the DMEM, washing with PBS (10 ml), using 1× trypsin-EDTA (2 ml; 5 min), and resuspended in supplemented DMEM (10 ml). Two flasks were used for young and old (3% oxygen) cells and 5 flasks were used for senescent cells. The cells for each time-point were then pooled to a final volume of 20 ml with DMEM. An aliquot (500 ul) was removed and used for cell counting via a hemocytometer. Cell density for each time-point was normalized to 7 $\times 10^6$ cells by removing an appropriate amount of each cell suspension. The cells were then

centrifuged (750 ×g; 2 min) and decanted, washed twice with 10 ml of ice-cold PBS and decanted, with an intermediate and final centrifugation step (750 ×g; 2 min). The cell pellets were then resuspended in ice-cold methanol (125 ul) and sonicated (15 sec) at 60% power on ice. Ice-cold water (125 ul) and chloroform (250 ul) were added, the suspension was vortexed and rocked (300rpm; 15 min) at 4 °C, vortexed again, and centrifuged (14000 ×g; 5 min) at 4 °C. The aqueous phase was removed and added to a new tube and stored at -20 °C.

MALDI TOF/TOF Mass Spectrometry. A volume of 0.5 μl of sample was mixed with 0.5 ul of 9 mg/ml 9-aminoacridine (matrix made in acetonitrile with 10 mmol of ammonium acetate). The mixture (1 μl) was spotted on an Opti-TOF 384-well plate and allowed to air dry. MS analyses were performed on a 4800 MALDI-TOF/TOF analyzer (Applied Biosystems/MDS-Sciex). Initial analysis using standards indicated that the negative ion mode was more sensitive than positive ion mode, so all subsequent analysis of standards and samples utilized the MS Reflector Negative operating mode. For MS/MS analysis, the MS/MS 1kV Negative operating mode was used (without CID gas). For glycolytic and TCA cycle intermediates, data were collected for an m/z range from 50 to 350. For nucleotides, the range was from 300 to 800. When utilizing the ATP signal for normalization, the entire m/z range from 50 to 800 was collected at one time. Typically, data for 500 to 1000 shots were collected and averaged for each sample spot. Samples were spotted in technical triplicates, and these three spectra were averaged. Then the average of three technical triplicates for three independent biological triplicates was averaged to generate one averaged spectrum per sample type. Averaging of spectra was performed using the Data Explorer software that accompanies the 4000 Series Applied Biosystems mass spectrometers. Peak lists containing m/z and signal intensity data were generated using the Data Explorer software and summarized using Microsoft Excel.

Optimized Extraction and LC-MS/MS Conditions for Primary Fibroblast Analysis. In order to detect all the metabolites of interest in primary fibroblasts, a total of 7-9 $\times 10^6$ cells were needed in 140 μl of extraction solvent. This cell number was achieved at 80% confluency for both young (3 and 20% oxygen) and old (3% oxygen) fibroblasts (Imr90 and BJ) in 3 T-150 flasks.

Senescent fibroblasts (Imr90 and BJ; 20% oxygen) required 6 T-150 flasks.

The final metabolite extraction protocol utilized the trypsinization method without a PBS wash (Fig. 4.1). Media was changed 2 hours before extraction. Cells were harvested at 80% confluency by using 1× trypsin-EDTA (2 ml; 10 min) in the incubator following the removal of DMEM and washed with PBS (10 ml). Cells were then resuspended in 8 ml of supplemented DMEM per flask used, removed and pooled into 1 test tube, and incubated at 37 °C (10 min) following the removal of 500 µl for cell counting. The cells were then centrifuged (750 ×g; 2 min), the media was decanted and the cells were resuspended in ice-cold methanol (70 µl), vortexed, and flash frozen in liquid nitrogen. The cell suspension was then allowed to thaw in an ice bath (5 min) and kept on ice while adding H_2O (70 µl) and chloroform (140 µl). N-acetyl glutamine (NAG) (1 µl) was also added as an internal standard to yield a final concentration of 1 ug/ml. The suspension was then vortexed, mixed in a rotator (10 min) at 4 °C, vortexed again, and centrifuged (14000 ×g; 5 min) at 4 °C. The aqueous layer (130 µl) was carefully removed, flash frozen in liquid nitrogen, and stored at -80 °C. Prior to analysis the samples were thawed in an ice-bath for 5 minutes and aliquots (40 ul) were put in 250 ul test tubes, flash frozen, and stored at -80 °C. The aliquots were then thawed as needed in an ice-bath for 5 minutes and used for sample analysis.

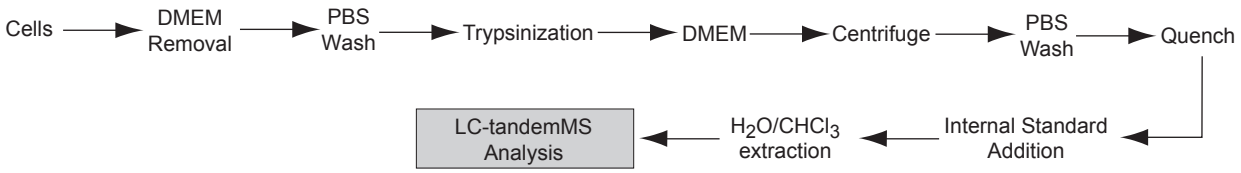

Fig. 4.1. *Optimized metabolite extraction method for LC-MS/MS*.

Samples were injected (10 µl) and analyzed by LC-MS/MS in the ESI mode on a 4000 QTrap interfaced with the Ultimate microLC system (LC Packings/Dionex). ESI spray voltage was -4500 V in negative mode. Nitrogen was used as sheath gas at 20 psi, as Gas 1 at 25 psi, as Gas 2 at 50 psi, and as the collision gas was set to high. The interface heater was on and the temperature was set to 200 °C. LC separation was performed on a Luna NH_2 aminopropyl column (Phenomenex) at pH 9.4 in HILIC mode. The column dimensions were 50 mm x 2 mm and the particles were 5 um in diameter and with pore size of 100 angstroms. The LC solvents were Solvent A: 20mM

ammonium acetate + 20mM ammonium hydroxide in 95:5 water:acetonitrile, pH 9.45; Solvent B: acetonitrile. The flow rate was 60 μl/min for the actual MS/MS run (0-125 min) and then was increased to 150 μl/min for column re-equilibration (125-150 min). The solvent gradient was t = 0 min, 100% B; t = 15 min, 100% B; t = 30 min, 100% A; t = 125 min, 100% A, 50 ul/min; t = 135 min, 100% A, 150 ul/min; t = 140 min, 100% B; t = 148 min, 100% B, 150 ul/min; t = 150 min, 100% B, 50 ul/min. A group of samples were also dried to completion to determine the effects of concentration on the metabolite profile. Flash frozen samples (500 ul) were used and dried to completion in a CentriVap Concentrator (Labconco). The samples were then resuspended in 50% methanol (500 ul). These samples were then analyzed by LC-MS/MS in technical triplicate for comparison to the original non-dried flash frozen samples.

Averaging of peak area spectra for each metabolite in biological triplicate was performed using the Analyst software that accompanies the 4000 QTrap and summarized using Microsoft Excel. Each metabolite was normalized to both the internal standard NAG and cell number to enable cross-sample comparison. NAG has been used before as an internal standard for metabolites of glycolysis and TCA and shown to perform similarly to isotopically labeled internal standards for the corresponding metabolites of interest [18].

Results and Discussion

A successful outcome for this work necessitated that a robust method of primary cell extraction be established. This is not a trivial problem for primary senescent cells where obtaining enough cell mass for analysis can be an enormous challenge. In order to establish proof of concept, preliminary metabolite profiling data was achieved utilizing MALDI TOF/TOF on the Imr90 cell cultures derived from the young, old, and senescent cell stocks that were created under 3% and 20% O_2. MALDI TOF/TOF mass spectrometry, while more traditionally used for peptide and large molecule analyses, can also be used for small polar metabolite analysis as long as an appropriate matrix can be found that has relatively few matrix ions in the mass range of interest [19]. Its speed and high throughput makes it an excellent choice for preliminary work. However,

as a quantitative tool it suffers from a very high percent error when quantifying either peak height or peak area. In addition, matrices generally provide a high background in the low mass range, leading to difficulties in metabolite detection and accurate quantification.

An evaluation of several matrices (data not shown) indicated that 9-aminoacridine performed the best for primary carbon metabolites and provided the least background, as reported in the literature [20-22]. Metabolite analyses showed changes in levels with senescence and age under 3% and 20% O_2 (Fig. 4.2). Detectable metabolites included malate (Mal), Iso/citrate (Iso/Cit), α-ketoglutarate (α-KG), pyruvate (Pyr), fumarate (Fum), succinate (Suc), oxaloacetate (Oaa), 2,3 phosphoglycerate (2,3PG), glucose/fructose-6-phosphate (G/F6P), fructose-1,6-bisphosphate (F1,6BP), NAD, NADH, AMP, ADP, and ATP (Fig. 4.2A).

As ATP levels showed no change for all conditions (Fig. 4.2B), metabolite levels were normalized to the ATP levels of young cells at 20% oxygen (*i.e.*, standard growth conditions). This is in contrast to previous reports that ATP levels decreased significantly with age and senescence [9, 12, 13]. Changes in TCA metabolites included increases in the levels of α-ketoglutarate, malate, pyruvate, fumarate, and succinate with senescence at 20% O_2 and a concurrent decrease in these metabolite levels with age at 3% O_2 (Fig. 4.3A). Changes observed in other nucleotides and cofactors included decreases in AMP levels with senescence at 20% O_2, no change in AMP levels with age at 3% O_2, and no change in NADH:NAD ratios for all conditions (Fig. 4.3B).

These results provided proof of concept that primary cell cultures in the senescent state can be obtained in sufficient quantities to permit MS analysis. The trends observed by MALDI were contrary in some respects to what has been reported previously. As there is some uncertainty as to the quantitative reliability of MALDI-TOF measurments, these trends were further explored on both BJ and Imr90 cells grown under conditions of 3% and 20% O_2 utilizing the LC-MS/MS platform.

There is presently a paucity of data related to the metabolome of primary mammalian cells upon entry into senescence under different levels of oxidative stress. Oxygen conditions of 3% and 20% O_2 were used as an ambient source of oxidative stress in an effort to determine what changes

A

Metabolite	[M-H]$^-$	Product ions	Main Product Ion
Pyr	87	79	79
Fum	115	73, 71	73
Suc	117	99, 73, 71	73
OAA	131	115, 87	87
Mal	133	115, 73, 71	115
α-KG	145	101	101
2/3PG	185	79	79
Iso/Cit	191	111, 73	111
G/F6P	259	97, 79	79
F1,6BP	339	97, 79	79
AMP	346	211, 97, 79	79
ADP	426	328, 134, 97, 79	79
ATP	506	408, 261, 79	261
NAD/H	663	408, 97, 79	79

B

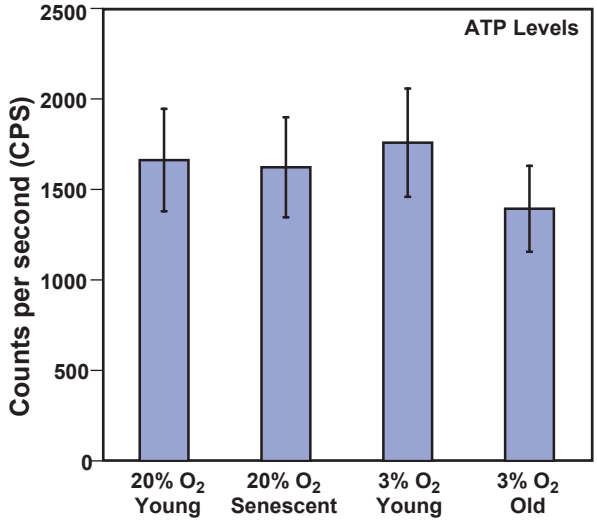

Fig. 4.2. *Preliminary data on Imr90 cells showing changes in metabolite levels of central carbon metabolism with age and senescence under conditions of 3% and 20% O_2 via MALDI TOF/TOF mass spectrometry.* (**A**) Parent and product ions of the metabolites detectable by MALDI TOF/TOF. All metabolite data represents average peak intensities of a technical triplicate. All samples were normalized via cell count to a population of 1x10^7 cells. (**B**) Average peak intensity in ion counts per second (cps) of ATP levels in young PD 31 and old PD 45 Imr90 cells at 3% and 20% oxygen. ATP levels showed no change throughout the various conditions. Therefore, all metabolite changes were normalized to 20% young ATP levels by dividing the average peak intensity of each metabolite by the average peak intensity of 20% young Imr90 cell ATP levels.

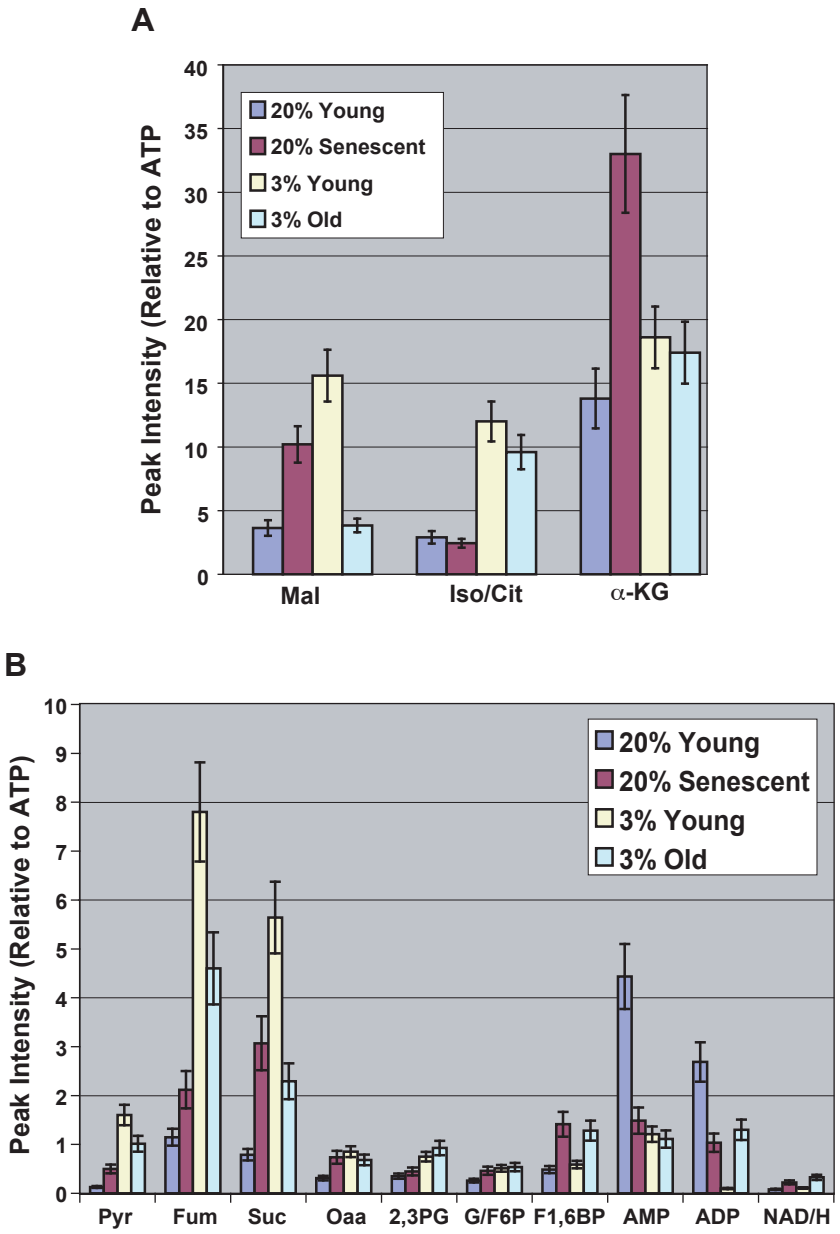

Fig. 4.3. *Relative levels of metabolites in Imr90 cells detected by MALDI TOF/TOF mass spectrometry in young and old Imr-90 cells grown under conditions of 3% and 20% O_2.* Standard deviation for all metabolites is approximately 20%, an error level that is similar to other literature reports [23, 24], and is presently a limitation of mass spectrometric analysis of small polar metabolites.

occur upon entry into senescence. Metabolite analyses were performed on BJ and Imr90 cells utilizing the LC-MS/MS method developed in Chapter 2. Metabolite data were collected on young, old, and senescent Imr90 and BJ cells at 3% and 20% O_2. Detectable metabolites included malate (Mal), Iso/citrate (Iso/Cit), α-ketoglutarate (α-KG), fumarate (Fum), succinate (Suc), oxaloacetate

(Oaa), lactate (Lac), dihydroxyacetone phosphate/ glyceraldehyde-3-phosphate (DHAP/G3P), 2,3 phosphoglycerate (2,3PG), glucose/fructose-6-phosphate (G/F6P), fructose-1,6-bisphosphate (F1,6BP), NADP, NAD, NADH, AMP, and ADP (See Appendix). ATP, NADPH, and pyruvate were unable to be detected in the biological samples. Metabolite levels for biological triplicates were normalized to the total cell population number for each replicate and then normalized to the internal standard NAG [18] to account for differences in sample concentration and complexity as well as inter-day variation in LC-MS/MS performance. The 20% young group was used as the baseline for comparison in both BJ and Imr90 cells.

The trends in the metabolite levels as determined by MALDI TOF/TOF and LC-MS/MS methodologies on Imr90 cells were comparable, even though the MALDI method was only meant to be used for proof of concept (Fig. 4.3, 4.4). However, both showed increases in most TCA metabolites upon senescence and a concurrent decrease or no change in these metabolite levels with age under 3% O_2 at the equivalent population doubling (*i.e.* age). Most of the TCA metabolites also showed higher levels in the 3% young group than in the 20% young group. Some differences between methods included the decrease in levels of AMP and ADP with senescence via MALDI and increase in these levels with senescence via LC-MS. These differences are presently attributed to the lack of accuracy provided by MALDI, arising from sample complexity and matrix interference, as well as the differences in the extraction methods. As shown in Chapter 2, the extraction method can have a significant impact on the metabolic profile. The MALDI method utilized only one product ion peak to determine each metabolite of interest, provided no separation of metabolites via chromatography, and was only performed in technical triplicate from one biological sample. This could lead to false increases in ion intensities for specific metabolites due to metabolites with similar mass/charge ratios. The more accurate LC-MS method determined each metabolite of interest from two product ion peaks for most metabolites of interest with the added specificity of retention times and normalization across samples via the internal standard NAG. For example, ATP was used as a internal standard for the MALDI because no changes in levels of ATP were seen. It also had the lowest intensity of all the metabolites measured via

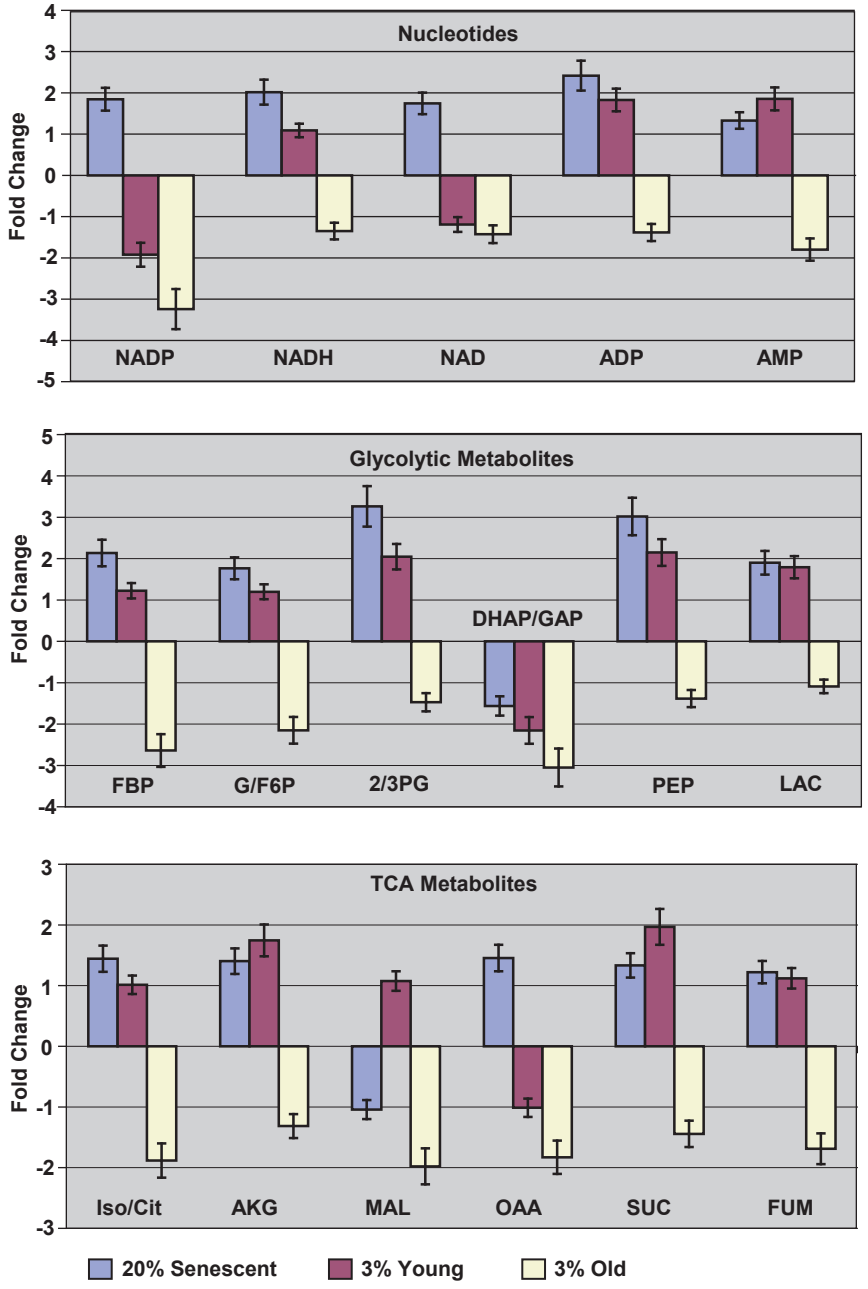

Fig. 4.4. *Changes in metabolite levels of central carbon metabolism in Imr90 cells with age and senescence under conditions of 3% and 20% O_2 via LC-MS/MS.* Metabolite data represents average peak intensities of biological triplicates. Samples were normalized both to total cell population number and the internal standard NAG. Metabolite changes are represented by fold changes from the baseline (20% young). The Imr90 20% young cells were at PD 31 and senescent cells were at PD 45. The Imr90 3% young cells were at PD 32 and the age matched old cells were at PD 47.

MALDI. Since decreases in ATP levels with age are well documented [9, 12, 13], this lack of change was unexpected. Changes in ATP levels may have been undetectable due to the very low ion intensity for this metabolite. In addition, the lack of specificity of the MALDI may have caused a false consistency in ATP measurements due to interfering molecules or matrix.

The changes in metabolite levels for BJ and Imr90 cells were similar (Fig. 4.4, 4.5). Most notably was an increase in the following metabolites with senescence at 20% O_2: NADP, NADH, NAD, ADP, FBP, 2/3PG, PEP, lactate, iso/citrate, α-ketoglutarate, oxaloacetate, succinate, and fumarate. Increases in the levels of FBP and PEP with senescence in human fibroblasts [12] and increases in the levels of lactate, isocitrate, succinate, and α-ketoglutarate with age in human serum have been previously reported [15, 16]. These metabolite level increases along with increased levels of fumarate were expected because their respective enzymes have been shown to be sensitive to OD [1-7]. The resulting attenuation in enzyme function due to OD leads a phenomenon that can be best described as a push and pull mechanism. For example, if an enzyme that forms a particular metabolite is damaged, then the product metabolite level decreases, and if an enzyme that utilizes a particular metabolite is damaged then the precursor metabolite level increases. This is further supported by no change or decreases in the levels of these metabolites with age and at the lower oxidative stress conditions (3% O_2). The decrease in metabolite levels under 3% O_2 supports previously cited *in vivo* results that show that these metabolites decline in neuronal cells in age related diseases such as Parkinson's and Alzheimer's [25, 26]. The accumulation of these metabolites during replicative senescence at 20% O_2 suggests a decrease in enzyme performance and/or a decline the catabolic activity of the cell. This has been suggested before due to characteristic increases in damaged proteins and impairment of protein turnover machinery with senescence, which leads to an increase in less effective enzymes, attenuating key biosynthetic pathways [27-30]. This is reflected in our metabolite study that shows increases with senescence in key metabolites such as lactate, G/F6P, citrate, oxaloacetate, and malate, which are precursors to the biosynthetic pathways of nucleotide, glycogen, and lipid synthesis. The above mentioned metabolite increases with senescence and decreases with age under 3% O_2 conditions are further

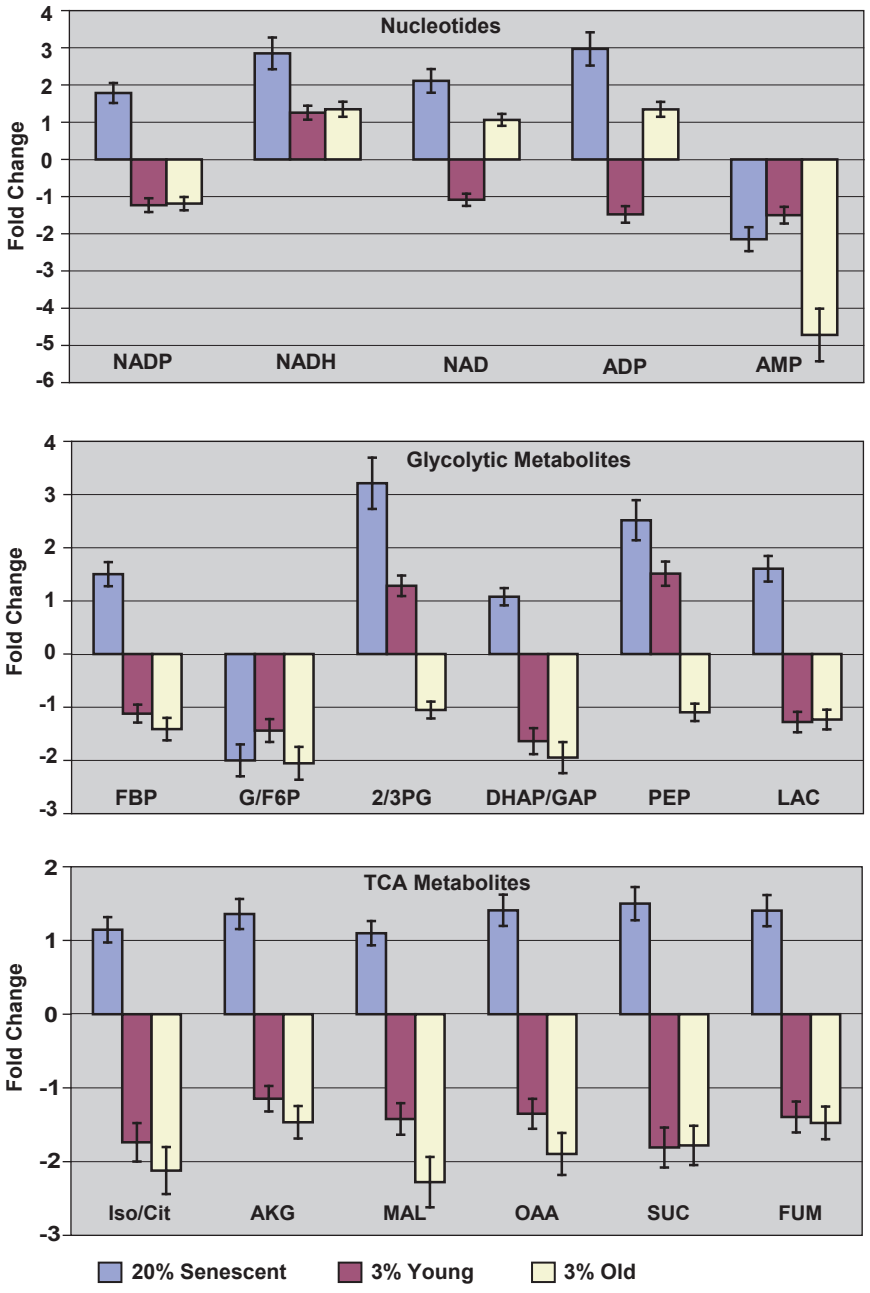

Fig. 4.5. *Changes in metabolite levels of central carbon metabolism in BJ cells with age and senescence under conditions of 3% and 20% O_2 via LC-MS/MS.* Metabolite data represents average peak intensities of biological triplicates. Samples were normalized both to total cell population number and the internal standard NAG. Metabolite changes are represented by fold changes from the baseline (20% young). The BJ 20% young cells were at PD 31 and senescent cells were at PD 55. The BJ 3% young cells are at PD 31 and the age matched old cells were at PD 57.

supported by increases and decreases in mitochondrial/cell volume under the corresponding conditions as shown in Chapter 3 (Fig. 3.5).

BJ and Imr90 cells respond differently to varying levels of oxidative stress as indicated by the changes in levels of metabolites at 3% O_2 when compared to 20% young cells (Fig. 4.4, 4.5). Note that the 3% cell stocks of young cells were created from the lines maintained by the ATCC. Both the Imr90 and BJ cells were cultivated for approximately 25 PDs before being exposed to 3% O_2. Therefore, the cells were grown for approximately 3 PDs under 3% O_2 prior to metabolite measurements in an effort to acclimate them to the new environment. Imr90 cells showed an increase in the levels of ADP, FBP, G/F6P, 2/3PG, PEP, lactate, iso/citrate, α-ketoglutarate, succinate, and fumarate in the 3% young group when compared to the 20% young group. This is followed by a decrease in these metabolites (below 20% young levels) with age at 3% O_2. This trend could be explained by the fact that mitochondrial/cellular volumes decreased significantly at 3% young in Imr90 cells, however these cells are sensitive to OD and hence take a longer time to adapt and eliminate damaged enzymes under 3% O_2 (Chapter 3, Fig. 3.5). This results in an increase in metabolite levels at 3% young and decrease in these metabolites with age under 3% O_2 in Imr90 cells (below 20% young levels). This hypothesis is further supported by decreased levels of many glycolytic and TCA metabolites in the 3% young group when compared to 20% young group of BJ cells. This can be explained by the BJ cells resistance to OD and therefore efficient degradation and removal of damaged enzymes. Therefore, decreases in metabolite levels of the 3% young group compared to the 20% young group correlate with decreases in mitochondrial/cellular volume under the respective conditions (Chapter 3, Fig. 3.5). Similar trends in both BJ and Imr90 cells were observed in the following nucleotides: NADP, ADP, and AMP. One difference from this trend was the observed increase in level with age under 3% O_2 of NAD, NADH, and ADP in BJ cells. This could be explained by the fact that the senescence process in OD resistant BJ cells may be less oxidatively stress dependent than Imr90 cells. Therefore, despite the decreased mitochondrial/cellular volumes under conditions of 3% O_2, these metabolites continue to increase with age under conditions of 3% O_2 as they did with senescence under conditions of 20% O_2

(Chapter 3, Fig 3.5). This indicates that these metabolites may be predominantly affected by cellular signaling pathways rather than OD and resultant attenuation in enzyme function.

There were also several notable differences in metabolite changes with senescence between Imr90 and BJ cells (Fig. 4.3, 4.4). AMP and G/F6P were shown to increase in level with senescence in Imr90 cells but decrease in level with senescence in BJ cells. DHAP/G3P and malate were shown to decrease in level with senescence in Imr90 cells but increase in level with senescence in BJ cells. The increases in AMP and GF/6P in Imr90 cells, and the increases in DHAP/G3P and malate in BJ cells were expected and followed the trends seen in the other metabolites. The unexpected decreases of AMP and GF/6P in BJ cells, and the decreases in DHAP/G3P and malate in Imr90 cells may be a result of their conversion into downstream metabolites of ADP, FBP, 1, 3 bisphosphoglycerate, and oxaloacetate. Their respective enzymes may be resistant to OD in a cell type specific manner.

This theory is supported by previous literature that show increases in AMP levels in lung fibroblasts and decreases in these levels in foreskin fibroblasts [10, 12]. The decrease in AMP levels with senescence in BJ cells, along with the other noted differences could be a result of cell line specific responses and/or metabolic enzyme resistances to OD. These differences may arise from the differences in tissue origin and the varying stress conditions that these types of tissue are exposed to in their natural environment. Fibroblasts in general form the structural framework of most connective tissues and are involved in wound repair. BJ are foreskin fibroblasts derived from a newborn. Since BJ cells are a part of the connective tissue underlying the epidermis and are responsible for wound repair, these cells would be expected to have superior protection mechanism against OD and other cellular stress. This would be necessary because of their exposure to environmental stresses such as hyperoxic conditions during a wound response. On the other hand, Imr90 cells are lung fibroblasts derived from a 16 week old fetus. Since Imr90 cells are a part of the connective tissue underlying pulmonary epithelium in a fetus, they are exposed to less environmental stresses and lower levels of oxygen then epidermal cells. Also since they have been derived from a fetus, these cells would be expected to have under developed stress response

mechanisms. Therefore these cells exhibit inferior protection mechanisms against OD and other cellular stresses. The differences in the response of BJ and Imr90 cells to oxidative stress have been noted in the previous literature [31, 32].

Summary and Conclusions

The purpose of the work described in this Chapter was to quantify changes in the metabolic profile of the central carbon metabolites of primary human fibroblasts (BJ and Imr90 cells) as they age and senesce under conditions of 3% and 20% O_2. An overall trend of increasing metabolite levels with senescence was observed in both BJ and Imr90 cells with a concurrent decrease or no change in these metabolite levels with age under 3% O_2 conditions. This trend included the following metabolites: NADP, FBP, 2/3PG, PEP, lactate, iso/citrate, α-ketoglutarate, oxaloacetate, succinate, and fumarate (Table 4.1). The observed changes in the metabolic profile suggest an attenuation of energy production along with a concurrent decrease in anabolic activity and are in part a result of OD. BJ and Imr90 cells were shown to respond and acclimate differently to 3% O_2 conditions and therefore oxidative stress. Imr90 cells that are sensitive to OD took longer to acclimate and degrade damaged enzymes under 3% O_2 growth conditions. This was exhibited by the increases in ADP, FBP, G/F6P, 2/3PG, PEP, lactate, iso/citrate, α-ketoglutarate, succinate, and fumarate with decreases in mitochondrial/cellular volume in the 3% young group when compared to the 20% young group. Eventually these metabolites decreased to levels below those of the 20% young group (Table 4.1).

Senescent metabolism in BJ and Imr90 cells exhibited cell type specific differences during senescence. These differences included the following metabolites: AMP, G/F6P, DHAP/G3P, and malate. A hypothesis to explain these results is that the enzymes for these metabolites exhibit cell type specific resistances to OD. This hypothesis is supported by reports of different levels of AMP with senescence in different types of fibroblasts [10, 12]. Imr90 cells are lung fibroblasts derived from a 16 week old fetus and therefore would be expected to have under-developed defense mechanisms to OD. BJ cells are foreskin fibroblasts derived from a newborn and therefore would be expected to have superior defense mechanisms in response to OD.

Table 4.1. *The metabolic profile trends of BJ and IMR90 cells at 3% and 20% O_2 during senescence and aging.*

	Imr90			BJ		
	20% Senescent	3% Young	3% Old	20% Senescent	3% Young	3% Old
NADP	1.85	-1.92	-3.24	1.78	-1.23	-1.19
FBP	2.14	1.22	-2.64	1.50	-1.12	-1.41
Iso/Cit	1.44	1.01	-1.88	1.15	-1.74	-2.12
2/3PG	3.26	2.05	-1.47	3.21	1.29	-1.05
PEP	3.02	2.15	-1.38	2.52	1.51	-1.10
AKG	1.40	1.75	-1.31	1.36	-1.15	-1.47
OAA	1.45	-1.01	-1.83	1.41	-1.35	-1.90
SUC	1.33	1.97	-1.44	1.50	-1.81	-1.78
FUM	1.22	1.12	-1.69	1.41	-1.40	-1.47
LAC	1.90	1.79	-1.09	1.61	-1.28	-1.23

The metabolic profile trends found in BJ and Imr90 cells during aging and senescence under 3% and 20% O_2 indicate that oxidative stress has a significant impact on energy metabolism during the aging process and is cell type specific. It also suggests that the energy processes involved in replicative senescence *in vitro* at 20% oxygen differ significantly from *in vivo* processes at normal physiological oxygen levels (about 3%). This suggests that further work in determining changes of the metabolic profile with age and/or senescence should be done *in vivo* for a more accurate reflection of aging in an organism.

References

1. Yarian, C.S., I. Rebrin, and R.S. Sohal, *Aconitase and ATP synthase are targets of malondialdehyde modification and undergo an age-related decrease in activity in mouse heart mitochondria.* Biochem Biophys Res Commun, 2005. **330**(1): p. 151-6.
2. Yarian, C.S., D. Toroser, and R.S. Sohal, *Aconitase is the main functional target of aging in the citric acid cycle of kidney mitochondria from mice.* Mech Ageing Dev, 2006. **127**(1): p. 79-84.
3. Kanski, J., A. Behring, J. Pelling, and C. Schoneich, *Proteomic identification of 3-nitrotyrosine-containing rat cardiac proteins: effects of biological aging.* Am J Physiol Heart Circ Physiol, 2005. **288**(1): p. H371-81.
4. Ji, L.L., D. Dillon, and E. Wu, *Myocardial aging: antioxidant enzyme systems and related biochemical properties.* Am J Physiol, 1991. **261**(2 Pt 2): p. R386-92.
5. Yan, L.J., R.L. Levine, and R.S. Sohal, *Oxidative damage during aging targets mitochondrial aconitase.* Proc Natl Acad Sci U S A, 1997. **94**(21): p. 11168-72.
6. Kil, I.S., J.H. Lee, A.H. Shin, and J.W. Park, *Glycation-induced inactivation of NADP(+)-dependent isocitrate dehydrogenase: implications for diabetes and aging.* Free Radic Biol Med, 2004. **37**(11): p. 1765-78.
7. Chakravarti, B., M. Oseguera, N. Dalal, P. Fathy, B. Mallik, A. Raval, and D.N. Chakravarti, *Proteomic profiling of aging in the mouse heart: Altered expression of mitochondrial proteins.* Arch Biochem Biophys, 2008. **474**(1): p. 22-31.
8. Takeyama, N., N. Matsuo, and T. Tanaka, *Oxidative damage to mitochondria is mediated by the Ca(2+)-dependent inner-membrane permeability transition.* Biochem J, 1993. **294 (Pt 3)**: p. 719-25.
9. Mansouri, A., F.L. Muller, Y. Liu, R. Ng, J. Faulkner, M. Hamilton, A. Richardson, T.T. Huang, C.J. Epstein, and H. Van Remmen, *Alterations in mitochondrial function, hydrogen peroxide release and oxidative damage in mouse hind-limb skeletal muscle during aging.* Mech Ageing Dev, 2006. **127**(3): p. 298-306.
10. Wang, W., X. Yang, I. Lopez de Silanes, D. Carling, and M. Gorospe, *Increased AMP:ATP ratio and AMP-activated protein kinase activity during cellular senescence linked to reduced HuR function.* J Biol Chem, 2003. **278**(29): p. 27016-23.
11. Yarian, C.S. and R.S. Sohal, *In the aging housefly aconitase is the only citric acid cycle enzyme to decline significantly.* J Bioenerg Biomembr, 2005. **37**(2): p. 91-6.
12. Zwerschke, W., S. Mazurek, P. Stockl, E. Hutter, E. Eigenbrodt, and P. Jansen-Durr, *Metabolic analysis of senescent human fibroblasts reveals a role for AMP in cellular senescence.* Biochem J, 2003. **376**(Pt 2): p. 403-11.
13. Sastre, J., F.V. Pallardo, R. Pla, A. Pellin, G. Juan, J.E. O'Connor, J.M. Estrela, J. Miquel, and J. Vina, *Aging of the liver: age-associated mitochondrial damage in intact hepatocytes.* Hepatology, 1996. **24**(5): p. 1199-205.
14. Zhang, X., H. Liu, J. Wu, M. Liu, and Y. Wang, *Metabonomic alterations in hippocampus, temporal and prefrontal cortex with age in rats.* Neurochem Int, 2009. **54**(8): p. 481-7.
15. Lawton, K.A., A. Berger, M. Mitchell, K.E. Milgram, A.M. Evans, L. Guo, R.W. Hanson, S.C. Kalhan, J.A. Ryals, and M.V. Milburn, *Analysis of the adult human plasma metabolome.* Pharmacogenomics, 2008. **9**(4): p. 383-97.
16. Jiang, H., S. Zhang, Q. Guan, C. Chen, F. Gao, and Y. Zhang, *1H NMR investigations of inclusion complexes between beta-cyclodextrin and 1-hexadecanol.* Curr Drug Discov Technol, 2007. **4**(4): p. 295-7.
17. Gu, H., Z. Pan, B. Xi, B.E. Hainline, N. Shanaiah, V. Asiago, G.A. Gowda, and D. Raftery, *(1)H NMR metabolomics study of age profiling in children.* NMR Biomed, 2009.

18. Bajad, S.U., W. Lu, E.H. Kimball, J. Yuan, C. Peterson, and J.D. Rabinowitz, *Separation and quantitation of water soluble cellular metabolites by hydrophilic interaction chromatography-tandem mass spectrometry.* J Chromatogr A, 2006. **1125**(1): p. 76-88.
19. Vaidyanathan, S., S. Gaskell, and R. Goodacre, *Matrix-suppressed laser desorption/ionisation mass spectrometry and its suitability for metabolome analyses.* Rapid Commun Mass Spectrom, 2006. **20**(8): p. 1192-8.
20. Vaidyanathan, S. and R. Goodacre, *Quantitative detection of metabolites using matrix-assisted laser desorption/ionization mass spectrometry with 9-aminoacridine as the matrix.* Rapid Commun Mass Spectrom, 2007. **21**(13): p. 2072-8.
21. Nordstrom, A., E. Want, T. Northen, J. Lehtio, and G. Siuzdak, *Multiple ionization mass spectrometry strategy used to reveal the complexity of metabolomics.* Anal Chem, 2008. **80**(2): p. 421-9.
22. Sun, G., K. Yang, Z. Zhao, S. Guan, X. Han, and R.W. Gross, *Shotgun metabolomics approach for the analysis of negatively charged water-soluble cellular metabolites from mouse heart tissue.* Anal Chem, 2007. **79**(17): p. 6629-40.
23. Munger, J., S.U. Bajad, H.A. Coller, T. Shenk, and J.D. Rabinowitz, *Dynamics of the cellular metabolome during human cytomegalovirus infection.* PLoS Pathog, 2006. **2**(12): p. e132.
24. Rabinowitz, J.D. and E. Kimball, *Acidic acetonitrile for cellular metabolome extraction from Escherichia coli.* Anal Chem, 2007. **79**(16): p. 6167-73.
25. Bubber, P., V. Haroutunian, G. Fisch, J.P. Blass, and G.E. Gibson, *Mitochondrial abnormalities in Alzheimer brain: mechanistic implications.* Ann Neurol, 2005. **57**(5): p. 695-703.
26. Ames, B.N., H. Atamna, and D.W. Killilea, *Mineral and vitamin deficiencies can accelerate the mitochondrial decay of aging.* Mol Aspects Med, 2005. **26**(4-5): p. 363-78.
27. Fujii, J. and N. Taniguchi, *Down regulation of superoxide dismutases and glutathione peroxidase by reactive oxygen and nitrogen species.* Free Radic Res, 1999. **31**(4): p. 301-8.
28. Rattan, S.I. and B.F. Clark, *Intracellular protein synthesis, modifications and aging.* Biochem Soc Trans, 1996. **24**(4): p. 1043-9.
29. Ando, K., K. Nagata, M. Beppu, K. Kikugawa, T. Kawabata, K. Hasegawa, and M. Suzuki, *Effect of n-3 fatty acid supplementation on lipid peroxidation and protein aggregation in rat erythrocyte membranes.* Lipids, 1998. **33**(5): p. 505-12.
30. Davies, K.J., *Oxidative stress, antioxidant defenses, and damage removal, repair, and replacement systems.* IUBMB Life, 2000. **50**(4-5): p. 279-89.
31. Chen, Q., A. Fischer, J.D. Reagan, L.J. Yan, and B.N. Ames, *Oxidative DNA damage and senescence of human diploid fibroblast cells.* Proc Natl Acad Sci U S A, 1995. **92**(10): p. 4337-41.
32. Lorenz, M., G. Saretzki, N. Sitte, S. Metzkow, and T. von Zglinicki, *BJ fibroblasts display high antioxidant capacity and slow telomere shortening independent of hTERT transfection.* Free Radic Biol Med, 2001. **31**(6): p. 824-31.

Chapter 5

Transcriptional and Protein Array Analyses of Signaling in Imr90 Cells with Age and Senescence under Growth Conditions of 3% and 20% Oxygen

Abstract

This study investigates the global changes in gene expression that occur with age under 3% and 20% oxygen conditions, and subsequent ties with changes in protein kinase activity at 20% oxygen. Unlike previous work, this study did not confine itself to selected pathways but rather investigated multiple pathways and their interactions via protein kinase array and transcriptional profiling. The observed changes not only confirm major pathways involved in senescence (p53/p21, PTEN/p27, and RTK/Raf/MAPK) but also display changes in gene expression and protein kinase activity with different levels of environmental stress and senescence that have not been previously associated with senescence. The majority of these changes were related to pathways involved in cellular stress, cell cycle control, and survival response. The correlation of the transcriptome and proteome data with the metabolome expounded on the overlapping cellular pathways involved in senescence and oxidative stress. Changes in genes related to glycolysis and energy pathways correlated with the data of the metabolite analysis; attenuated function was mirrored by an up regulation of gene expression as a compensatory mechanism. Overall, senescent cells displayed an alternate signaling profile that is directly related to their resistance to apoptosis and suggested role in preventing uncontrolled growth (cancer).

Introduction

Senescence is an irreversible form of cell cycle arrest initiated by damaged cell constituents and subsequent pro-oncogenic signaling. The natural entry into the senescent state is presently considered a preventive measure against cancer formation as it is induced and maintained through the cooperative effects of different signaling cascade mechanisms [1-5]. Transcriptional profiling has been employed by several groups in an attempt to understand the senescent state [1, 6-9]. Critical review of these datasets indicates that there is very little correlation between human cell-based experiments, even among the same cell types (See Appendix) [1, 6-8]. This lack of agreement is due in part to the initial absence of standardized protocols for processing (RNA extraction), analysis (one dye vs. two dye platforms as well as bioinformatic tools), and reporting microarray data. Standardized protocols for acquiring and improved interpretation of these datasets have eliminated much of the experimental and lab-based variations.

Transcriptional profiling combined with targeted protein analysis has provided insight into several pathways involved with signaling during replicative senescence. In brief, cell cycle arrest during senescence has been shown to be regulated by the p16/Rb and p53/p21 pathways [4, 5, 10]. The cascade of arrest through these pathways is a result of increased senescence-associated inflammatory signaling and perturbations in growth hormone receptor signaling [2, 3, 5]. The senescence process affects three major mitogen activated protein kinase pathways (MAPK) which are involved in process of cell growth, differentiation, apoptosis, cell survival, and stress response (Fig. 5.1). These include mitogen activated protein kinase/extracellular regulated kinase (MAPK/ERK), p38 MAPK, and Jun-N-terminal kinase/signal activated protein kinase/c-Jun kinase (JNK/SAPK). Senescence associated changes in these pathways include increases in p38 in response to inflammatory signaling and increases in JNK in response to cellular stress [4, 11]. Increases in the MAPK/ERK pathway via increases in Ras and Raf (both oncogenic proteins) with uncharacteristic downstream inhibition of the final targets Erk 1 and 2 are also characteristic of the senescent

phenotype [2, 3, 11-14]. These signaling cascades ultimately cause and maintain cell cycle arrest through the p16/Rb and/or p53/p21 pathways (also see Chapter 1).

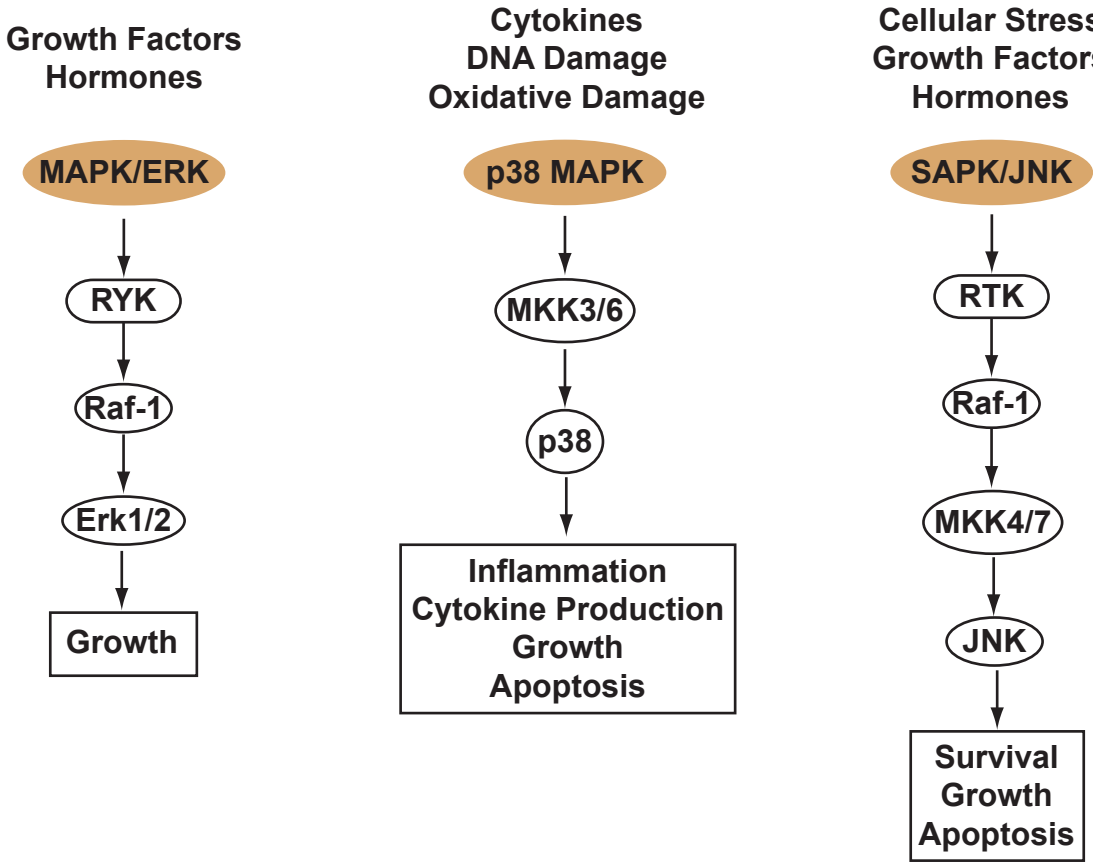

Fig. 5.1. *MAPK signaling cascades involved in the replicative senescence process.*

There are no studies that have explored the global changes in gene expression that occur with age under 3% O_2 growth conditions and subsequent parallels with expression levels at 20% O_2. Despite many more narrowly-focused studies on protein changes in a small number of specific signaling pathways, there are also no broad analyses of multiple pathways and their simultaneous changes in protein levels during the senescence process. Our studies explore and define both of these important aspects of senescence with particular emphasis on changes that are related to oxidative stress. Combining the transcriptome and protein array data with the metabolite data (Chapter 4) provides a "theoretical senescence model" of replicative senescence in human fibroblasts. The complementary nature of the results permits comparisons across the genome, proteome and metabolome, a key step in fully detemining the processes underlying the senescence

process.

Experimental Procedures

Cell Growth. BJ (human foreskin fibroblast) and Imr90 (human lung fibroblast) cells were obtained from ATCC at population doublings (PD) 21 and 27 respectively. Cells were cultured as monolayers in Dubelco's modified medium (DMEM; ATCC) supplemented with 10% (v/v) fetal bovine serum (FBS; Atlanta Biologicals) and 5% CO_2 humidified air at 37 °C. Monolayers were grown to 80% confluency in T-150 flasks with the growth medium (25 ml) changed every 2-3 days. Separate incubators were used for both the 3% and 20% oxygen growth conditions. Nitrogen gas was used to maintain steady levels of 3% oxygen in the 3% oxygen incubator. Cells were passaged by removing the DMEM, washing with phosphate-buffered saline (PBS, 10 ml; Gibco), and treating the cultures with 2 ml of 1× trypsin-EDTA (Gibco) for 5 minutes in the incubator. The released cells were then resuspended in supplemented DMEM (8 ml), with 200 ul aliquots removed for cell counting and 2 ml aliquots removed for the seeding of new flasks for cell growth containing supplemented DMEM (30ml). Population doublings were calculated by the following formula: log (N/Ni) ×3.33 (N = number of cells, Ni = initial seeded number of cells). Dimethyl sulfoxide (DMSO; Sigma) was added to the remaining cell suspension in order to provide a 10% DMSO and DMEM cocktail. Five aliquots (2 ml each) were frozen at -80 °C for 4 hrs using cryotube vials (Nunc). These vials were then transferred to a Biocane (Thermolyne) for storage in liquid nitrogen.

Protein Kinase Microarrays. A protein kinase profiling experiment was performed on young (PD 31) and senescent (PD 46) Imr90 cells under 20% oxygen growth conditions. The array work was performed by Kinexus (Vancouver, CA) with protein isolation performed according to their recommended protocol. All chemicals unless otherwise noted were from Sigma. Lysis buffer was composed of 20 mM MOPS, pH 7.0, 2 mM EGTA, 5 mM EDTA, 0.5% NP-40, 1 mM DTT, and 30 ul of 100× stock of Halt phosphatase inhibitor cocktail (pH 7.2; Pierce) was added fresh. Cells were collected at 80% confluency by removing the DMEM, washing with PBS (10

ml), treating the cells with 1× trypsin-EDTA (2 ml; 5 min), and resuspending the released cells in supplemented DMEM (8 ml). Following resuspension, the cells were centrifuged (750 ×g; 2 min), washed twice with ice-cold PBS (10 ml; with an intermediate centrifugation step at 750 ×g for 2 min), and centrifuged (750 ×g; 2 min). The PBS was decanted and ice-cold lysis buffer (300 ul) was added to the cell pellet. The cells were then sonicated (4 × for 10 sec; 1 min pause between cycles) on ice, and centrifuged (14000 ×g; 30 min) at 4 °C. The supernatant was transferred to a clean test tube, and the protein concentration was quantified on a Beckman Coulter DU520 spectrophotometer using the Bradford assay (Pierce) according to manufacturer's instructions. Aliquots of each sample (100 μg) at young (PD30) and senescent (PD46) conditions of Imr90 cells were then provided to Kinexus for analysis.

Protein kinase changes were detected on the Kinex KAM-1.1 antibody microarray and uploaded to the KiNET on-line databank. The Kinex KAM-1.1 microarray labels non-denatured proteins with the same dye for both protein samples for comparison to reduce false negatives and positives. It consists of over 650 antibodies (270 phospho-site specific) that include 240 protein kinases, 28 phosphatases, and 90 other cell signaling proteins involved in cell proliferation, stress, and apoptosis [15]. The Kinex service performs the dye-labeling of proteins, scanning, and quantification of the antibody spots. It then delivers a summary report of protein changes in an Excel file with an Excel data filter to summarize results. Control and experimental samples were normalized to a net signal median (actual signal intensity after the background is subtracted) with the assumption that the sum of intensity of all the spots between the control and experimental samples are essentially the same. This gives a more conservative measure of changes in protein expression [16]. Changes deemed significant had a S/N ratio of above 2, a total percent error below 15%, and an above average (23) %CFC (percent change from control, which measures the change in normalized signal intensity averages between the experimental sample and control sample).

Transcriptional Profiling. A transcriptional profiling experiment was performed on young (PD 30 at 3% and 20% oxygen), old (PD 53 at 3% oxygen), and senescent (PD 48 at 20% oxygen)

Imr90 cells. Microarray protocols, equipment, and data were fully MIAME compliant and are available at the Gene Expression Omnibus. RNA was extracted using TRIzol Reagent (Invitrogen) following the manufacturer's protocol. Briefly, cells were collected at 80% confluency and then resuspended in supplemented DMEM (10 ml). No more than $5\times10^{\wedge6}$ cells were used for the extraction. Cells were centrifuged (750 ×g; 2 min) and resuspended in TRIzol reagent (1 ml) and incubated for 5 minutes. Chloroform (0.2 ml) was added and the solution was mixed vigorously, followed by centrifugation (12000 ×g; 15 min). The aqueous phase was transferred to a new tube, isopropyl alcohol (0.5 ml) was added, and the suspension was incubated for 10 minutes. Following incubation, the suspension was then centrifuged (12000 ×g; 10 min) and the supernatant was removed. The RNA pellet was washed with 75% ethanol and centrifuged (7000 ×g; 5 min). The supernatant was removed and the pellet was resuspended in RNase free water (20 ul). Quantity and quality of the RNA was measured by using a Gene Quant pro RNA/DNA calculator, and a 260/280 ratio was used to determine the quality of the RNA extraction to ensure a high purity RNA sample for generation of cDNA. Between 1 and 10 μg of total RNA from each sample was used to generate a high fidelity cDNA, which was modified at the 3' end to contain an initiation site for T7 RNA polymerase. Samples were subjected to gene expression analysis via the Affymetrix Human U133A oligonucleotide array which queries 22,000 human probe sets. Hybridization, staining, and washing of all arrays were performed in the Affymetrix fluidics module as per the manufacturer's protocol. Streptavidin-phycoerythrin stain (SAPE; Molecular Probes) is the fluorescent conjugate used to detect hybridized target sequences. The detection and quantitation of target hybridization was performed with a GeneArray Scanner 3000, set to scan each array twice at a factory set PMT level and resolution. All arrays referred to in this study were assessed for "array performance" prior to data analysis by statistical analysis of control transcripts that were spiked into the samples and the hybridization cocktail. In addition, several genes were identified on each array to help assess the overall quality of signal intensity from all arrays, this analysis helped validate the reproducibility of each array at baseline to define the lower limit of sensitivity.

Raw data were normalized and analyzed using ArrayAssist (Stratagene). The Robust

Multichip Averaging (RMA) aligorithm was used for background subtraction, normalization, and summarization of data. An unpaired t-test (asymptotic) was used to determine the significance of transcriptional alterations. The data was permuted from all spots randomly 100 times to determine the false discovery rate (FDR). The FDR was corrected for multiple testing using the Benjamini-Hochberg approach. The Q-Value cutoff for the experiment was 0.05 with probe sets with Q-values greater than 0.05 considered insignificant expressors across the experiment. Young Imr90 cells at 20% oxygen (PD 30) were used as control for baseline comparison. Spots showing changes of 2 fold or more across all time-points were considered significant.

Results and Discussion

Imr90 cells were passaged to the senescent state and isolates were prepared for both transcriptional profiling and an antibody based protein kinase array. Transcriptional profiling was performed in young (PD 30 at 3% and 20% oxygen), old (PD 48 at 3% oxygen), and senescent (PD 46 at 20% oxygen) Imr90 cells. All data were normalized to young cells grown at 20% O_2 essentially because this is the standard protocol used in most laboratories for tissue culture. Several key changes in gene expression due to senescence and the 3% O_2 growth conditions are listed in Table 5.1. Further discussion of these genes will be reserved until after presentation of the protein array data.

Along with the transcriptional profiling, a protein kinase microarray on young (PD 30) and senescent (PD 46) Imr90 cells under normal cell culture oxygen conditions was performed by Kinexus Bioinformatics (http://www.kinexus.ca/). A summary of the key changes in protein kinase levels are listed in Table 5.2. Several phosphorylated proteins reflecting activated kinase signaling cascades involved in cell cycle progression and stress/survival response displayed prominent changes, as would be expected for transition into a senescent state (Table 5.1). CDK 4, CDK 6, and CDK 2, cell cycle proteins that are active during the G1 phase, are decreased in the senescent cells indicating cell cycle arrest (Fig. 1.4) [10, 17, 18]. These decreases can be attributed to the observed increase in phosphorylated protein levels of p53 and p21. This elevation indicates that

the p53/p21 tumor suppressor pathway, as opposed to the p16/Rb pathway, is activated in Imr90 cells with senescence. Further supporting evidence for the induction of the p53/p21 pathway was indicated by increased levels of c-Jun N-terminal kinase (JNK). JNK has been associated with senescence and shown to increase p53's half-life [19]. Increased phosphorylation levels of PTEN and p27 were also seen, supporting the apparent role of the PTEN/p27 pathway in senescence [20-22].

Table 5.1. *Changes in gene expression levels of Imr90 cells with age relative to 20% O_2 young cells.*

Genes	20% Senescent PD 46	3% Young PD 30	3% Old PD 48
ATPase	-3	-3	-3
BCL2	5	4	4
CLDN1	2	-5	-4
CTHRC1	-9	-1	1
DEPDC1	-1	5	8
NR4A2	-1	2	6
PDK	4	3	3
PEPCK	3	4	4
PFK2	4	3	3
PGK1	3	2	2
PTGIS	-30	4	1
PTGS2	-3	5	8
PTHLH	-21	-13	-19
SEPP1	-20	-8	-13

When senescent cells enter into the irreversible state of cell cycle arrest, they adopt an altered cellular signaling profile and exhibit a resistance to apoptosis [23, 24]. The following information is a summary of activated signaling cascades involved in various stress responses with senescence in Imr90 cells grown under 20% O_2. The predominately activated pathway, as indicated by observed changes in phosphorylated protein levels, was the RTK/Raf/MAPK pathway, a pathway which mainly responds to growth factors and hormones and has been recently associated with cellular stress, senescence, and age-related human diseases (Fig. 5.2) [2, 25-27]. The JNK protein, which promotes survival/apoptosis under various stress stimuli [25, 26, 28, 29], seemed to be activated

very specifically through only the receptor tyrosine kinases (RTK)s. This specific activation was supported by an increase in phosphorylated levels of the Receptor-like Tyrosine Kinase (RYK) [30], downstream affectors p21/Cdc42/Rac1-activated kinase 1 (PAK1) [31], mitogen activated protein kinase kinase 7 (MKK4/7) [25, 26], and Raf-1 [27], with no other observed signaling through upstream MKK's or p38 (Table 5.2; Fig. 5.1).

Table 5.2. *Changes in phosphorylated (activated) protein levels in Imr90 cells with age based upon analysis by protein kinase array.* Phosphorylated protein levels higher in senescent Imr90 cells (PD 46, 20% oxygen) relative to young Imr90 cells (PD 30; 20% oxygen) are on the left and those in lower levels are on the right. %CFC represents percent change from control (young Imr90 cells).

Protein	% CFC		Protein	% CFC
p21	107		p38	-43
p27	119		Bad	-92
p53	129		CDK2	-23
Akt	27		CDK4	-53
Bcl-2	26		Erk1	-30
CTNNB	44		Erk2	-70
c-Raf	193		GYS1	-45
JNK	101		H2B	-28
MKK 4	112		JAK1	-16
MKK 7	86			
MKK 3/6	161			
NF-kB	57			
PAK1	173			
PI3K	97			
PTEN	296			
SOCS4	58			
RYK	116			

Increases in levels of suppressor of cytokine signaling 4 (SOCS4) [32], and decreases in levels of Janus Kinase 1 (JAK1) [32, 33] and p38 [28, 34] further promote RTK/Raf/MAPK as the major pathway (Table 5.2; Fig. 5.1). These trends in protein signaling suggest that the senescent state is being maintained via growth factors, cellular stress, and hormonal signaling rather than cytokine signaling such interleukin 6 and 8 (IL-6 and 8) (Fig. 5.3). Therefore, senescent Imr90 cells seem to be in an atypical, nonresponsive state to cytokine signaling. This could be explained by differences in signaling due to cell type, because the inflammatory response (IL-6 and 8, p38)

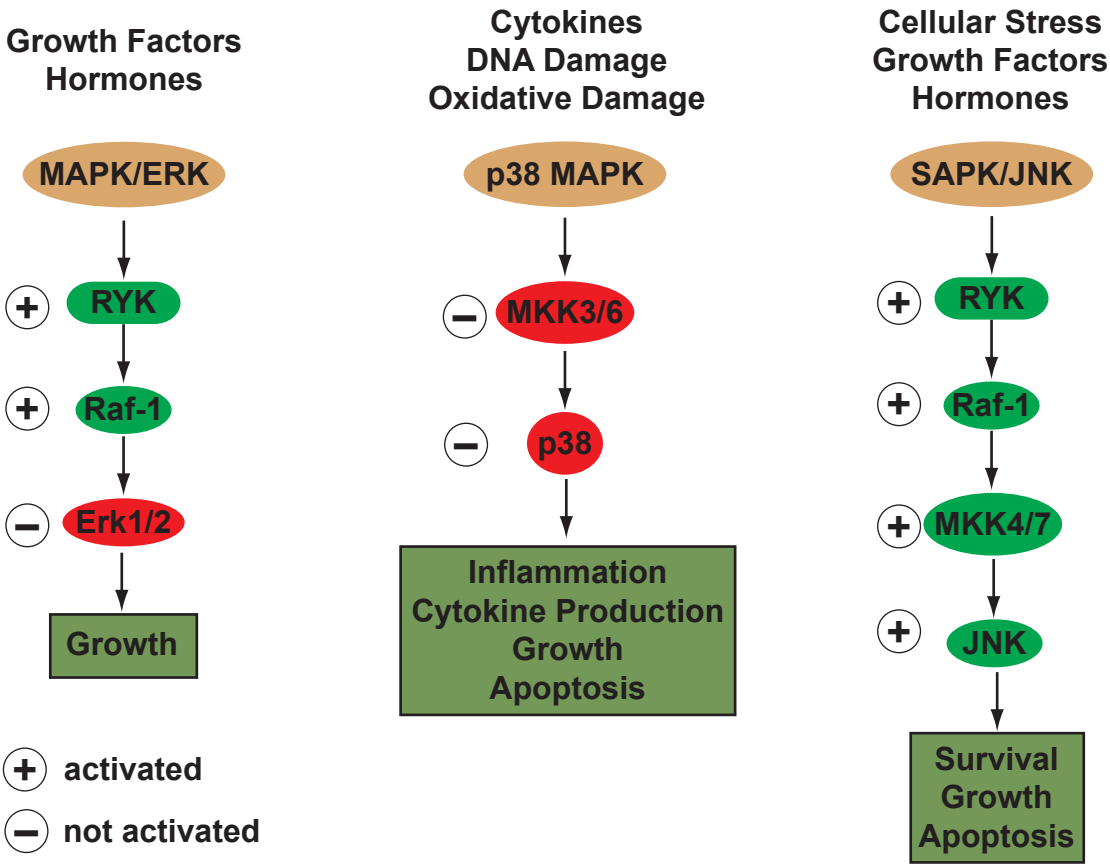

Fig. 5.2. *MAPK signaling cascades involved in the replicative senescence process.* Proteins with a "+" indicate activation and "-" indicate no activation as seen in the protein array.

has been shown to be a mediator in cellular senescence in other cell types [24, 28, 32-34]. Also of note is the increase in levels of the oncogenic protein Raf-1. Raf-1 expression is dysregulated in many cancers and accompanied by increased levels of extracellular signaling regulated kinase 1 and 2 (Erk 1 and 2). These promote cell growth and differentiation and are a requirement for G1 to S phase progression [35]. However, as expected with a senescent state and complementing the observed G1 cell cycle arrest, phosphorylation levels of Erk 1 and 2 are decreased with senescence. This indicates an unknown regulatory event downstream of Raf-1 that is suppressing Erk signaling (Table 5.2). This type of downstream inhibition in the face of properly activated RTK signaling pathways has been reported before in senescent cultures [5].

The RTK/Raf/MAPK pathway has also been associated with the Wnt/beta-catenin signaling pathway (also activated in the protein array). This relationship is indicated by the increased phosphorylated protein levels of RYK and beta-catenin (CTNNB) (Table 5.2). The Wnt/β-catenin pathway may be responsible, along with PAK1 activation and downstream signaling, for the cadherin stimulation and actin reorganization resulting in flattened cell morphology [26, 36-38].

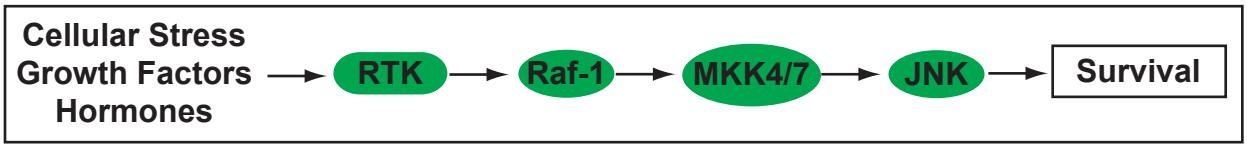

Fig 5.3. *Diagram of the RTK/Raf/MAPK signaling pathway in senescence.*

The Akt signaling pathway, which acts as an energy sensor and promotes cell survival and proliferation, was also activated in the protein kinase array. Increased phosphorylated levels of Akt, phosphoinositol-3-phosphate kinase (PI3K), and Bcl-2 were observed along with decreased levels of Bad [39] (Table 5.2). Bcl-2 and Bad are proteins that regulate mitochondrial membrane permeability and therefore apoptosis [40]. Activation of the Akt signaling pathway was further supported by results from separate transcriptional and metabolite profiling, which showed increases in both fructose-6-phosphate levels and expression levels of phosphofructose kinase 2 (PFK2). PFK2 is a metabolic enzyme which has been reported to increase in response to increased levels of Akt [39] (Table 5.1). PFK2 is bifunctional, either forming or hydrolyzing fructose 2, 6 bisphosphate, which directs the cell to undergo either glycolysis or gluconeogenesis and simultaneously inhibits the opposing pathway. Metabolic enzymes like PFK2 have shown hallmark attenuation in function with a subsequent increase in enzyme levels that accumulate with age due to OD (Chapter 1). The overexpression of PFK2 could be a compensatory mechanism for the cells with altered metabolism and attenuated metabolic function. When metabolite enzymes become attenuated, one expects a pooling effect to occur because substrate metabolites are not converted to product as efficiently due to the decline in both energy production and biosynthesis with senescence. Overexpression likely takes place due to changes in signaling in the Akt pathway, which acts as an energy sensor

via glycolytic flux and ATP levels [39]. Sensing a large concentration of precursor metabolites, a lack of recognizable final products (*i.e.*, ATP), and attenuated energy metabolism, the Akt pathway proceeds to ramp up metabolic gene expression. This rationale is supported by the increase in levels of the precursor metabolites such as fructose-6-phosphate with senescence as shown in Chapter 4, as well as increases in energy metabolites such as PEP, FBP, lactate, and succinate previously reported in the literature (Chapter 1) (Fig. 4.3). Also, increased protein levels of Akt have been shown to increase lactate dehydrogenase (LDH) levels. LDH converts pyruvate into lactate and, contrary to literature, seems to be resistant to OD. It does not become attenuated with age, as indicated by the increase in expression of LDH and subsequent increase in its end product lactate. Such increases have been previously reported in literature and were also confirmed by the metabolite analyses described in Chapter 4 (Fig. 4.3) [41, 42].

Changes in LDH and PFK2 are two examples of how senescent signaling can change the metabolic profile of a cell during replicative senescence. Also of note is the decreased levels of glycogen sythetase GYS1 with senescence (Table 5.2). This suggests a shift away from anabolic cellular activities. Such a shift would be expected with senescence, since the senescent cell no longer has the steep energy demand requirements for cell division and proliferation compared to an active, cycling cell.

Several significant changes in the transcriptional profile of Imr90 cells occurred during both senescence at 20% O_2 and under growth conditions of 3% O_2 with age. These changes involved genes in cell signaling (cell cycle control and stress response) and energy metabolism. These changes correlated with changes found in the protein array work described above. Notable changes in gene expression were summarized in Table 5.1, and the cell signalling genes are shown graphically in Fig. 5.4. Changes as a result of senescence include the parathyroid hormone-like hormone (PTHLH) and claudin-1 (CLDN1) genes which both showed a decrease in expression. The PTHLH is a member of the parathyroid hormone family and is involved in growth, differentiation, proliferation, and apoptosis [43, 44]. Increased levels of PTHLH have been associated with cancer as well as invasion and migration [45-47]. PTHLH expression also has a putative effect on Erk

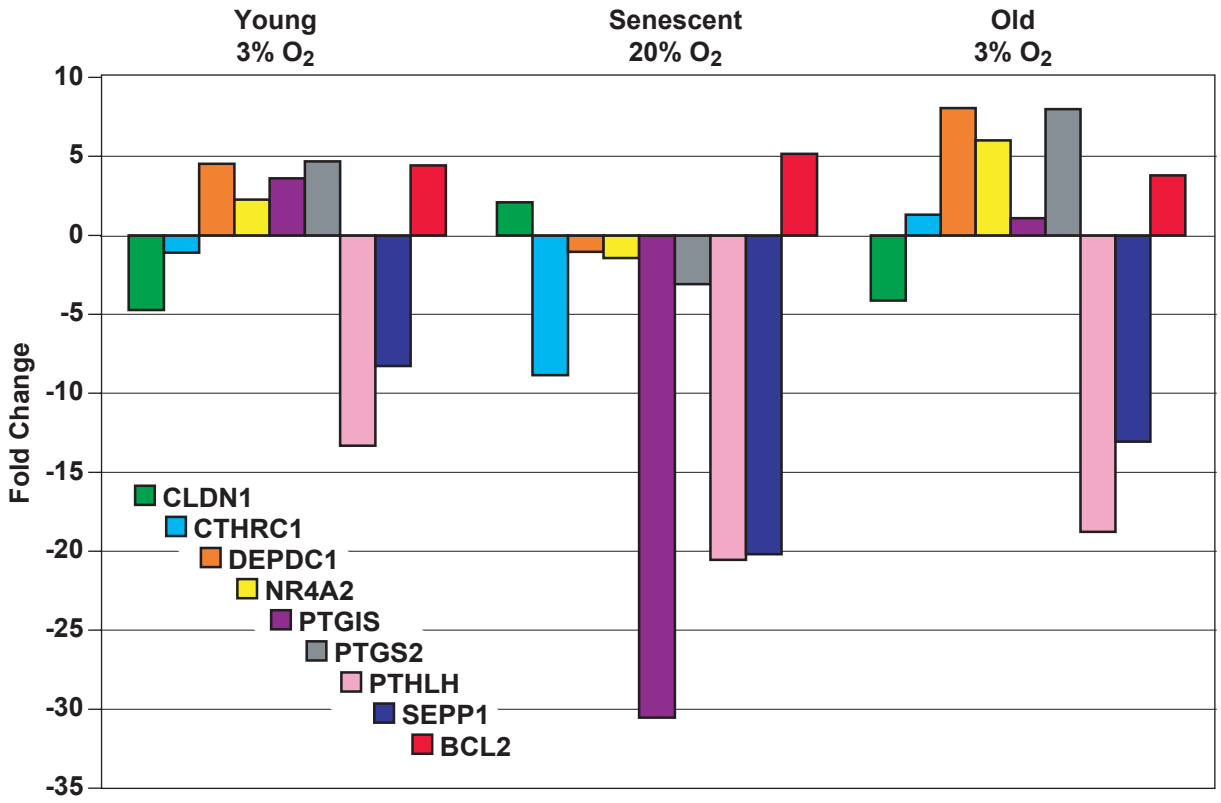

Fig. 5.4. Differences in expression levels of genes involved in cell signaling. Graph represents significant changes in gene expression levels of Imr90 cells under conditions of 3 and 20 percent oxygen with age relative to young cells grown in 20% oxygen. Conditions include: 3% young, 20% senescent, and 3% old.

1 and 2 phosphorylation that are involved in various cellular processes in response to a variety of extracellular signals [35, 47]. PTHLH levels decreased significantly in Imr90 cells with senescence and was accompanied by the aforementioned decrease in phosphorylated Erk 1 and 2 levels as shown in the Kinexus data (Table 5.2). This effect is slightly alleviated under growth conditions of 3% O_2, but continues to decline with age.

CLDN1, also known as senescence associated epithelial membrane protein, is an integral part of tight junctions. Changes in expression of junction proteins are a hallmark of cell invasion and metastasis [48]. CLDN1 expression has been shown to decrease in breast cancer and increase with senescence [49, 50], and has a purported role in tumor suppression [51]. CLDN1 expression

increases with senescence in Imr90 cells but decreases significantly under conditions of 3% O_2, suggesting that CLDN1 is involved in a senescence pathway that is responsive to oxidative stress. Other major gene expression changes with senescence include selenoprotein P (SEPP1), which is involved in oxidant scavenging, and collagen triple helix repeat containing 1 (CTHRC1), which is involved in anti-oncogenic responses [52-55] .

One of the most significant changes in gene expression was the prostaglandin I2 synthase (PTGIS; Fig. 5.4). PTGIS encodes for a endoplasmic reticulum membrane protein that is part of the arachidonic pathway, a protein that has been implicated as being important in colon and lung cancers as well as inflammatory diseases [56]. PTGIS over-expression suppresses phosphorylation of p38 MAPK in smooth muscle cells [57]. p38 plays major roles in stress-induced responses such as apoptosis, cytokine expression, proliferation, and survival [57]. PTGIS expression is increased under conditions of 3% O_2 compared to 20% O_2. Its expression decreases significantly with senescence and is accompanied by decreases in levels of p38 MAPK as shown in the Kinexus data (Table 5.2). Another significant change in gene expression was prostaglandin-endoperoxide synthase (PTGS), also known as cyclooxygenase, a key enzyme in prostaglandin biosynthesis that acts both as a dioxygenase and as a peroxidase. PTGS is purported to have roles in inflammation, aging, and oxidative stress, which in turn relates to age-related diseases such as Alzheimer's and Parkinson's [58, 59]. The expression of this gene is deregulated in epithelial tumors and is responsible for tumor viability, growth, and metastasis [60]. It also has been suggested to inhibit p53 activity and protect against DNA damage due to oxidative stress [59, 61, 62]. PTGS expression decreases with senescence and is accompanied by increases in p53 protein levels as shown in the Kinexus data (Table 5.2). Under conditions of 3% oxygen, PTGS expression is increased compared to 20 percent oxygen. Other gene expression changes observed with 3 vs. 20% O_2 include the oncogenic DEP domain containing 1 (DEPDC1) and nuclear receptor subfamily 4 (NR4A2), both of which are involved in Parkinson's disease and have been shown to be phosphorylated by Erk 2 [63-66]. Erk 2, DEPDC1, NR4A2 decrease in expression and protein levels with senescence (Table 5.1 and Fig. 5.4)

Changes in expression of genes involved in metabolism with both senescence and 3% O_2 growth conditions were also seen (Fig. 5.5). ATPase, a mitochondrial metabolism enzyme that converts ADP and inorganic phosphate to ATP via the electron transport chain, decreased in activity with senescence and under conditions of 3% O_2. Phosphoenolpyruvate kinase (PEPCK), pyruvate kinase (PDK), phosphofructose kinase 2 (PFK2), and phosphoglycerate kinase (PGK), all of which are glycolytic/gluconeogenic enzymes, were shown to increase in expression with senescence and under conditions of 3% O_2. No significant changes in these enzymes were seen between 20% senescent, 3% young, and age matched 3% old conditions. The altered expression of mitochondrial and glycolytic enzymes can be explained by the fact the mitochondria have their own autonomous protein degradation machinery that differs from cytosolic protein degradation machinery [67]. The gene expression profiles of these genes could represent steady state expression levels of these metabolic regulatory proteins under the conditions specified. These changes coincide with the changes in mitochondrial volume per cell volume (Chapter 3). Mitochondrial volume per cell volume was not shown to differ significantly under conditions of 20% senescence, 3% young, and 3% old; however all three of these conditions differed significantly from 20% young, showing a decrease in mitochondrial volume per cell volume when compared to 20% young (Fig. 3.3). This would account for the lower steady state expression levels of ATPase in the conditions of 20% senescence, 3% young, and 3% old when compared to 20% young. The subsequent increase in steady state expression levels of the glycolytic genes under the same conditions could be a result of the cell attempting to compensate for the loss of ATP (via loss of mitochondria volume per cell) by promoting ATP production through glycolysis. This process is similar to the Warburg effect exhibited by cancer cells [68].

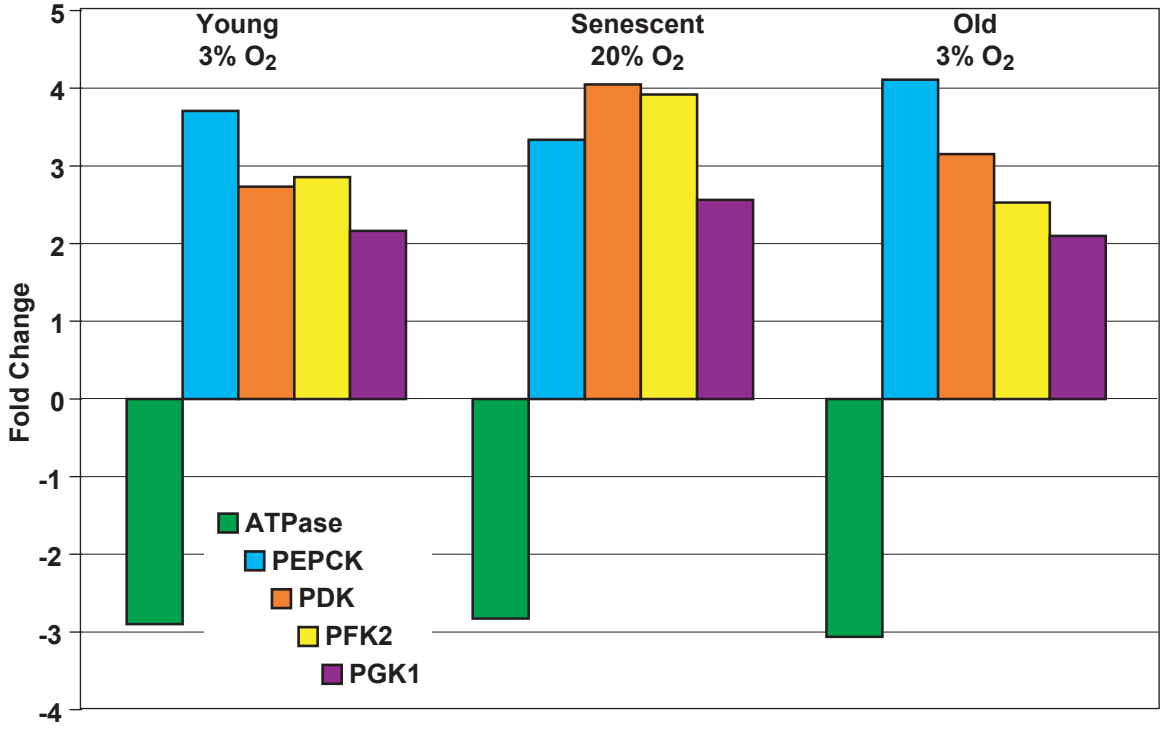

Fig. 5.5. *Differences in expression of genes involved energy metabolism.* Graph represents changes in gene expression levels for Imr90 cells under conditions of 3 and 20 percent oxygen with age relative to young cells grown in 20% oxygen. Conditions include: 3% young, 20% senescent, and 3% old.

Summary and Conclusions

The results of the protein array indicated cell cycle arrest occurred with senescence through the p53/p21 pathway, with potential PTEN/p27 pathway involvement as well. The transcriptional profiling data provided changes in gene expression with different levels of constant environmental stress and senescence. Both analyses show correlative changes in gene expression and protein levels involved in the RTK/Raf/MAPK, Akt, and Wnt/beta-catenin pathways during replicative senescence in response to oxidative stress. These changes involve genes with roles in cellular stress, cell cycle control, and survival responses. Many of these gene expression changes seen in 3 vs. 20% O_2 have ties to senescence via p53, p38, and Erk 1 and 2 as shown in the protein array. Transcriptome, proteome, and metabolome data elucidated the interaction of multiple cell signaling pathways and related metabolic pathways in replicative senescence. This provides insight

as to how cell signaling affects the metabolic profile of the cell, and how the metabolic profile influences cell signaling. For example, it was shown that replicative senescence is regulated by the RTK/Raf/MAPK pathway in Imr90 cells with associated increases in the Akt pathway. In this example, Akt signaling bridges the gap between cell signaling and metabolic control, a relationship exemplified by the induction of PFK2, a critical metabolic enzyme involved in both glycolysis and gluconeogenesis. The Akt signaling pathway was also associated with the Wnt/β-catenin pathway, which may be responsible for the changes observed in cell and mitochondrial morphology as discussed in Chapter 3. Steady state expression levels of certain regulatory enzymes may also be affected predominantly by the mitochondrial morphology (mitochondrial volume per cell volume) with possible altered regulation of mitochondrial enzyme expression compared to glycolytic expression. In summary, as opposed to being limited in focus in terms of a particular pathway or product, the work described in Chapters 3 - 5 ties together multiple facets of replicative senescence, from mitochondrial morphology to gene/protein expression to metabolite profile. This provides a more complete picture of the replicative senescent process in BJ and Imr90 cells under conditions of 3% and 20% O_2.

References

1. Passos, J.F., G. Saretzki, S. Ahmed, G. Nelson, T. Richter, H. Peters, I. Wappler, M.J. Birket, G. Harold, K. Schaeuble, M.A. Birch-Machin, T.B. Kirkwood, and T. von Zglinicki, *Mitochondrial dysfunction accounts for the stochastic heterogeneity in telomere-dependent senescence.* PLoS Biol, 2007. **5**(5): p. e110.
2. Zhu, J., D. Woods, M. McMahon, and J.M. Bishop, *Senescence of human fibroblasts induced by oncogenic Raf.* Genes Dev, 1998. **12**(19): p. 2997-3007.
3. Lin, A.W., M. Barradas, J.C. Stone, L. van Aelst, M. Serrano, and S.W. Lowe, *Premature senescence involving p53 and p16 is activated in response to constitutive MEK/MAPK mitogenic signaling.* Genes Dev, 1998. **12**(19): p. 3008-19.
4. Jiang, H., S. Zhang, Q. Guan, C. Chen, F. Gao, and Y. Zhang, *1H NMR investigations of inclusion complexes between beta-cyclodextrin and 1-hexadecanol.* Curr Drug Discov Technol, 2007. **4**(4): p. 295-7.
5. Cristofalo, V.J., A. Lorenzini, R.G. Allen, C. Torres, and M. Tresini, *Replicative senescence: a critical review.* Mech Ageing Dev, 2004. **125**(10-11): p. 827-48.
6. Shelton, D.N., E. Chang, P.S. Whittier, D. Choi, and W.D. Funk, *Microarray analysis of replicative senescence.* Curr Biol, 1999. **9**(17): p. 939-45.
7. Zhang, H., K.H. Pan, and S.N. Cohen, *Senescence-specific gene expression fingerprints reveal cell-type-dependent physical clustering of up-regulated chromosomal loci.* Proc Natl Acad Sci U S A, 2003. **100**(6): p. 3251-6.
8. Yoon, I.K., H.K. Kim, Y.K. Kim, I.H. Song, W. Kim, S. Kim, S.H. Baek, J.H. Kim, and J.R. Kim, *Exploration of replicative senescence-associated genes in human dermal fibroblasts by cDNA microarray technology.* Exp Gerontol, 2004. **39**(9): p. 1369-78.
9. de Magalhaes, J.P., J. Curado, and G.M. Church, *Meta-analysis of age-related gene expression profiles identifies common signatures of aging.* Bioinformatics, 2009. **25**(7): p. 875-81.
10. Coller, H.A., *What's taking so long? S-phase entry from quiescence versus proliferation.* Nat Rev Mol Cell Biol, 2007. **8**(8): p. 667-70.
11. Marshall, C.J., *Ras effectors.* Curr Opin Cell Biol, 1996. **8**(2): p. 197-204.
12. Medrano, E.E., F. Yang, R. Boissy, J. Farooqui, V. Shah, K. Matsumoto, J.J. Nordlund, and H.Y. Park, *Terminal differentiation and senescence in the human melanocyte: repression of tyrosine-phosphorylation of the extracellular signal-regulated kinase 2 selectively defines the two phenotypes.* Mol Biol Cell, 1994. **5**(4): p. 497-509.
13. Bose, C., C. Bhuvaneswaran, and K.B. Udupa, *Altered mitogen-activated protein kinase signal transduction in human skin fibroblasts during in vitro aging: differential expression of low-density lipoprotein receptor.* J Gerontol A Biol Sci Med Sci, 2004. **59**(2): p. 126-35.
14. Lim, I.K., K. Won Hong, I.H. Kwak, G. Yoon, and S.C. Park, *Cytoplasmic retention of p-Erk1/2 and nuclear accumulation of actin proteins during cellular senescence in human diploid fibroblasts.* Mech Ageing Dev, 2000. **119**(3): p. 113-30.
15. Kinexus, *Antibody MicroArrays.* 09.
16. Kinexus, *Info Package.* 09.
17. Harbour, J.W., R.X. Luo, A. Dei Santi, A.A. Postigo, and D.C. Dean, *Cdk phosphorylation triggers sequential intramolecular interactions that progressively block Rb functions as cells move through G1.* Cell, 1999. **98**(6): p. 859-69.
18. Campisi, J. and F. d'Adda di Fagagna, *Cellular senescence: when bad things happen to good cells.* Nat Rev Mol Cell Biol, 2007. **8**(9): p. 729-40.
19. Fuchs, S.Y., V. Adler, M.R. Pincus, and Z. Ronai, *MEKK1/JNK signaling stabilizes and activates p53.* Proc Natl Acad Sci U S A, 1998. **95**(18): p. 10541-6.

20. Jonason, J.H., N. Gavrilova, M. Wu, H. Zhang, and H. Sun, *Regulation of SCF(SKP2) ubiquitin E3 ligase assembly and p27(KIP1) proteolysis by the PTEN pathway and cyclin D1.* Cell Cycle, 2007. **6**(8): p. 951-61.
21. Mamillapalli, R., N. Gavrilova, V.T. Mihaylova, L.M. Tsvetkov, H. Wu, H. Zhang, and H. Sun, *PTEN regulates the ubiquitin-dependent degradation of the CDK inhibitor p27(KIP1) through the ubiquitin E3 ligase SCF(SKP2).* Curr Biol, 2001. **11**(4): p. 263-7.
22. Bringold, F. and M. Serrano, *Tumor suppressors and oncogenes in cellular senescence.* Exp Gerontol, 2000. **35**(3): p. 317-29.
23. Raffetto, J.D., M. Leverkus, H.Y. Park, and J.O. Menzoian, *Synopsis on cellular senescence and apoptosis.* J Vasc Surg, 2001. **34**(1): p. 173-7.
24. Ren, J.L., J.S. Pan, Y.P. Lu, P. Sun, and J. Han, *Inflammatory signaling and cellular senescence.* Cell Signal, 2009. **21**(3): p. 378-83.
25. Carlson, M.E., H.S. Silva, and I.M. Conboy, *Aging of signal transduction pathways, and pathology.* Exp Cell Res, 2008. **314**(9): p. 1951-61.
26. Sundaram, M.V., *RTK/Ras/MAPK signaling.* WormBook, 2006: p. 1-19.
27. Avruch, J., A. Khokhlatchev, J.M. Kyriakis, Z. Luo, G. Tzivion, D. Vavvas, and X.F. Zhang, *Ras activation of the Raf kinase: tyrosine kinase recruitment of the MAP kinase cascade.* Recent Prog Horm Res, 2001. **56**: p. 127-55.
28. Raman, M., W. Chen, and M.H. Cobb, *Differential regulation and properties of MAPKs.* Oncogene, 2007. **26**(22): p. 3100-12.
29. Vlahopoulos, S. and V.C. Zoumpourlis, *JNK: a key modulator of intracellular signaling.* Biochemistry (Mosc), 2004. **69**(8): p. 844-54.
30. Lu, W., V. Yamamoto, B. Ortega, and D. Baltimore, *Mammalian Ryk is a Wnt coreceptor required for stimulation of neurite outgrowth.* Cell, 2004. **119**(1): p. 97-108.
31. Chi, S., S. Chang, and D. Park, *Pak regulates calpain-dependent degradation of E3b1.* Biochem Biophys Res Commun, 2004. **319**(2): p. 683-9.
32. Himpe, E. and R. Kooijman, *Insulin-like growth factor-I receptor signal transduction and the Janus Kinase/Signal Transducer and Activator of Transcription (JAK-STAT) pathway.* Biofactors, 2009. **35**(1): p. 76-81.
33. Kisseleva, T., S. Bhattacharya, J. Braunstein, and C.W. Schindler, *Signaling through the JAK/STAT pathway, recent advances and future challenges.* Gene, 2002. **285**(1-2): p. 1-24.
34. Thornton, T.M. and M. Rincon, *Non-classical p38 map kinase functions: cell cycle checkpoints and survival.* Int J Biol Sci, 2009. **5**(1): p. 44-51.
35. Meloche, S. and J. Pouyssegur, *The ERK1/2 mitogen-activated protein kinase pathway as a master regulator of the G1- to S-phase transition.* Oncogene, 2007. **26**(22): p. 3227-39.
36. Angers, S. and R.T. Moon, *Proximal events in Wnt signal transduction.* Nat Rev Mol Cell Biol, 2009. **10**(7): p. 468-77.
37. Lilien, J. and J. Balsamo, *The regulation of cadherin-mediated adhesion by tyrosine phosphorylation/dephosphorylation of beta-catenin.* Curr Opin Cell Biol, 2005. **17**(5): p. 459-65.
38. Abramovici, H., P. Mojtabaie, R.J. Parks, X.P. Zhong, G.A. Koretzky, M.K. Topham, and S.H. Gee, *Diacylglycerol kinase zeta regulates actin cytoskeleton reorganization through dissociation of Rac1 from RhoGDI.* Mol Biol Cell, 2009. **20**(7): p. 2049-59.
39. Robey, R.B. and N. Hay, *Is Akt the "Warburg kinase"?-Akt-energy metabolism interactions and oncogenesis.* Semin Cancer Biol, 2009. **19**(1): p. 25-31.
40. Zamzami, N., C. Brenner, I. Marzo, S.A. Susin, and G. Kroemer, *Subcellular and submitochondrial mode of action of Bcl-2-like oncoproteins.* Oncogene, 1998. **16**(17): p. 2265-82.
41. Zhang, X., H. Liu, J. Wu, M. Liu, and Y. Wang, *Metabonomic alterations in hippocampus, temporal and prefrontal cortex with age in rats.* Neurochem Int, 2009. **54**(8): p. 481-7.

42. Chakravarti, B., M. Oseguera, N. Dalal, P. Fathy, B. Mallik, A. Raval, and D.N. Chakravarti, *Proteomic profiling of aging in the mouse heart: Altered expression of mitochondrial proteins.* Arch Biochem Biophys, 2008. **474**(1): p. 22-31.
43. Wysolmerski, J.J. and A.F. Stewart, *The physiology of parathyroid hormone-related protein: an emerging role as a developmental factor.* Annu Rev Physiol, 1998. **60**: p. 431-60.
44. Burrell, H.E., A.W. Simpson, S. Mehat, D.T. McCreavy, B. Durham, W.D. Fraser, G.R. Sharpe, and J.A. Gallagher, *Potentiation of ATP- and bradykinin-induced [Ca2+]c responses by PTHrP peptides in the HaCaT cell line.* J Invest Dermatol, 2008. **128**(5): p. 1107-15.
45. Shen, X. and M. Falzon, *PTH-related protein modulates PC-3 prostate cancer cell adhesion and integrin subunit profile.* Mol Cell Endocrinol, 2003. **199**(1-2): p. 165-77.
46. Sellers, R.S., A.I. Luchin, V. Richard, R.M. Brena, D. Lima, and T.J. Rosol, *Alternative splicing of parathyroid hormone-related protein mRNA: expression and stability.* J Mol Endocrinol, 2004. **33**(1): p. 227-41.
47. Dittmer, A., D. Schunke, and J. Dittmer, *PTHrP promotes homotypic aggregation of breast cancer cells in three-dimensional cultures.* Cancer Lett, 2008. **260**(1-2): p. 56-61.
48. Dhawan, P., A.B. Singh, N.G. Deane, Y. No, S.R. Shiou, C. Schmidt, J. Neff, M.K. Washington, and R.D. Beauchamp, *Claudin-1 regulates cellular transformation and metastatic behavior in colon cancer.* J Clin Invest, 2005. **115**(7): p. 1765-76.
49. Paschoud, S., M. Bongiovanni, J.C. Pache, and S. Citi, *Claudin-1 and claudin-5 expression patterns differentiate lung squamous cell carcinomas from adenocarcinomas.* Mod Pathol, 2007. **20**(9): p. 947-54.
50. Swisshelm, K., A. Machl, S. Planitzer, R. Robertson, M. Kubbies, and S. Hosier, *SEMP1, a senescence-associated cDNA isolated from human mammary epithelial cells, is a member of an epithelial membrane protein superfamily.* Gene, 1999. **226**(2): p. 285-95.
51. Swisshelm, K., R. Macek, and M. Kubbies, *Role of claudins in tumorigenesis.* Adv Drug Deliv Rev, 2005. **57**(6): p. 919-28.
52. Tang, L., D.L. Dai, M. Su, M. Martinka, G. Li, and Y. Zhou, *Aberrant expression of collagen triple helix repeat containing 1 in human solid cancers.* Clin Cancer Res, 2006. **12**(12): p. 3716-22.
53. Pyagay, P., M. Heroult, Q. Wang, W. Lehnert, J. Belden, L. Liaw, R.E. Friesel, and V. Lindner, *Collagen triple helix repeat containing 1, a novel secreted protein in injured and diseased arteries, inhibits collagen expression and promotes cell migration.* Circ Res, 2005. **96**(2): p. 261-8.
54. Mostert, V., *Selenoprotein P: properties, functions, and regulation.* Arch Biochem Biophys, 2000. **376**(2): p. 433-8.
55. Kabuyama, Y., K. Oshima, T. Kitamura, M. Homma, J. Yamaki, M. Munakata, and Y. Homma, *Involvement of selenoprotein P in the regulation of redox balance and myofibroblast viability in idiopathic pulmonary fibrosis.* Genes Cells, 2007. **12**(11): p. 1235-44.
56. Stearman, R.S., M.C. Grady, P. Nana-Sinkam, M. Varella-Garcia, and M.W. Geraci, *Genetic and epigenetic regulation of the human prostacyclin synthase promoter in lung cancer cell lines.* Mol Cancer Res, 2007. **5**(3): p. 295-308.
57. Imai, H., Y. Numaguchi, M. Ishii, R. Kubota, K. Yokouchi, Y. Ogawa, T. Kondo, K. Okumura, and T. Murohara, *Prostacyclin synthase gene transfer inhibits neointimal formation by suppressing PPAR delta expression.* Atherosclerosis, 2007. **195**(2): p. 322-32.
58. Dore, S., T. Otsuka, T. Mito, N. Sugo, T. Hand, L. Wu, P.D. Hurn, R.J. Traystman, and K. Andreasson, *Neuronal overexpression of cyclooxygenase-2 increases cerebral infarction.* Ann Neurol, 2003. **54**(2): p. 155-62.

59. Lee, J., B. Kosaras, H. Aleyasin, J.A. Han, D.S. Park, R.R. Ratan, N.W. Kowall, R.J. Ferrante, S.W. Lee, and H. Ryu, *Role of cyclooxygenase-2 induction by transcription factor Sp1 and Sp3 in neuronal oxidative and DNA damage response.* FASEB J, 2006. **20**(13): p. 2375-7.
60. Koki, A.T., N.K. Khan, B.M. Woerner, K. Seibert, J.L. Harmon, A.J. Dannenberg, R.A. Soslow, and J.L. Masferrer, *Characterization of cyclooxygenase-2 (COX-2) during tumorigenesis in human epithelial cancers: evidence for potential clinical utility of COX-2 inhibitors in epithelial cancers.* Prostaglandins Leukot Essent Fatty Acids, 2002. **66**(1): p. 13-8.
61. Corcoran, C.A., Q. He, Y. Huang, and M.S. Sheikh, *Cyclooxygenase-2 interacts with p53 and interferes with p53-dependent transcription and apoptosis.* Oncogene, 2005. **24**(9): p. 1634-40.
62. Choi, E.M., J.I. Heo, J.Y. Oh, Y.M. Kim, K.S. Ha, J.I. Kim, and J.A. Han, *COX-2 regulates p53 activity and inhibits DNA damage-induced apoptosis.* Biochem Biophys Res Commun, 2005. **328**(4): p. 1107-12.
63. Le, W. and S.H. Appel, *Mutant genes responsible for Parkinson's disease.* Curr Opin Pharmacol, 2004. **4**(1): p. 79-84.
64. Zhang, T., N. Jia, E. Fei, P. Wang, Z. Liao, L. Ding, M. Yan, N. Nukina, J. Zhou, and G. Wang, *Nurr1 is phosphorylated by ERK2 in vitro and its phosphorylation upregulates tyrosine hydroxylase expression in SH-SY5Y cells.* Neurosci Lett, 2007. **423**(2): p. 118-22.
65. Chu, Y., W. Le, K. Kompoliti, J. Jankovic, E.J. Mufson, and J.H. Kordower, *Nurr1 in Parkinson's disease and related disorders.* J Comp Neurol, 2006. **494**(3): p. 495-514.
66. Kanehira, M., Y. Harada, R. Takata, T. Shuin, T. Miki, T. Fujioka, Y. Nakamura, and T. Katagiri, *Involvement of upregulation of DEPDC1 (DEP domain containing 1) in bladder carcinogenesis.* Oncogene, 2007. **26**(44): p. 6448-55.
67. Kaser, M. and T. Langer, *Protein degradation in mitochondria.* Semin Cell Dev Biol, 2000. **11**(3): p. 181-90.
68. Garber, K., *Energy boost: the Warburg effect returns in a new theory of cancer.* J Natl Cancer Inst, 2004. **96**(24): p. 1805-6.

Chapter 6

Summary and Future Work

Senescence is a process defined by irreversible cell cycle arrest at the G1 phase. This arrest and its associated cellular changes can be modeled *in vitro* by serial passaging of primary cells, a protocol termed replicative senescence. Replicative senescence can be used to determine the underlying mechanisms involved in cellular aging *in vivo*, although its accuracy in representing actual *in vivo* processes is presently controversial (Chapter 1). However, as of now, it is the best tissue culture-based method for modeling *in vivo* processes and is widely used to monitor cellular responses of primary mammalian cells to environmental stresses over time. The work described in Chapters 2-5 attempts to tie together multiple molecular processes involved during replicative senescence and aging in BJ and Imr90 fibroblast cells under conditions of 3% and 20% oxygen. Specific emphasis was placed on the role of the mitochondria in these processes by characterizing both mitochondria-specific metabolites and morphological changes. Profiling of the transcriptome, proteome, and metabolome, along with characterization of mitochondrial dynamics, were performed during the induction of replicative senescence under conditions of 3% and 20% oxygen.

The most challenging work in this study was to develop an effective method for cell quenching, metabolite extraction, and LC-MS analysis of metabolites of interest (Chapter 2). This proved to be an extremely difficult because of the extremely low cell population densities of primary fibroblasts grown as adherent monolayers. These low cell densities resulted in very low yields of metabolites, making analysis difficult, especially with cells in the senescent state where proliferation was no longer occurring. After testing various other methods, it was found that a trypsinization protocol that incorporates a phosphate wash step was superior to the fast quenching and drying methodologies previously published for use in high cell population density samples. An ESI LC-MS/MS method utilizing an extended gradient was also developed specifically for these low yield analyses and proceeded to outperform the previously cited HILIC LC-MS/MS

methods.

The second step was to define the "visual" processes of replicative senescence in both BJ and Imr90 cells via lifespan, SA β-Gal, and SAHF assays, and mitochondrial numbers and volume (Chapter 3). Utilization of a image analysis protocol developed for use in microbial biofilm analysis proved to be very useful in automating the mitochondrial number and volume measurements. In accordance with previous literature, it was found that with attenuation of mitochondrial function and lack of fission there is compensatory mitochondrial hypertrophy or organelle enlargement. This relationship between function and morphology was exemplified by changes in MMP, membrane integrity, and mitochondrial volume/morphology during senescence and aging under conditions of 3% and 20% O_2. Changes in mitochondrial dynamics were shown to be partly a result of oxidative stress based on the lack of hypertrophy during aging under conditions of 3% O_2. These results were uniform across both BJ and Imr90 cells with senescence, suggesting that changes in mitochondrial dynamics are conserved across multiple cell types. The increases in mitochondrial and cellular volumes with age under both 3% and 20% O_2 suggest that *in vitro* changes in mitochondrial morphology may accurately reflect *in vivo* changes with age.

To parallel the mitochondrial data, changes in the metabolite profile of central carbon metabolism was also examined (Chapter 4). Replicative senescence under 20% O_2 conditions resulted in an overall increase in nucleotide, glycolytic, and TCA metabolites which was attributed to attenuations in energy metabolism via OD of metabolic enzymes. Conversely, under 3% O_2 conditions, these metabolite levels decreased with age after acclimation when compared to the 20% O_2. In spite of the similarities in mitochondrial morphological data across cell types the senescent metabolite profiles of BJ and Imr90 cells differed, which may be attributed to the origin of each (foreskin *vs.* fetal lung). In their natural state prior to harvest, fibroblasts of the fetal lung are not exposed to the same O_2 concentrations as foreskin, and therefore experience lower levels of oxidative stress. Such "oxidatively naïve" cells may require extended periods to recover from oxidative stress unlike foreskin cells that have experienced prior exposure to such conditions.

An antibody-based protein array and mRNA transcriptional profiling were also performed to

determine signaling pathways and changes in gene expression that occur with senescence (Chapter 5). The predominantly activated pathways involved in replicative senescence were the RTK/Raf/MAPK, Akt, and Wnt/β-catenin, with cell cycle arrest occurring through p53/p21 and PTEN/p27. Transcriptional profiling was performed under conditions of 3% and 20% O_2 in order to determine gene expression changes in response to oxidative stress. The changes in protein levels associated with senescence correlated with the observed changes in gene expression, particularly with regards to genes involved in stress signaling and metabolic pathways. The specific changes in glycolytic and mitochondrial enzyme expression that were observed may also be affected by aforementioned changes in mitochondrial dynamics.

This study was initiated in order to analyze the effects of replicative senescence and oxidative damage at the genomic, proteomic, and metabolomic levels, a rather complex goal for a single graduate student dissertation. While data were collected at all the aforementioned levels, it has only scratched the surface of this complex physiogical event. Future efforts should be direceted at more targeted proteomic work and potentially more extensive metabolic profiling. Targeted proteomic work should focus on metabolic enzyme levels involved glycolysis, gluconeogenesis, and the pentose phosphate pathway as well as other anabolic and catabolic pathways with emphasis on determining the extent of oxidative damage to these enzymes upon reaching the senescent state. Assessment of the protein degradation pathways may also provide insight into core senescence processes. The possibility exists that oxidatively-damaged proteins are not rapidly recognized by the degradation machinery permitting levels of less effective enzymes to increase.

There is justification for additional metabolite work, and efforts at monitoring pentose phosphate intermediates may provide new insights into maintenance of the redox state of the cell over time. Additional time-points during aging under conditions of 3% and 20% O_2 should be used to provide a better indication of the oxidative stress tolerance of the metabolic enzymes of interest. More targeted analyses using isotope dilution methods (^{13}C-labeled standards) would afford increased accuracy and sensitivity of key metabolites. Before embarking on such a study, it would be useful to explore the possibility of finding better chromatographic supports for separating the

metabolites of interest as well as increasing the life expectancy of the columns used. At present, due to the alkaline nature of the mobile phase, the life expectancy of the column is on the order of just a couple of weeks of full time use. In the course of this thesis work, four separate columns were needed to provide the data presented. As HPLC columns are relatively expensive, this cost could become prohibitive if more extensive profiling were to be performed. While there is some justification for a more open-ended metabolomics project, at present there is no evidence that any major metabolite is changing to a very large degree. If such a project were initiated, it would be best if the broad analysis quickly moved into a targeted, quantitative effort.

As seen in this study, fibroblasts derived from different source material provide different responses to oxidative stress over time, suggesting that varied enzymatic profiles may be present in different cell lines. This complicates the situation as using multiple cell lines increases the experimentation exponentially. Addition of a senescent time-point for 3% O_2 conditions would also provide further insight into telomere-dependent senescence and may be more reflective of *in vivo* aging. In particular, the Akt pathway should be of extreme interest and targeted for both proteomic and metabolic work to explore metabolic control of cell signaling. The Akt response is ideal for this type of study because it is affected by both metabolite levels and cell signaling cascades.

Finally, in moving towards more relevant or translational research, efforts directed at quantifying the proteomes and metabolomes of muscle biopsies or human naevi (moles) from a cohort of individuals of specific ages may provide a completely new approach to understanding the mechanisms of aging and senescence.

APPENDIX

The main manuscript text focuses on specific metabolome, transcriptome, and proteome changes found during senescence and aging under 20% and 3% oxygen conditions. Comprehensive results of all changes found in the metabolome, transcriptome, and proteome analyses are provided here.

Table S-1: *Known isomers of the metabolites investigated*. When measuring mass and fragmentation patterns of low mass ions, the distinct possibility exists that more than one compound can have the same mass. Below is a listing of isomers that are known components of metabolism indicated by the Ecocyc database (www.ecocyc.org).

Metabolite	Parent Mass	Isomers
Fumarate	115	Maleate
Succinate	117	Methylmalonate
Malate	133	(R)- Malate
Dihydroxyacetone phosphate	169	D-Glyceraldehyde-3-phosphate
3-Phosphoglycerate	185	2-Phosphoglycerate
Citrate	191	2,5-Diketo-D-gluconate, 5-keto-4-deoxy-D-glucarate, Isocitrate, 2,3-Diketo-L-gulonate
Glucose-6-phosphate	259	Hexose phosphates, Inositol phosphates
Fructose-1,6-bisphosphate	339	Glucose-1,6-bisphosphate,Tagatose-1,6-bisphosphate
AMP	348	dGMP
ATP	506	dGTP

Remaining Tables and Page Number

Table S-2. *MS/MS parameters and LC-MS/MS performance characteristics for metabolites quantified in this investigation.* Metabolites of interest are listed with characteristic parent and product ion peaks, limits of detection (LOD), and retention times (RT). LOD was determined by internal standards of the respective metabolites of interest. Average % error for each metabolite across cell lines and biological triplicates is indicated when applicable. The average peak area of a biological triplicate for each metabolite of interest normalized to cell population number and the internal standard NAG are listed for conditions of 20% young (20% Y), 20% senescent (20% O), age-matched 3% young (3% Y), and age-matched 3% old (3% O) for both Imr90 and BJ primary fibroblasts.

IMR90							20% Oxygen		3% Oxygen	
							Y	O	Y	O
Metabolite	Parent Ion	Product Ions		Retention Time (min)	Limit of Detection (ng/ml)	Avg. % Error	Avg. Peak Area	Avg. Peak Area	Avg. Peak Area	Avg. Peak Area
NADPH	744.12	Major	78.8	97	3000	-	-	-	-	-
		Minor	408			-	-	-	-	-
NADP	742.18	Major	620.3	58	100	10.49	4.78E+04	8.82E+04	2.49E+04	1.48E+04
		Minor	78.7			12.02	1.28E+04	2.36E+04	6.63E+03	4.08E+03
NADH	664.22	Major	79	55	1000	14.58	1.90E+04	3.82E+04	2.07E+04	1.40E+04
		Minor	158.6			12.25	3.11E+03	6.22E+03	3.66E+03	2.20E+03
NAD	662.21	Major	540	40	150	12.33	1.48E+05	2.58E+05	1.24E+05	1.04E+05
		Minor	78.8			11.62	5.31E+04	9.27E+04	4.00E+04	3.70E+04
ATP	506.01	Major	78.8	99	1000	-	-	-	-	-
		Minor	158.5			-	-	-	-	-
ADP	426.05	Major	78.9	67	200	10.78	5.19E+03	1.25E+04	9.47E+03	3.75E+03
		Minor	133.9			6.71	2.20E+03	5.05E+03	4.26E+03	1.60E+03
AMP	346.05	Major	78.8	54	50	5.28	1.95E+03	2.59E+03	3.61E+03	1.08E+03
		Minor	134			7.44	5.52E+02	7.58E+02	1.07E+03	3.17E+02
FBP	338.98	Major	240.9	70	300	5.87	7.81E+04	1.67E+05	9.57E+04	2.96E+04
G/F6P	258.94	Major	168.9	55	1000	14.45	3.40E+04	6.00E+04	4.07E+04	1.58E+04
Iso/Cit	190.95	Major	110.8	58	20	13.26	1.27E+06	1.84E+06	1.29E+06	6.76E+05
CIT	190.96	Major	86.8	58	20	15.43	4.81E+05	7.08E+05	4.74E+05	2.62E+05
ISOCIT	190.95	Major	172.8	58	20	12.3	9.23E+04	1.32E+05	1.05E+05	5.57E+04
2/3PG	184.93	Major	96.9	58	200	7.90	1.79E+04	5.83E+04	3.66E+04	1.21E+04
DHAP/GAP	168.84	Major	96.9	55	3000	9.08	3.44E+04	2.20E+04	1.60E+04	1.13E+04
		Minor	62.9			5.39	6.16E+02	3.33E+02	4.52E+02	2.69E+02
PEP	166.88	Major	78.8	63	100	14.64	1.95E+04	5.90E+04	4.20E+04	1.41E+04
		Minor	62.8			9.37	5.30E+02	1.89E+03	1.31E+03	4.26E+02
AKG	144.91	Major	100.9	55	200	16.85	3.70E+04	5.20E+04	6.47E+04	2.82E+04
		Minor	57.1			15.45	5.65E+03	8.18E+03	1.01E+04	3.89E+03
MAL	132.94	Major	115	55	30	8.92	4.44E+05	4.26E+05	4.77E+05	2.24E+05
		Minor	70.9			8.79	2.10E+05	2.03E+05	2.07E+05	1.07E+05
OAA	130.92	Major	86.8	55	2000	10.43	1.97E+03	2.87E+03	1.95E+03	1.08E+03
SUC	116.97	Major	73	55	1500	12.58	1.19E+04	1.58E+04	2.33E+04	8.22E+03
		Minor	98.9			13.69	1.13E+03	1.54E+03	2.36E+03	7.53E+02
FUM	114.94	Major	70.9	55	1000	11.06	2.73E+04	3.34E+04	3.06E+04	1.62E+04
LAC	88.9	Major	70.9	37	2000	8.53	2.07E+04	3.93E+04	3.71E+04	1.90E+04
PYR	86.92	Major	43.1	32	2000	-	-	-	-	-
		Minor	58.9			-	-	-	-	-

BJ							20% Oxygen		3% Oxygen	
							Y	O	Y	O
Metabolite	Parent Ion	Product Ions		Retention Time (min)	Limit of Detection (ng/ml)	Avg. % Error	Avg. Peak Area	Avg. Peak Area	Avg. Peak Area	Avg. Peak Area
NADPH	744.116	Major	78.8	97	3000	-	-	-	-	-
		Minor	408			-	-	-	-	-
NADP	742.179	Major	620.3	58	100	10.49	5.64E+04	1.01E+05	4.59E+04	4.74E+04
		Minor	78.7			12.02	1.49E+04	2.77E+04	1.24E+04	1.26E+04
NADH	664.22	Major	79	55	1000	14.58	1.30E+04	3.70E+04	1.63E+04	1.75E+04
		Minor	158.6			12.25	2.25E+03	6.70E+03	2.86E+03	3.00E+03
NAD	662.211	Major	540	40	150	12.33	1.29E+05	2.73E+05	1.19E+05	1.38E+05
		Minor	78.8			11.62	4.66E+04	9.44E+04	4.01E+04	4.83E+04
ATP	506.013	Major	78.8	99	1000	-	-	-	-	-
		Minor	158.5			-	-	-	-	-
ADP	426.046	Major	78.9	67	200	10.78	5.27E+03	1.57E+04	3.56E+03	7.09E+03
		Minor	133.9			6.71	2.03E+03	7.19E+03	1.41E+03	3.08E+03
AMP	346.05	Major	78.8	54	50	5.28	9.85E+03	4.59E+03	6.57E+03	2.09E+03
		Minor	97			7.44	2.58E+03	1.30E+03	1.81E+03	6.20E+02
FBP	338.984	Major	240.9	70	300	5.87	9.03E+04	1.36E+05	8.07E+04	6.40E+04
G/F6P	258.941	Major	96.7	55	1000	14.45	5.44E+03	2.72E+03	3.79E+03	2.65E+03
Iso/Cit	190.95	Major	110.8	58	20	13.26	1.48E+06	1.70E+06	8.53E+05	6.99E+05
CIT	190.96	Major	86.8	58	20	15.43	5.54E+05	6.48E+05	3.42E+05	2.51E+05
ISOCIT	190.95	Major	172.8	58	20	12.3	1.08E+05	1.23E+05	6.85E+04	5.60E+04
2/3PG	184.93	Major	96.9	58	200	7.90	1.02E+04	3.29E+04	1.32E+04	9.73E+03
		Minor	78.9			8.87	4.17E+02	1.33E+03	5.85E+02	4.81E+02
DHAP/GAP	168.838	Major	96.9	55	3000	9.08	2.46E+04	2.65E+04	1.50E+04	1.26E+04
		Minor	78.8			5.39	7.22E+02	6.54E+02	2.49E+02	2.53E+02
PEP	166.882	Major	78.8	63	100	14.64	8.14E+03	2.05E+04	1.23E+04	7.43E+03
		Minor	62.8			9.37	2.71E+02	5.52E+02	4.04E+02	2.13E+02
AKG	144.913	Major	100.9	55	200	16.85	2.66E+04	3.61E+04	2.32E+04	1.81E+04
		Minor	57.1			15.45	4.66E+03	6.04E+03	3.59E+03	2.58E+03
MAL	132.943	Major	115	55	30	8.92	5.27E+05	5.79E+05	3.71E+05	2.31E+05
		Minor	70.9			8.79	2.46E+05	2.71E+05	1.68E+05	1.08E+05
OAA	130.915	Major	86.8	55	2000	10.43	2.20E+03	3.10E+03	1.63E+03	1.16E+03
SUC	116.969	Major	73	55	1500	12.58	1.06E+04	1.59E+04	5.88E+03	5.97E+03
		Minor	98.9			13.69	1.23E+03	1.39E+03	5.40E+02	6.10E+02
FUM	114.943	Major	70.9	55	1000	11.06	3.09E+04	4.34E+04	2.21E+04	2.09E+04
LAC	88.9	Major	70.9	37	2000	8.53	1.92E+04	3.08E+04	1.50E+04	1.56E+04
PYR	86.917	Major	43.1	32	2000	-	-	-	-	-
		Minor	58.9			-	-	-	-	-

Table S-3. *Comparison of mRNA profiling data from recently published works on human cells during replicative senescence*. Gene expression change is represented by a mix of LOG values and fold change. Highlighted genes (grey boxes) are those with similar expression changes across published papers. Relatively few genes match across the individual datasets.

Genes	Shelton, D.N., et al., Curr Biol, 1999. **9**(17): p. 939-45.			Zhang, H. et al., Proc Natl Acad Sci USA, 2003. **100**(6): p. 3251-6.			Yoon, I.K. et al., Exp. Gerontol, 2004. **39**(9): p. 1369-78.	Passos, J.F. et al., PLoS Biol, 2007. 5(5): p. e110.
Cell Lines	**BJ**	**RPE340**	**HUVEC**	**WS1**	**WI38**	**BJ**	**HDF**	**MRC-5**
Adhesion								
ACAN	-	-	-	-	-	-	down .45	-
ADAMTS1	-	-	-	-	-	-	up 3	-
CD 36	-	-	-	-	-	-	up 4	-
CDH12	-	-	-	-	-	-	up 2	-
CDH13	-	-	-	-	-	-	-	-
DPT	-	-	-	-	-	-	down .40	-
ENG	-	-	-	-	-	-	down .34	-
HNT	-	-	-	-	-	-	down .41	-
ICAM1	up 4	-	up 6	-	-	-	-	-
ISLR	-	-	-	-	-	-	down .35	-
MMP3	up 4	-	-	-	-	-	-	-
PCDHGC3	-	-	-	-	-	-	down .32	-
POSTN	-	-	-	-	-	-	-	-
VCAM1	-	-	-	-	-	-	-	-
Cell Cycle								
p21	up 5	up 7	-	-	-	-	-	-
CCNA2	down 7	-	-	down 2	down 2	down 2	down 0.5	-
CCNB1	down 5	down 5	down 2	-	-	-	-	-
CCNC	-	-	-	down .5	down .8	down .6	-	-
CCND1	-	-	-	up 2	up2	up 1	up 2	-
CCNDBP1	-	-	-	up 1	up 1	up.5	-	-
CCNI	-	-	-	down .6	down .5	down .3	down .36	-
CDC2	down 5	down 5	down 2	down 1	down 1	down 1	-	-
CDK1	down 5	down 5	-	-	-	-	-	-
CDC37	-	-	-	up .6	up .7	up .4	-	-
MYBL2	down 5	-	-	-	-	-	-	-
Cell Growth								
BAP1	-	-	-	-	-	-	down .09	-
CLDN1	-	-	-	-	-	-	-	-
CTSK	up 5	up 3	-	-	-	-	-	-
FLT1	-	-	-	-	-	-	-	-
GAS1	up 4	-	-	-	-	-	-	-
GAS6	-	-	-	up 2	up 1.5	up 1	down .46	-
GAS7	-	-	-	up .7	up .5	up .4	-	-
IGF2	-	-	-	-	-	-	down .32	-
IGFBP2	up 4	up 25	-	-	-	-	-	-
IGFBP3	-	-	-	-	-	-	up 4	up 2
IGFBP5	up 5	up 5	up 15	-	-	-	up 7	-

IGFBP7	-	-	-	up 1.5	up 1.5	up 2	-	-
SERPINB2	-	-	-	up 3	up 2	up 2	-	-
SERPINB7	-	-	-	up 2	up 2	up .5	-	-
SERPINF1	-	-	-	-	-	-	-	-
RUNX2	-	-	-	-	-	-	down .27	-
STC2	up 5	-	-	-	-	-	-	-
TGFBR2	up 5	-	-	-	-	-	-	up 3
TPD52L1	-	-	-	-	-	-	up 3	-
Cytoskeleton								
COL1A1	down 5	up 5	-	-	-	-	-	-
COL3A1	down 5	-	up 5	-	-	-	-	-
COL14A1	-	-	-	-	-	-	-	-
COL6A1	-	-	-	down .8	down .4	down .5	-	-
CO6A2	-	-	-	down .8	down .4	down .5	-	-
CTHRC1	-	-	-	-	-	-	-	-
ELN	down 10	-	-	-	-	-	down 0.49	-
KRT7	down 5	-	-	-	-	-	-	-
KRT14	-	-	-	-	-	-	up 2	-
KRT19	-	-	-	-	-	-	up 4	-
KRTAP4-12	-	-	-	-	-	-	-	-
FBN2	-	-	-	-	-	-	down .36	-
FGL2	-	-	-	-	-	-	-	-
MMP1	-	-	-	-	-	-	down .45	-
Metabolism								
ACOT8	-	-	-	-	-	-	-	up 2
ACSL5	-	-	-	-	-	-	-	up 2
ALDH1A1	-	-	-	-	-	-	-	up 3
ALDH8A1	-	-	-	-	-	-	-	down .5
AK1	-	-	-	up .4	up .7	up .4	-	-
AK3	-	-	-	-	-	-	-	up 3
AK3L1	-	-	-	-	-	-	-	-
AKGDH	-	-	-	-	-	-	-	up 2
ALDH2	-	-	-	-	-	-	down.48	-
ASK	-	-	-	-	-	-	-	down .5
ATP5J	-	-	-	-	-	-	-	-
ATP6IP1	-	-	-	up .7	up 1	up 1	-	-
ATP6VoC	-	-	-	up .8	up.8	up .5	-	-
ATP6Vo1	-	-	-	up .7	up 1	up .4	-	-
ATP8B1	-	-	-	-	-	-	-	up 2
ATP8B4	-	-	-	-	-	-	-	-
CPT1A	-	-	-	-	-	-	-	up 2
CS	-	-	-	-	-	-	down .32	-
FABP4	-	-	-	-	-	-	-	up 2
GALNT5	-	-	-	-	-	-	-	up 1
GALNT10	-	-	-	-	-	-	-	up 2
GCLM	-	-	-	-	-	-	-	up 2

GLS	-	-	-	up 1	up.7	up 2	-	up 3
GLUL	-	-	-	-	-	-	-	down .5
GRIA4	-	-	-	-	-	-	-	down .3
GRIK4	-	-	-	-	-	-	-	-
GSR	-	-	-	down .5	down .7	down 1	-	-
HK2	-	-	-	-	-	-	up 2	up 2
HSD17B12	-	-	-	-	-	-	-	up 3
LOX	-	-	-	-	-	-	-	up 2
LOXL2	-	-	-	-	-	-	-	-
NDUFV2	-	-	-	-	-	-	down .34	-
PCK2	-	-	-	-	-	-	-	-
PDK1	-	-	-	-	-	-	-	-
PDK4	-	-	-	-	-	-	-	up 3
PDP2	-	-	-	-	-	-	-	up 2
PGK1	-	-	-	-	-	-	-	-
SCD	-	-	-	-	-	-	down .32	down .3
TK1	down 5	-	-	up 4	up 9	up 5	-	-
TYMS	down 5	-	-	-	-	-	-	-
Mitochondrial Function								
CPS1	-	-	-	-	-	-	-	down .3
MAOA	-	-	-	-	-	-	-	up 3
MIPEP	-	-	-	-	-	-	-	down .5
MTUS1	-	-	-	-	-	-	-	down .4
NRF1	-	-	-	-	-	-	-	down .5
SLC1A1	-	-	-	-	-	-	-	-
SLC2A1	-	-	-	-	-	-	-	-
SLC16A2	-	-	-	up .5	up1	up.6	-	-
SLC5A3	-	-	-	-	-	-	-	up 2
SLC16A3	-	-	-	up 1	up 1	up 1	-	-
SLC16A6	-	-	-	up .5	up 1	up 1	-	-
SLC20A2	-	-	-	up 1	up 2	up 1	-	-
SLC25A4	-	-	-	up .6	up .4	up 1	-	-
SLC30A1	-	-	-	-	-	-	-	-
SLC31A2	-	-	-	up 1	up 2	up 1	-	-
SLC39A4	-	-	-	down .4	down .3	down 1	-	-
UAP1L1	-	-	-	-	-	-	-	down .5
UCP2	-	-	-	-	-	-	-	up 2
Inflammation								
COX2	-	-	-	-	-	-	up 3	-
CXCL1	up 7	-	-	-	-	-	up 6	-
CCL2	-	-	-	-	-	-	-	-
CXCL6								
CXCL7	-	-	-	-	-	-	up 3	-
CXCL8	-	-	-	-	-	-	up 3	-
CXCL11	-	-	-	-	-	-	up 3	-
IL1B	up 5	-	-	-	-	-	-	-

IL1R1	-	-	-	-	-	-	-	-
IL6	-	-	-	-	-	-	up 3	-
IL15	up 4	-	-	-	-	-	-	-
MX1	-	-	-	-	-	-	up 4	-
PTX3	-	-	-	-	-	-	-	-
TLR4	up 7	-	-	-	-	-	-	-
Immune Response								
B2M	-	-	-	-	-	-	up 2	-
CFP	-	-	-	-	-	-	up 3	-
DPP4	-	-	-	-	-	-	up 2	-
HLA-A	-	-	-	-	-	-	up 2	-
HLA-B	-	-	-	-	-	-	up 2	-
HLA-C	-	-	-	-	-	-	up 2	-
IFI6	-	-	-	-	-	-	up 4	-
IFIT1	-	-	-	-	-	-	up 3	-
ISG15	-	-	-	-	-	-	up 2	-
LTBP1	down 5	-	-	-	-	-	-	-
OAS1	-	-	-	-	-	-	up 2	-
Signal Transduction								
NPR2	-	-	-	-	-	-	up 2	-
PENK	-	-	-	-	-	-	up 3	-
MEK3	-	-	-	up .5	up .7	up .3	-	up 2
RGS4	-	-	-	-	-	-	-	-
RGS5	-	-	-	-	-	-	-	-
STK17A	-	-	-	-	-	-	-	-
STK24	-	-	-	down .6	down .3	down 1	-	-
SOCS2	-	-	-	-	-	-	-	-
SOCS5	-	-	-	down 1	down 1	down .2	-	-
TRPA1	-	-	-	-	-	-	-	-
Oxidative Stress and Apoptosis								
BCL2L1	-	-	-	up 1	up 1	up 1	-	up 2
BCL2L11	-	-	-	-	-	-	-	up .3
BCOR	-	-	-	-	-	-	-	down .3
CARD10	-	-	-	-	-	-	-	down .5
CASP7	-	-	-	up .8	up 1	up 1	-	-
CCAR1	-	-	-	-	-	-	-	down .3
DDIT	up 4	-	up 5	-	-	-	-	-
NAPOR	-	-	-	-	-	-	down .31	-
PAWR	-	-	-	-	-	-	-	up 3
SEPP1	-	-	-	-	-	-	-	-
SOD2	up 7	-	-	-	-	-	-	up 1
TNFRSF10C	-	-	-	up 2	up .5	up 1	-	-
TNFRSF21	-	-	-	-	-	-	-	-
Unknown/Other								
ABCG1	-	-	-	-	-	-	-	-
ADAM12	-	-	-	down .4	down .9	down 1	-	-

ADAMTS8	-	-	-	-	-	-	-	-
CAPN6	-	-	-	-	-	-	down .33	-
CPE	-	-	-	-	-	-	-	-
CRIP1	-	-	-	-	-	-	down .37	-
CYTL1	-	-	-	-	-	-	-	-
EEA1	-	-	-	-	-	-	down .36	-
EPPK1	-	-	-	-	-	-	-	-
HEPH	-	-	-	-	-	-	-	-
ID4	-	-	-	-	-	-	-	-
IQGAP3	-	-	-	-	-	-	-	-
KIF4A	-	-	-	-	-	-	down .38	-
MYCT1	-	-	-	-	-	-	-	-
PAM	up 4	-	-	-	-	-	-	-
PDE4D	-	-	-	-	-	-	-	-
PKN2	-	-	-	-	-	-	down .46	-
FUBP1	-	-	-	-	-	-	down .42	-
SOX9	-	-	-	-	-	-	down .37	-
SOX22	-	-	-	down .7	down .6	down .5	-	-

Table S-4. *Gene expression changes found during aging and senescence under 20% and 3% oxygen conditions.* Fold changes of LOG values are listed for genes showing a 2-fold or more change in expression at all four conditions: 20% young, 20% senescent, age-matched 3% young, age-matched 3% old.

Probe Level Analysis: Robust Multichip Analysis(RMA)
T-test: unpaired
P-Value Computation: Asymptotic, 100 permutations
P-Value Correction: Benjamini Hochberg FDR
Differential Expression Analysis: P-Value=0.05, Filter: min-max=2.0
Baseline Transformation: Y20 as control comparison
Sample Average Computation: Average for each probe set across condition/time point

Gene Symbol	20% Young	20% Senescent	3% Young	3% Old
ABCG1	-1	2.078193947	4.525621092	13.73511705
ADAMTS8	1.00000011	-2.817338476	-3.787494254	-3.00419071
ADAMTS8	1.00000022	-13.47878546	-18.78875673	-14.36203223
ADH1B	-1	-2.109759427	-2.048005089	-2.265704951
AK3L1	1.00000022	2.770105649	2.38502816	2.015332945
AK3L1	-1.00000022	6.985348046	4.694793492	3.437642218
AKR1C1	-1.00000022	-3.401550717	-4.594651696	-2.983737671
AKR1C2	-1	-2.633114212	-3.509528696	-2.59435553
AKR1C2	-1.00000022	-2.964565968	-3.454670463	-2.654599283
ANGPTL2	-1.000000661	-2.946842388	-2.920278982	-2.514751946
ANKH	1.00000022	-2.431816551	-2.041026763	-2.230219796
ANKH	1.000000441	-3.098186517	-2.493302105	-3.122262424
ANKH	1.00000022	-2.37223741	-2.135950332	-2.456045861
AQP3	1.00000022	-10.71671471	-4.598055883	-4.571742034
ARHGEF3	-1.000000331	-2.659117264	-3.062218653	-3.621601979
ASNS	-1	2.712899305	2.51782585	2.902776106
ATP5J	-1	-2.828017014	-2.898783525	-3.061185349
ATP8B4	1.000000331	-2.080512707	-2.138705594	-2.278462143
B3GALNT1	1.00000011	-6.396163421	-2.070052274	-2.590248658
B4GALT6	1.00000011	-4.729711219	-2.205285284	-6.122758585
BCAT1	1.000000331	2.09939204	2.255991294	2.204074669
BNIP3	-1	5.154222437	4.432097134	3.787864701
BNIP3	1.00000022	4.394718629	3.505702326	3.114256987
C1R	-1.00000022	-3.279107275	-3.152849052	-3.978380597
C1S	-1	-2.511126139	-3.323592024	-2.863278297
C20orf100	-1.00000011	2.274634903	2.036728953	2.49137726
CCL2	-1	-2.564349672	-6.308338168	-16.22361032
CD226	-1.000000331	-2.668933945	-2.183628149	-2.795785156
CDH13	-1.00000011	2.134510708	2.073144102	2.302208504
CEBPD	1.00000022	2.191208245	2.007631796	2.016609857
CFH /// CFHR1	-1.00000011	-6.214434866	-4.530263606	-4.688424824
CHRDL2	-1.000000331	-2.182401892	-2.872335955	-2.599460981
CLDN1	-1.00000022	2.097818698	-4.724807003	-4.135663486
CLU	-1.00000022	-2.269348692	-5.2646886	-6.083683923

CLU	1.000000441	-2.207161046	-5.029237554	-6.218609821
COL14A1	1.000000331	-6.806033253	-5.709236397	-5.416879507
COL14A1	-1	-13.9441704	-9.997705288	-10.0259539
CORIN	-1	-6.622129391	-2.243110357	-3.602210776
CPE	1.00000022	-13.08360496	-6.737635117	-10.60179467
CPEB2	-1.00000011	-2.503137427	-2.126935966	-2.393920927
CROT	1.00000022	-2.03391121	-2.455364825	-2.058578551
CSS3	-1.00000011	-2.393149459	-2.230982195	-2.446793078
CYTL1	-1.000000331	-5.136281239	-11.03160194	-11.86260622
DACH1	1.00000011	-2.309946119	-2.558211068	-2.132406079
DCN	1.000000441	-2.272346907	-3.705881114	-3.175762006
DCN	1.00000022	-3.197270486	-5.49139999	-4.796383448
DCN	-1.00000022	-2.109459223	-3.599498956	-3.024119815
DCN	1.000000441	-2.392143605	-4.024258555	-3.392046859
DDB2	-1	2.055924664	2.261809933	2.487835681
DDIT4	-1	3.987853746	6.036370256	6.885882676
DGKI	-1.00000011	-5.45546322	-3.464799334	-3.877794631
DIO2	-1.00000022	-2.512488164	-3.367515299	-2.273365418
DIO2	1.00000022	-3.583022989	-4.257415807	-2.639386449
DNM3	-1	-3.549747483	-3.111137376	-2.526942436
DSP	-1.00000011	2.324707493	2.686525999	4.044655142
EGLN1	-1	2.630210745	2.74218366	2.555811967
EGLN1	-1	2.118611121	2.222342381	2.146445735
EGR3	1.00000022	-6.988006741	-3.884339766	-6.187834453
EIF2C2	1.00000022	-2.873907246	-2.840104276	-2.455165367
EIF4EBP1	-1.00000022	2.116894102	2.205039042	2.085480034
ENAH	-1	-2.353908432	-2.029363072	-2.095095489
ENAH	1.00000022	-2.869023728	-2.129344385	-2.042898604
ENO2	-1	5.449556787	3.770726468	3.474984397
EPOR	1.000000331	2.820365621	2.488318052	3.420587654
EPOR	1.000000331	2.629557237	2.346325388	3.306388612
EPPK1	1.00000022	-10.60838401	-2.869020944	-4.924895115
ERO1L	-1	3.167066806	2.049949401	2.14207011
ERO1L	-1	4.547566705	3.291046703	3.401543644
ETV6	1.00000011	-2.101260021	-2.067018928	-2.044677486
FAM13A1	-1.00000022	3.622543716	2.810677058	3.220929761
FAM38B	-1	-4.830419882	-4.535826007	-3.295978428
FAM38B	1.00000022	-3.078849185	-2.91230913	-2.448879524
FAT3	1.00000011	-2.189356663	-4.349118445	-5.873335294
FBLN1	1.00000011	-3.852068344	-3.91766544	-3.828370349
FGL2	-1.00000022	-31.34846724	-2.211434175	-3.237432919
FLT1	-1.000000661	-2.880960539	-8.555049487	-13.48704141
FLT1	-1.000000441	-3.376635612	-7.921408622	-12.30720795
FOS	1.00000011	-5.756370293	-5.064038594	-3.338097283
FOSB	1.000000331	-2.49338558	-2.463607115	-2.763648432
FZD8	1.00000011	-3.760333191	-2.072166171	-2.266468327

GALNACT-2	1.00000022	-2.104716472	-2.497907581	-2.198465511
GALNACT-2	1.00000022	-2.346963329	-2.900227756	-2.239137619
GAS7	1.00000011	-2.081692248	-2.550155641	-2.253864055
GCH1	1.00000011	-2.141636304	-2.28996905	-3.21883539
GEM	-1.00000022	-3.720982486	-2.121149196	-2.644312533
GGH	-1.00000022	2.094752796	4.684340995	4.756369514
GPC4	1.00000022	-6.059981124	-2.451971992	-3.331274181
GREM2	1.00000022	-5.941460868	-3.79127367	-3.464058514
GREM2	-1.00000022	-8.527669939	-4.740328369	-3.811364006
GRIK2	-1	3.080625265	2.852582279	3.509816243
GUCY1A3	1.000000441	-2.291307841	-2.063582905	-2.823776686
GUCY1B3	-1	-2.646818558	-2.84059588	-4.082861984
HBEGF	1.00000022	-4.14684637	-5.08084904	-7.978259228
HBEGF	-1	-3.516900942	-4.287004703	-5.850982893
HIG2	1.00000011	2.630402545	2.285596449	2.298847398
HIST1H2AC	1.000000441	2.048589751	-2.008574816	-2.368459332
HNMT	1.00000011	-3.445821812	-2.817284969	-2.581827477
HSD17B6	-1	-2.100693672	-2.630336726	-2.513696898
HSPC111	1.000000441	-3.681980791	-2.878491396	-2.811251255
HSPC111	1.00000022	-3.355318223	-2.156246179	-2.703026957
ID4	-1	-2.978972488	2.263638845	3.10423225
IGFBP3	1.000000441	2.324999168	2.847150193	2.11763831
IL1R1	-1	-3.1765997	-2.232876565	-2.693630758
INHBE	-1.000000331	2.401556915	4.377723391	4.563902591
IQGAP3	1.00000022	2.037906696	9.777598738	11.42526007
ITGAV /// PLTP	1.00000022	-2.021695892	-2.800834815	-2.319748176
ITGB8	1.00000011	-2.315027289	-2.224196113	-3.773117949
KAL1	1.00000011	-2.798839582	-2.124510833	-2.05112185
KATNAL1	1.00000022	2.010380803	2.18287815	2.428080579
KBTBD8	1.00000022	-2.627898037	-3.145862468	-3.700614358
KCTD12	1.00000022	-4.433878693	-4.126585694	-3.442112141
KCTD12	-1	-4.406481658	-4.656655967	-4.184513785
KIAA1211	-1.00000022	-3.064593241	-2.703322065	-3.204037426
KRTAP4-12	1.00000011	-4.634859481	-5.922664236	-8.67726266
LEF1	-1.00000022	-5.539782365	-6.635431561	-3.86706523
LFNG	-1.00000011	-2.514764844	-2.417705297	-2.810384452
LIF	1.000000441	-4.441736471	-4.514215213	-7.592157913
LOX	-1.00000022	3.484162953	2.94850226	2.070256894
LOXL2	-1.00000022	2.340426892	2.541340347	2.258971705
LRRC8B	1.000000331	-2.105517549	-2.738398486	-3.54332918
LRRN1	-1	-3.971529171	-3.390309306	-4.062068026
LXN	1.000000661	-2.68277916	-2.040917832	-2.191601202
MAN1A1	-1.00000022	-2.314946577	-3.450678586	-2.235007078
MAN1C1	-1	-2.669965315	-4.883475639	-6.349522493
MFAP4	-1	-3.625163087	-4.968877242	-5.544891382
MKI67IP	-1.00000022	-2.462147514	-2.16805176	-2.98559919

MRVI1	1.00000022	-2.017936533	-2.382526565	-2.007877843
MXI1	-1.00000011	5.100735884	3.631627421	3.399478864
MYCT1	1.00000011	2.536141604	8.97740325	7.149137996
MYH11	1.00000011	-2.264418162	-2.047906715	-2.005914898
MYLK	-1	-2.346800818	-2.984542711	-3.186896575
NAV3	-1	-2.009333868	-2.440180385	-2.65106051
NDRG1	1.000000441	5.005145469	5.239718841	6.238564493
NFASC	-1	-2.184250014	-2.119919085	-2.334193884
NFIL3	1.00000011	2.084551623	2.605679062	2.89932769
NRK	-1.00000011	-3.409926635	-2.18849517	-2.958488321
NRXN3	1.000000441	-2.718051327	-2.235446316	-2.754213122
NUFIP1	1.000000441	-2.493515896	-2.076588561	-2.402425345
OLFML2A	1.000000441	-3.368040298	-6.610162324	-6.280134686
PCK2	-1.000000441	3.335735736	3.709190076	4.110486057
PCSK5	1.00000022	-3.013379552	-3.171919154	-4.690576339
PDE4D	1.000000331	2.878928981	8.600369834	10.2423297
PDE4D	1.00000011	2.458422371	8.61116242	11.00116572
PDGFD	1.000000441	-7.655547721	-5.171350177	-4.773032633
PDK1	-1	4.047919781	2.731773746	3.153223212
PDLIM4	-1	-2.279724993	-2.189984714	-2.564401575
PDPN	-1	-5.940990576	-4.242035223	-4.796948996
PELO	-1.00000011	-2.066324449	-2.489489792	-2.089769032
PFKFB4	-1	3.919325517	2.855939069	2.528149012
PGK1	-1	2.563433372	2.164215708	2.099337616
PGK1	-1	2.640181845	2.308256101	2.164815539
PGK1	-1	2.572889682	2.269266111	2.023272866
PHF14	1.00000011	-2.978840546	-2.691216396	-2.750679402
PHF21A	1.00000011	2.617838687	2.171760029	2.410340391
PLAGL1	-1.00000022	2.264360088	2.085109284	2.271408516
PLAGL1	-1.00000022	2.298942847	2.093524498	2.302626474
PLAU	-1.00000022	-2.687387199	-3.161825395	-2.286985946
PLEKHA2	1.000000441	2.309554995	2.927279495	3.140746276
PLEKHA2	1.00000011	2.125578735	2.156738555	2.875698648
PNO1	1.00000011	-2.614432821	-2.412841587	-2.656642685
POSTN	1.000000441	-2.31125878	-3.859886431	-9.367361877
POSTN	-1	-2.695234685	-2.473721353	-2.678035342
PROS1	-1	-3.544357677	-3.975363545	-3.284492566
PSAT1	-1	2.166502648	2.166906194	2.720573113
PSAT1	1.00000022	2.801584875	2.754670383	3.02297448
PSG5	1.00000022	7.368147283	3.945633352	2.945950113
PSPC1	1.00000011	-3.34393499	-2.206758263	-2.183053066
PTGS2	-1.000000441	-3.086760822	4.679172775	7.99551133
PTHLH	1.00000011	-10.42359189	-7.377953518	-8.421637047
PTHLH	-1.00000022	-2.675847505	-2.362055232	-2.934854131
PTHLH	-1.00000022	-4.91747937	-3.277307629	-4.049927832
PTHLH	-1.00000022	-20.54583416	-13.31348904	-18.77161277

PTPRB	1.00000011	2.112749173	3.845403263	2.255006044
PTX3	1.00000022	-3.982542893	-10.18318246	-19.80717191
RARRES1	-1.00000011	-4.36999158	-2.392780237	-3.61067508
RARRES2	1.00000022	-8.216605494	-8.314897044	-7.360884836
RASSF2	1.000000661	-2.823339852	-3.648024959	-3.181156834
RGS4	-1	-2.088250234	-2.331439997	-8.600062831
RGS5	-1.00000022	-2.119591284	-5.578674977	-8.439085675
RHOJ	1.00000011	-3.655894909	-2.056386007	-4.682410114
RHOJ	1.00000022	-3.57897558	-2.254417319	-5.029859146
RIOK2	-1.000000441	-2.126923435	-2.276753655	-2.380454247
RNF128	-1	-3.461191584	-4.107662643	-5.593962956
ROR1	-1.00000011	-3.150992674	-2.439007171	-5.503223037
RORA	1.00000011	3.107459309	3.44936907	3.252409694
RRM2	-1.000000441	-2.057898319	2.355664204	2.406817914
SCG5	1.00000022	-6.970642796	-2.658646379	-3.080872546
SCN2A2	-1.00000011	-2.597440317	-2.134047813	-2.68739614
SEPP1	1.00000022	-20.18549415	-8.279903766	-13.07062751
SERPINB2	1.00000022	-4.933674716	-3.063192642	-10.60466028
SERPINB7	1.00000011	6.79098149	4.163693003	3.588008977
SERPINF1	-1	-5.708648763	-6.788143201	-9.631173551
SFRS2IP	-1.00000011	-3.90978073	-2.741825775	-3.005632248
SFRS3	1.000000441	-3.175189728	-2.385672655	-2.128036948
SFRS7	1.00000022	-3.10617971	-2.29984718	-2.798002594
SGCD	-1	-2.140213319	-3.144756472	-2.667227344
SLC16A6	-1.00000022	-2.778152895	-7.06775877	-2.10066688
SLC1A1	1.00000022	2.60038998	2.075410617	5.077835646
SLC2A1	1.00000022	3.181036443	2.972931248	2.824445573
SLC30A1	-1	-2.350254518	-2.736069164	-2.673825472
SOCS2	-1.00000011	2.572397157	5.573343217	7.792202122
SPOCD1	-1.000000331	-2.478891111	-2.710003848	-2.451515528
SPON1	-1	-2.135356575	-2.107304507	-2.578299394
SPON1	-1.00000022	-4.505670147	-2.754619403	-5.100569716
SPRY4	-1	-2.472241021	-2.043600367	-2.094683828
STC2	-1.000000441	2.286060841	2.110197308	2.325001102
STK17A	1.00000022	-2.355891177	-2.105116827	-2.367865114
SVEP1	-1.00000022	-2.181346567	-4.52973421	-5.5208121
SYNE1	-1.00000022	-2.211906496	-2.755596403	-2.28635781
TMEM119	1.00000011	-2.067461838	-2.277179946	-2.39103956
TMEM176A	-1.000000441	-6.274133383	-6.623173264	-6.804234204
TMEM176B	1.00000011	-5.273454709	-5.87104372	-6.296819445
TMEM5	-1.00000011	-2.298418962	-2.23560251	-2.138244012
TMEM56	-1.00000022	-2.11906303	-2.092761927	-2.295379982
TMTC2	1.00000022	-6.769660574	-3.943179812	-5.95279825
TNC	-1.00000022	-2.624357568	-2.8210775	-2.586814675
TNC	-1.00000022	-2.55718015	-2.148868649	-3.083278696
TNC	1.000000331	-3.226609083	-3.16582169	-2.997731562

TNFAIP6	-1	-7.701415854	-2.284922131	-3.110262401
TNFRSF21	-1.00000022	-2.007066196	-7.349180065	-2.427588346
TNFRSF21	-1.00000022	-2.066721368	-7.032228748	-2.532100909
TP53RK	-1	-2.323278008	-2.34531483	-2.127788123
TPM2	1.00000011	-2.304609793	-2.422484945	-2.197169697
TRPA1	-1.00000011	-3.57410867	-3.487308752	-2.263043945
TRPA1	-1.00000022	-8.366237769	-10.01815963	-2.798847536
TSLP	-1.00000022	-2.094539803	-5.388375158	-4.918415784
VCAM1	-1.000000881	-2.397467736	-9.947129783	-31.96670191
VLDLR	-1	2.609479196	2.178675603	2.287717958
WDR54	1.00000011	2.571481545	2.23766288	2.186050153
XIST	-1	-2.617473625	-2.436725772	-2.859258585
ZFP36	-1	-3.071589029	-2.998295549	-3.57876373
ZNF365	-1.00000011	-2.012556102	-2.457671511	-2.21684761
ZNF395	1.00000011	5.64658577	7.916444388	6.292097385
ZNF551	1.00000011	-2.940438263	-3.017594392	-2.74011036

Table S-5. *Changes in protein level during senescence (raw Kinexus data).* Changes in protein expression between young (control) and senescent (treated) Imr90 cells under conditions of 20% oxygen relative to the control (young cells at 20% oxygen). When the low intensity and high error proteins are removed, there are approximately 150 proteins that exhibit significant changes.

Target Protein Name	Phospho Site (Human)	Control Average	Treated Average	Total % Error Range	% CFC
PKCg	T514	2	20	200	1086
Rb	S807+S811	15	101	26	589
RafB	Pan-specific	440	2185	3	397
PDGFRb	Y716	173	725	44	320
STAT5A	Y694	16	65	58	308
PRKAB1	Pan-specific	20	79	11	300
PTEN	Pan-specific	515	2037	16	296
PDGFRa/b	Y572+Y574/Y579+Y581	264	1019	7	286
Tau	S720	6	21	443	263
Pyk2	Pan-specific	460	1631	2	255
RSK1	Pan-specific	636	2249	9	253
Mn SOD	Pan-specific	17	56	12	223
S6Ka	Pan-specific	443	1423	7	221
STAT2	Pan-specific	415	1275	19	207
STAT5B	Pan-specific	178	533	5	200
MEK5	Pan-specific	299	897	13	200
TBK1	Pan-specific	211	626	6	196
Raf1	Pan-specific	399	1167	0	193
STAT5A	Pan-specific	445	1271	9	185
PKR	Pan-specific	572	1633	18	185
STAT4	Pan-specific	556	1579	3	184
Rb	T356	647	1799	72	178
PKCa/b2	T638/T641	23	64	24	177
MEK1	T385	40	110	8	174
PAK1	Pan-specific	389	1063	5	173
STAT3	Pan-specific	445	1206	6	171
MST3	Pan-specific	5	12	45	166
PKCz	Pan-specific	524	1377	2	163
GSK3a/b	S21	74	193	18	162
MEK3	Pan-specific	463	1208	3	161
STAT1	Pan-specific	449	1165	4	160
Mcl1	Pan-specific	499	1288	6	158
AMPKa1/2	T174/T172	278	692	20	149
PAK3	Pan-specific	312	776	6	149
Tyk2	Pan-specific	224	557	37	148
PAC1	Pan-specific	580	1402	18	142
PKCd	Pan-specific	344	800	5	133
PRKWNK4	Pan-specific	629	1457	3	132
TEK	Pan-specific	351	810	65	131
p53	Pan-specific	465	1064	1	129
SPHK2	Pan-specific	806	1821	1	126

PDK1	Pan-specific	713	1610	15	126
Trail	Pan-specific	378	849	2	125
PKD (PKCm)	Pan-specific	256	569	6	122
hHR23B	Pan-specific	547	1215	38	122
Tyro10	Pan-specific	366	803	88	120
p27 Kip1	Pan-specific	972	2132	4	119
PTEN	S380+S382+S385	663	1438	15	117
RYK	Pan-specific	598	1293	4	116
PKCb1	Pan-specific	324	686	8	112
MEK4	Pan-specific	239	506	5	112
Pyk2	Y579	705	1481	15	110
PKCg	Pan-specific	339	711	10	110
EGFR	Pan-specific	2202	4607	1	109
p21 CDKI1	Pan-specific	790	1637	4	107
PTP1C	Pan-specific	599	1232	11	106
MEK1	T291	55	111	20	104
ROS	Pan-specific	888	1810	1	104
SPHK1	Pan-specific	570	1155	2	103
STAT6	Pan-specific	247	500	23	103
JNK	T183/Y185	636	1280	3	101
Nek2	Pan-specific	722	1445	13	100
PRP4K (PRP4)	Pan-specific	776	1550	10	100
PI3KR4	Pan-specific	704	1390	6	97
S6Kb	Pan-specific	782	1534	4	96
Nip1	Pan-specific	609	1181	7	94
MEK3/6	S189/S207	58	111	33	91
PKCl	Pan-specific	402	768	4	91
RSK1/2	S363/S369	224	426	22	90
PKC-nu	Pan-specific	931	1764	4	89
RIPK	Pan-specific	740	1397	34	89
RSK1/2	S221/S227	614	1147	21	87
Hsp60	Pan-specific	636	1185	6	86
MEK7	Pan-specific	337	626	11	86
PKCe	Pan-specific	363	672	5	85
PI4KCB	Pan-specific	607	1119	6	84
Msk1	S376	29	52	59	83
SLK	Pan-specific	892	1632	4	83
Abl	Pan-specific	2569	4676	9	82
PI4K2b	Pan-specific	588	1066	2	81
KHS	Pan-specific	333	602	3	81
PDK2	Pan-specific	771	1388	4	80
PIP5K2a	Pan-specific	445	800	2	80
PCK2	Pan-specific	636	1130	5	78
S6	S235	769	1365	25	78
ROCK-I/ROKb	Pan-specific	596	1056	1	77
p38a MAPK	T180+Y182	583	1029	13	76

FAK	Pan-specific	1130	1992	3	76
Pax2	S394	654	1152	7	76
Smac/DIABLO	Pan-specific	183	317	14	74
SOD (Cu/Zn)	Pan-specific	170	288	15	70
IkBb	Pan-specific	604	1025	8	70
NFkB p65 (Rel A)	S276	1247	2094	14	68
PKCg	T674	463	775	5	67
Lck	Y504	391	652	8	67
Tlk1	Pan-specific	57	95	14	67
PAK6	Pan-specific	858	1432	5	67
PKBb (Akt2)	Pan-specific	665	1100	4	65
Wee1	Pan-specific	631	1044	9	65
RSK1/2	S380/S386	743	1227	19	65
SGK3	Pan-specific	932	1537	0	65
Tlk1	Pan-specific	577	950	4	65
p38d MAPK	Pan-specific	643	1050	3	63
p35	Pan-specific	1034	1674	3	62
ROKa	Pan-specific	866	1393	17	61
TAK1	Pan-specific	604	970	2	61
MEK1	T385	704	1130	17	60
Chk2	Pan-specific	1669	2666	1	60
Rac1/cdc42	S71	707	1129	7	60
PCTK1	Pan-specific	1026	1638	10	60
RSK2	Pan-specific	626	994	8	59
IkBa	Pan-specific	720	1143	7	59
p38 gamma	Pan-specific	753	1194	0	58
SOCS4	Pan-specific	1166	1842	3	58
NFkappaB p65	Pan-specific	1340	2110	11	57
RSK4	Pan-specific	790	1245	22	57
TAK1	Pan-specific	218	343	21	57
Src	Pan-specific	876	1374	2	57
Rb	Pan-specific	858	1343	14	57
IKKa	Pan-specific	629	968	7	54
MAK	Pan-specific	1031	1566	2	52
NR1	S896	61	92	21	51
Rad17	S645	668	1004	5	50
CytoC	Pan-specific	1370	2045	13	49
TBK1	Pan-specific	363	538	3	48
CASP1	Pan-specific	2013	2968	1	47
STAT3	S727	781	1147	3	47
Rac1	Pan-specific	751	1099	2	46
MARK	Pan-specific	1011	1478	4	46
PKA R2a (PKR2)	Pan-specific	587	858	8	46
PAK5	Pan-specific	1012	1479	2	46
SOX9	S181	688	1004	8	46
PKM2	Pan-specific	617	900	5	46

JNK2	Pan-specific	345	503	6	46
P5/PPT (same as PP5C)	Pan-specific	769	1116	21	45
MAPKAPK2	T222	909	1318	2	45
TrkB	Pan-specific	664	962	3	45
Cyclin B1	Pan-specific	1374	1992	11	45
Catenin b	Pan-specific	2039	2947	2	45
VHR	Pan-specific	598	859	10	44
Hsp40	Pan-specific	1036	1484	7	43
Synapsin 1	S9	21	30	68	43
JAK1	Pan-specific	496	709	2	43
TrkA	Pan-specific	737	1052	6	43
Vrk1	Pan-specific	833	1186	9	42
MEK1	T291	884	1255	6	42
PKN	Pan-specific	385	546	25	42
Hsc70	Pan-specific	894	1262	4	41
Tau	T231	741	1044	5	41
MAPKAPK2	Pan-specific	528	739	1	40
MAPK14 Ctr Antibody	Pan-specific	1051	1469	2	40
Cyclin G1	Pan-specific	1177	1644	3	40
NT5E	Pan-specific	1297	1806	15	39
b-Arrestin	Pan-specific	724	1002	25	38
PP1/Ca	Pan-specific	965	1333	3	38
Erk4	Pan-specific	1698	2345	1	38
IRAK3	Pan-specific	936	1285	1	37
Jun	Pan-specific	781	1065	16	36
NMDAR2B	Y1474	32	43	0	36
Shc1	Y349+Y350	766	1043	6	36
AIF	Pan-specific	1733	2351	10	36
Krs2	Pan-specific	336	455	8	35
Hsp90	Pan-specific	960	1294	5	35
JIK	Pan-specific	1074	1447	2	35
MRLC2 (MLC)	S18	861	1156	1	34
p38a MAPK	T180+Y182	52	70	29	34
Plk2 (SNK)	Pan-specific	881	1176	1	33
Nek4	Pan-specific	1070	1425	15	33
Plk3 (CNK)	Pan-specific	1064	1416	8	33
CaMK1d	Pan-specific	2094	2777	3	33
PKA Cb	S338	241	319	8	32
PKAR1A	Pan-specific	663	874	3	32
Smad2	S465+S467	156	205	1	31
PKCd	Y313	745	975	2	31
PP2Cab	Pan-specific	700	915	3	31
MST2	Pan-specific	1276	1658	9	30
ErbB2	Pan-specific	1787	2316	4	30
PRK2	Pan-specific	1355	1755	11	29

Btk	Pan-specific	1901	2453	3	29
PKBa (Akt1)	S473	696	896	6	29
FAK	Y576	159	204	27	29
CAMK2g	Pan-specific	1961	2521	4	29
TTK	Pan-specific	760	977	1	29
p53	S392	396	507	43	28
PyDK2 (PDK2)	Pan-specific	594	761	27	28
MLK3	T277+S281	973	1244	3	28
Mnk2	Pan-specific	1162	1485	16	28
Lyn	Y507	106	135	23	28
Bcl2	Pan-specific	459	585	0	27
PKBa (Akt1)	Pan-specific	458	583	4	27
MEK3b	Pan-specific	630	802	20	27
Src	Y529	634	805	9	27
Histone H3	S28	1401	1754	7	25
Syk	Pan-specific	545	681	1	25
MST1	Pan-specific	928	1151	1	24
Met	Pan-specific	1550	1914	5	24
p27 Kip1	S10	1309	1616	4	23
Mos	Pan-specific	875	1074	4	23
B23 (NPM)	T234	1026	1253	7	22
Tyro10	Pan-specific	844	1030	1	22
Paxillin	Pan-specific	785	957	12	22
Met	Y1003	267	324	20	21
Lyn	Pan-specific	681	826	2	21
CASP7	Pan-specific	1717	2079	3	21
PI3K p110 delta	Pan-specific	633	766	3	21
CAMK2b	Pan-specific	1883	2276	7	21
LATS1	Pan-specific	891	1076	1	21
MEKK2	Pan-specific	1002	1209	4	21
CaMK1d	Pan-specific	1926	2313	2	20
PP6C	Pan-specific	876	1049	9	20
PKA Ca/b	Pan-specific	830	993	11	20
Tau	S712	843	1007	23	19
PKCb1/2	T500	674	801	10	19
Yes	Pan-specific	651	772	6	19
ZAP70	Y319	443	525	6	19
PKBg (Akt3)	Pan-specific	943	1114	6	18
HSTK12 (Aurora 2)	Pan-specific	998	1175	9	18
Hpk1	Pan-specific	1056	1240	7	17
Chk1	Pan-specific	1622	1902	10	17
PDGFRa	Y754	1265	1484	3	17
IRAK1	Pan-specific	616	722	1	17
JNK	Pan-specific	1293	1515	3	17
APG1	Pan-specific	2052	2396	5	17
PKBb (Akt2)	Pan-specific	1062	1240	1	17

Smad1/5/9	S463+S465/S463+S465/ S465+S467	540	630	3	17
MRLC	S20	1081	1259	0	16
PKCb2	Pan-specific	778	904	1	16
SIRPa1	Pan-specific	549	637	5	16
PKCe	S729	154	178	7	16
MYPT1	T696	844	979	12	16
AK2	Pan-specific	1844	2138	0	16
MEKK4	Pan-specific	386	446	7	16
AcCoA carboxylase	S80	1735	1999	1	15
Paxillin 1	Y118	895	1028	2	15
PKR1	T451	854	980	22	15
S6Ka	T389	331	378	6	14
Histone H3	S10	1403	1599	5	14
Lck	Y191	779	883	2	13
Lck	S157	874	990	5	13
PAK1/2/3	S144/S141/S154	796	900	0	13
XIAP	Pan-specific	771	865	1	12
IGF1R	Pan-specific	1121	1253	5	12
Hsp105	Pan-specific	678	756	5	11
MEK2	Pan-specific	832	922	9	11
Raf1	S259	54	60	91	11
PKD (PKCm)	S910	866	959	5	11
CAMK2d	Pan-specific	2471	2728	18	10
Histone H2A.X	S139	373	410	23	10
IRAK2	Pan-specific	567	623	16	10
CaMK1g	Pan-specific	2117	2325	3	10
MKP1	Pan-specific	1080	1186	8	10
ROR2 (RON2)	Pan-specific	218	239	9	10
HO2	Pan-specific	1227	1347	23	10
PKA R2b	S114	138	151	18	10
Bax	Pan-specific	1863	2041	2	10
Arrestin b1	S412	1294	1415	1	9
Met	Y1230+Y1234+Y1235	182	199	41	9
PCNA	Pan-specific	540	587	21	9
eIF2a	Pan-specific	1186	1285	10	8
STK33	Pan-specific	517	560	6	8
PP1/Cg	Pan-specific	868	939	4	8
JAK3	Pan-specific	507	549	16	8
ASK1	Pan-specific	1999	2155	1	8
PKA R2a	S98	457	491	9	8
PKCd	S645	401	431	4	8
CDC42	Pan-specific	800	858	2	7
SODD	Pan-specific	829	889	2	7
Tau	S515	1062	1133	17	7
NME6	Pan-specific	1068	1138	2	7
DNAPK	Pan-specific	2528	2689	6	6

CK1d	Pan-specific	2003	2129	3	6
CDK2	Pan-specific	1783	1893	2	6
Cyclin E	Pan-specific	1738	1838	8	6
p107	Pan-specific	891	941	0	6
Bcl-xS/L	Pan-specific	1897	2001	11	5
PP1/Ca	T320	136	143	1	5
Abl	Y412	1285	1346	4	5
BMX (Etk)	Pan-specific	857	896	15	5
PP2A/Ca	Pan-specific	766	800	11	4
FAK	Y576	2140	2231	4	4
Bad	S75	1195	1242	8	4
PRK1/2	T774	437	453	2	4
LOK	Pan-specific	900	931	6	3
PKCh	T655	1275	1318	7	3
PKCe	S729	383	395	14	3
MEK1	S297	1127	1161	8	3
KAP	Pan-specific	351	361	1	3
PKBa (Akt1)	S473	336	344	10	2
Dok2	Y142	1367	1400	1	2
ACK1	Pan-specific	2224	2277	2	2
MEK6	Pan-specific	268	274	3	2
ICK	Pan-specific	1135	1161	4	2
CDK7	Pan-specific	1765	1802	13	2
CAMK2b	Pan-specific	1933	1964	8	2
APG2	Pan-specific	1902	1932	14	2
CASK/Lin2	Pan-specific	1538	1561	11	1
CDK9	Pan-specific	1868	1889	7	1
CASP2	Pan-specific	2143	2162	2	1
ILK1	Pan-specific	1119	1129	9	1
ALS2CR7	Pan-specific	1804	1815	6	1
PI3-Kinase	Pan-specific	748	751	31	0
PACSIN1	Pan-specific	637	639	17	0
MAPKAPK2	T334	112	112	38	0
Cyclin A	Pan-specific	1773	1774	11	0
MST1	Pan-specific	412	411	19	0
PKCd	T507	35	35	2	0
NME7	Pan-specific	1384	1379	9	0
Histone H3	T11	1507	1501	4	0
Jun	S73	1030	1025	7	0
Rb	S780	483	479	22	-1
MSH2	Pan-specific	1021	1010	26	-1
Paxillin 1	Y31	950	940	6	-1
eNos	T495	511	505	7	-1
PKBg (Akt3)	Pan-specific	573	565	11	-1
VEGFR2	Y1054+Y1059	1035	1020	15	-2
Ret	S696	391	385	10	-2

HO1	Pan-specific	1241	1220	0	-2
PKCd	S664	820	804	24	-2
Grp78	Pan-specific	2552	2494	5	-2
Rb	T821	1198	1170	25	-2
PKBa (Akt1)	T308	1014	988	3	-3
PED15 (PEA15)	S116	242	236	14	-3
Vinculin	Y821	795	772	6	-3
EGFR	Pan-specific	2038	1963	0	-4
IKKa	Pan-specific	1228	1181	16	-4
PKCd	Y313	1083	1041	9	-4
FAK	Y397	1483	1422	29	-4
IR	Y999	1238	1186	11	-4
FAK	S843	71	68	46	-4
CASP8	Pan-specific	2148	2043	4	-5
Fos	Pan-specific	2101	1996	5	-5
PKCg	T655	329	312	1	-5
CDK8	Pan-specific	1853	1755	4	-5
IKKa	Pan-specific	341	322	5	-5
JNK	T183/Y185	936	883	20	-6
Axl	Pan-specific	2294	2158	7	-6
c-IAP1	Pan-specific	1303	1225	11	-6
ANKRD3	Pan-specific	1915	1800	2	-6
CDK1 [p34(cdc2)]	Y15	1385	1300	4	-6
eEF2K	Pan-specific	1206	1129	15	-6
PKCa	Pan-specific	988	924	15	-6
CDK10	Pan-specific	979	914	2	-7
PP2Cd	Pan-specific	654	610	32	-7
CASP3	Pan-specific	1453	1355	1	-7
Hsp27	S15	1165	1083	2	-7
Kit	Y730	1185	1101	1	-7
Bak	Pan-specific	2196	2039	1	-7
MEKK1	Pan-specific	890	826	15	-7
STAT2	Y690	1259	1165	3	-7
CaMKK	Pan-specific	2421	2239	5	-8
Tau	S202	1047	968	2	-8
PERP	Pan-specific	326	300	9	-8
PKCq	T538	29	27	66	-8
Hip	Pan-specific	1844	1692	20	-8
p38a MAPK	T180+Y182	1013	929	21	-8
Nek7	Pan-specific	1252	1145	17	-9
PKCq	Pan-specific	1124	1027	7	-9
eIF2a	S51	1430	1300	1	-9
Rb	S807	1516	1375	3	-9
PKR1	Pan-specific	920	831	2	-10
PDK1	S244	382	343	17	-10
PKA Ca/b	T197	1154	1036	0	-10

Plk1	Pan-specific	605	542	16	-10
Kit	Y703	1302	1167	1	-10
Nek2	Pan-specific	1512	1354	18	-10
PP1/Cb	Pan-specific	1016	908	10	-11
RSK1/2	T573/T577	418	373	3	-11
eIF4E	Pan-specific	854	762	15	-11
BRD2	Pan-specific	1932	1723	17	-11
NFkappaB p50	Pan-specific	446	398	2	-11
PKCg	T514	365	325	17	-11
PDGFRa	Y742	1588	1402	4	-12
CK1g2	Pan-specific	2062	1819	3	-12
Fes	Pan-specific	1371	1209	19	-12
PP5C	Pan-specific	678	598	10	-12
ALK	Pan-specific	2814	2480	6	-12
DFF45	Pan-specific	1448	1275	7	-12
eIF4E	S209	1246	1097	0	-12
CASP4	Pan-specific	2407	2118	3	-12
CREB1	S129+S133	1179	1035	13	-12
p38a MAPK	Pan-specific	324	285	15	-12
Integrin b1	S785	1195	1046	2	-12
FAK	Y861	1105	964	9	-13
CDC2L5	Pan-specific	2207	1922	1	-13
Erk1/2	T202+Y204; T185/Y187	1059	922	13	-13
mTOR	Pan-specific	1730	1504	4	-13
ZIPK	Pan-specific	821	713	16	-13
eIF2a	S51	1584	1374	1	-13
Tau	S716	1105	957	1	-13
S6Ka	T229	176	152	39	-14
Vimentin	S33	353	304	33	-14
DGKZ	Pan-specific	1627	1403	1	-14
MEK6 (MKK6)	Pan-specific	226	194	5	-14
FAK	S722	1510	1294	2	-14
FAK	S910	1320	1130	4	-14
GFAP	S8	303	257	4	-15
MKP2	Pan-specific	1273	1081	19	-15
Bid	Pan-specific	2202	1869	8	-15
CASP5	Pan-specific	2711	2299	2	-15
MEK2 mouse	T394	1153	978	2	-15
EphA1	Pan-specific	2344	1984	15	-15
MEK1	T385	1126	953	3	-15
Aurora 3	Pan-specific	2541	2150	12	-15
Tau	S515+S518	1050	887	9	-15
Histone H3	T3	1747	1475	5	-16
PP2A/Aa/b	Pan-specific	1157	976	5	-16
JAK1	Pan-specific	2071	1736	0	-16
PKA	Pan-specific	884	739	9	-16

COX2	Pan-specific	1237	1034	1	-16
Kit	Y936	849	702	12	-17
p53	S392	883	728	8	-18
Erk5	T218+Y220	1298	1070	5	-18
SHP2	S576	185	152	20	-18
Hsp27	S82	1086	891	4	-18
Cofilin	Pan-specific	936	766	5	-18
JNK	T183/Y185	164	134	8	-18
Catenin b	S45	1458	1189	1	-18
CDK5	Pan-specific	2126	1730	6	-19
Cdc25B	Pan-specific	1269	1032	7	-19
TRADD	Pan-specific	982	798	1	-19
GRK3	Pan-specific	2179	1769	19	-19
Caveolin 2	S36	1524	1235	4	-19
Tau	S578	960	777	10	-19
RIP2/RICK	Pan-specific	693	560	12	-19
PP4/A'2	Pan-specific	1092	878	7	-20
PTP1B	Pan-specific	736	590	15	-20
S6Ka	T421+S424	376	301	0	-20
PKCl	T555	214	171	1	-20
GCK	Pan-specific	1481	1181	5	-20
Hsp60 (Myobact-Hsp65)	Pan-specific	896	711	6	-21
LAR	Pan-specific	754	597	6	-21
Caveolin 2	Pan-specific	1051	828	19	-21
p38a MAPK	T180+Y182	63	49	34	-21
MAPKAPK2	T334	1142	898	15	-21
MEK1 + B23(NPM)	S217+S221, S4	88	69	54	-22
Tyro3	Pan-specific	876	685	14	-22
CDK8	Pan-specific	1310	1022	4	-22
PKG1	Pan-specific	1797	1399	0	-22
Plk1	T210	1500	1166	1	-22
DAPK1	Pan-specific	1136	882	4	-22
LIMK1/2	Y508/T505	780	605	4	-22
CDK2	Pan-specific	1822	1409	7	-23
Lck	Pan-specific	1072	827	0	-23
Integrin a4	S988	1473	1128	5	-23
Hsp27	S78	1486	1136	25	-24
Erk1/2	T202+Y204	1503	1148	1	-24
14-3-3 z	Pan-specific	1885	1431	17	-24
STI1	Pan-specific	1061	805	8	-24
Dok1/p62dok	Pan-specific	1001	757	1	-24
PKCq	S676	1315	994	9	-24
PTP-PEST	Pan-specific	149	113	5	-24
MEK2	Pan-specific	1199	903	1	-25
CASP9	Pan-specific	1385	1042	1	-25
ZAP70	Y315+Y319	804	604	15	-25

Tau	S530	1073	800	15	-25
Ksr1	Pan-specific	165	122	38	-26
eIF4E	S209	1435	1067	1	-26
ERP72	Pan-specific	1653	1227	3	-26
GRK2	S670	2080	1540	7	-26
Hsp27	S15	2043	1512	10	-26
FGFR1	Pan-specific	2147	1585	1	-26
Dab1	Y198	1628	1201	22	-26
CAMK2d	Pan-specific	2034	1497	2	-26
Hsp70	Pan-specific	1034	758	26	-27
HSF4	Pan-specific	1320	967	6	-27
COT	Pan-specific	1309	958	8	-27
Huntington	S421	2243	1641	13	-27
PKBa (Akt1)	S473	192	141	3	-27
Cdc34	Pan-specific	1373	992	0	-28
Histone H2B	S14	2090	1509	1	-28
FAK	Y577	1768	1273	4	-28
PKCq	S695	1377	991	0	-28
MEK2 human	T394	1374	987	0	-28
Cofilin 2	S3	2126	1516	2	-29
CK2a	Pan-specific	1533	1092	2	-29
STAT1	S727	950	671	29	-29
Cdc25C	Pan-specific	1498	1054	1	-30
GNB2L1	Pan-specific	1813	1272	1	-30
ATF2	T51/T53	1738	1218	0	-30
Erk1	Pan-specific	2028	1421	0	-30
CREB1	S133	1678	1174	14	-30
AMPKb	Pan-specific	979	684	22	-30
ZIPK	Pan-specific	689	481	4	-30
Fyn	Pan-specific	1470	1025	4	-30
Rb	T826	834	571	8	-31
IKKb	Pan-specific	1342	920	1	-31
PRAS40	T246	1092	747	6	-32
MEK1	S297	1041	710	7	-32
Tyrosine Hydroxy-lase	S19	242	165	8	-32
DAXX	Pan-specific	1754	1194	15	-32
PP4C	Pan-specific	2004	1359	1	-32
DRAK1	Pan-specific	682	460	11	-33
p18 INK4c	Pan-specific	1512	1018	11	-33
GroEL	Pan-specific	2483	1652	9	-33
GRK2	Pan-specific	1745	1155	8	-34
IRAK4	Pan-specific	906	592	13	-35
Crystallin aB	S19	1186	771	19	-35
PKD (PKCm)	S738+S742	167	108	18	-35
Paxillin 1	Y118	392	253	51	-36
ErbB2	Y1248	1983	1276	9	-36

Crystallin aB	S45	1478	949	13	-36
IRAK4	Pan-specific	299	192	10	-36
GSK3ab	Y279	114	73	14	-36
PKCz/l	T410/T403	709	449	28	-37
Erk6	Pan-specific	733	462	18	-37
p16 INK4	Pan-specific	1564	985	7	-37
PKCh	S674	429	270	24	-37
B23 (NPM)	T199	1630	1019	2	-37
Btk	Y223	663	411	1	-38
ZAP70	Pan-specific	615	379	13	-38
Mnk1	T209+T214	552	338	5	-39
Nek2	Pan-specific	3028	1851	14	-39
Alk	Pan-specific	1802	1090	23	-39
Aurora 2 (Aurora A)	Pan-specific	616	372	18	-40
Lck	Pan-specific	315	190	24	-40
Tau	S422	1037	623	10	-40
EGFR	Y1068	1401	838	3	-40
FGFR2	Pan-specific	2189	1308	2	-40
CK1e	Pan-specific	1092	650	4	-40
CPG16/CaMKinase VI	Pan-specific	955	568	18	-41
DRAK2	Pan-specific	1449	857	3	-41
RSK1/2 (p90RSK)	T359/T365	69	41	1	-41
Cyclin D1	Pan-specific	1705	1007	12	-41
CDK7	Pan-specific	1880	1103	18	-41
Hsp25	S86	381	222	25	-42
FAS	Pan-specific	1479	862	7	-42
MAPK14/p38a	Pan-specific	1423	817	18	-43
ErbB2	Y1139	1829	1046	0	-43
LIMK1	Pan-specific	760	433	12	-43
FLT4	Pan-specific	2372	1351	12	-43
Cortactin	Y470	1425	809	4	-43
PKCb2	T641	248	139	6	-44
Glycogen Synthase	S640	3561	1980	4	-44
CD45	Pan-specific	1366	759	0	-44
VEGFR2	Y1054	1470	817	1	-44
PKCa	S657	669	366	27	-45
Grp75	Pan-specific	3381	1848	0	-45
IKKg/NEMO	Pan-specific	1041	568	7	-45
Csk	Pan-specific	1168	637	4	-46
Erk3	Pan-specific	929	506	4	-46
RONa	Pan-specific	774	418	22	-46
FasL	Pan-specific	2021	1090	10	-46
Smad2/3	Pan-specific	648	349	32	-46
MEK1	Pan-specific	1397	750	1	-46
MEK4	S257+T261	849	447	5	-47
Jun	S73	774	405	32	-48

DAPK2	Pan-specific	1553	814	19	-48
Rb	S612	1102	569	22	-48
CAS	Pan-specific	1435	739	17	-49
Synapsin 1	S603	45	23	44	-49
RSK1	S380/S386	84	42	39	-49
MEK1	T291	36	18	26	-50
BLNK	Y84	1942	975	9	-50
Src	Y418	274	136	8	-50
FAK	Y425	1968	973	11	-51
Adducin a/g	S726	945	465	29	-51
Haspin	Pan-specific	1848	906	3	-51
Tyrosine Hydroxy-lase	S71	76	37	97	-51
Hsp27	S82	205	100	54	-51
Progesterone Recep-tor	S294	212	103	20	-52
CASP12	Pan-specific	631	305	68	-52
ATM PK	S1981	4612	2225	5	-52
CDK6	Pan-specific	1491	714	5	-52
BUB1A	Pan-specific	2074	987	21	-52
eIF2Be	S540	98	47	35	-53
JAK2	Pan-specific	411	195	5	-53
ILK1	Pan-specific	842	395	3	-53
IRS1	Y612	1266	593	2	-53
CDK1	Pan-specific	784	366	2	-53
CDK4	Pan-specific	1815	844	21	-53
BLK	Pan-specific	2221	1024	2	-54
PTP1D	Pan-specific	1557	717	18	-54
Hsp47	Pan-specific	5127	2318	5	-55
PP2B/Aa	Pan-specific	75	33	21	-56
ZAP70	Y292	492	217	23	-56
CaMK2a	T286	1139	500	16	-56
ATF2	T53	1282	560	14	-56
GSK3a/b	Y279/ Y216	242	105	17	-57
Bad	S99	1736	754	13	-57
HspBP1	Pan-specific	836	360	3	-57
Grp94	Pan-specific	897	383	24	-57
FAK	S732	365	155	29	-58
PKBa (Akt1)	T308	170	72	9	-58
Histone H1	phospho CDK1 sites	589	241	1	-59
PARP1	Pan-specific	191	78	37	-59
eIF4G	S1107	677	260	2	-62
ErbB2	Y1248	1594	610	6	-62
PKD (PKCm)	S910	118	44	71	-63
4E-BP1	S65	163	58	24	-64
BMX (Etk)	Y40	399	140	9	-65
JAK2	Y1007/1008	405	141	16	-65

CDK1/2	Y15	555	192	20	-65
IRS1	Y1179	992	343	29	-65
EGFR	Y1148	675	232	2	-66
p53	S392	56	19	13	-66
Cofilin 1	S3	1081	333	7	-69
Erk1/2	T202+Y204; T185/Y187	1701	518	3	-70
CASP6	Pan-specific	1424	427	1	-70
STAT1	Y701	75	22	7	-71
BRCA1	S1497	1225	346	16	-72
Fos	T232	412	110	31	-73
CaMK2a	T286	830	221	7	-73
Erk2	Pan-specific	1998	530	2	-73
FKHRL1	T32	245	64	39	-74
MARCKS	S158+S162	100	25	1	-75
ErbB2	Y1139	69	17	17	-75
GAP-43	S41	737	178	69	-76
GSK3a/b	Pan-specific	79	18	17	-77
CDK1/2	T161/T160	1761	373	32	-79
Jun	S73	1411	288	2	-80
IR/IGF1R	Y1189/Y1190	339	65	22	-81
Hsp25	Pan-specific	162	29	26	-82
Caldesmon	S789	339	60	8	-82
Jun	S63	349	59	60	-83
CDK1/2	T14+Y15	1387	224	8	-84
Caveolin 2	S23	68	11	13	-84
ERP57	Pan-specific	456	61	14	-87
MARCKS	S158+S162	162	21	8	-87
CASP8	Pan-specific	57	7	38	-88
Insulin Receptor b	Pan-specific	79	10	109	-88
Integrin b1	T783	430	51	19	-88
CDK1/2	Y15	234	27	45	-89
Bad	S91	1122	95	6	-92
PTEN	S370	185	11	30	-94
IKKb	Pan-specific	36	2	21	-96
IKKa/b	S180	65	0	14	-99